The Encounter of Comet Shoemaker-Levy 9 with Jupiter

An extraordinary event took place in July 1994: the collision of a comet with Jupiter (Comet Shoemaker-Levy 9). There is every indication that this is an extremely rare event. For this reason the planetary astronomers in the world organized and carried out extensive observations of the encounter. The data obtained are truly unique.

This issue of the Messenger presents first results obtained at ESO La Silla (see pages 28–49).

Latest Developments Around Paranal

R. GIACCONI, Director General of ESO

There have been a number of important developments around the Paranal issue since my last report in the ESO Messenger (June 1994). In particular, Council decided to continue the construction of the VLT Observatory at Paranal, while at the same time requesting the ESO Management to pursue the ongoing studies of alternative solutions. During the past months, progress has also been achieved towards the conclusion of negotiations of a Supplementary Treaty between Chile and ESO.

The Council Decisions

The ESO Council met in extraordinary session at the ESO Headquarters on August 8 and 9, 1994. The main agenda items were concerned with the recent developments around ESO's relations with the Republic of Chile, as well as the status of the VLT project at Paranal.

This meeting followed continued consultations at different levels within the ESO member states and included careful consideration of all aspects of the current situation. Council took note of recent positive developments which have occurred since the May 1994 round of discussions with the Chilean authorities in Santiago. The confirmation of ESO's immunities as an International Organization in Chile, contained in a number of important statements and documents, is considered a significant step by the Chilean Government to insure to ESO the unhindered erection and later operation of the VLT on Paranal.

Under these circumstances and in order to maintain progress on the VLT project, the ESO Council authorized the ESO Management to continue the on-site work at Paranal.

Council also took note of the desire expressed by the Chilean Government to complete negotiation of a Supplementary and Amending Agreement, and it was decided that a Council Delegation shall conclude as soon as possible the negotiation of this Agreement. Council noted that the Chilean Delegation has accepted ESO's invitation to hold the final round of negotiations in Europe and proposed that it shall be held in the early autumn 1994, i.e. well before the next Council meeting on November 30–December 1, 1994.

Nonetheless, Council also expressed its preoccupation with regard to remain-

1

ing ambiguities contained in some official statements according to which the formal recognition of ESO's status on Paranal would depend on the conclusion of the above-mentioned Agreement. At the May 1994 meetings in Santiago, understanding had been reached that this Agreement will merely confirm the already existing legal situation. The main objective is to expand the cooperation between Chile and ESO by granting ensured access for Chilean astronomers to ESO's facilities and incorporate elements of Chilean labour legislation into the ESO internal staff regulations.

In view of these circumstances, and pending the successful conclusion of these negotiations, Council therefore instructed the ESO Management to continue exploring alternative sites for the VLT.

In a final statement, the ESO Council again expressed its hope that the scientific co-operation between Europe and Chile in the field of astronomy which began in 1963 will continue to develop and expand well into the next century to the mutual benefit of science in both communities.

The Continuation of the VLT Project at Paranal

In practical terms, the above decision by Council implies that ESO is now taking the steps necessary to move from Europe to Paranal the main mechanical parts of the rotating dome (total weight around 500 tons) for the first VLT 8.2-metre unit telescope. The transport will begin in late September and it is ex-pected that the ship will unload its precious cargo in Antofagasta sometime in November. The assembly at Paranal will begin soon thereafter, once the concrete base, now under construction, is ready. This will enable the VLT project to stay within the planned timeline for completion just after the year 2000.

A Visit to Chile

In order to assess the current situation in Chile, I paid a visit to this country in the period August 23–26, 1994, together with the Head of the VLT project, Prof. M. Tarenghi. On August 24 we visited the Paranal site together with the Antofagasta authorities, including members of the Regional Government and also the Members of the Chilean Parliament from the Second Region, Senator A. Alessandri, Messrs. R. Gajardo and F. Valenzuela. The Mayor of Taltal also joined the visitors on the mountain top.

Both the site and the foundation layout were very impressive, and for the first time it was possible to get a feeling of the full magnitude of this enormous project. There were many positive comments by the visitors and this was an excellent opportunity for ESO to show its VLT project and future ambitions to the local authorities.

Later that day, the ESO Management made a thorough presentation of the VLT project in the presence of more than 150 persons at Hotel Antofagasta in that city. Among those present were the Members of the Parliament, various authorities from the Antofagasta and Taltal municipalities and also many local business-men. This event confirmed the positive mood and the profound support which ESO enjoys in the Second Region. This was also obvious during a visit which Daniel Hofstadt and I paid to the Intendente (Governor) the next day.

Travelling on to Santiago the next day, our delegation met with the Ambassadors of the ESO member states and we gave a report on the latest developments at the ESO Council, as well as the status of the relations with the Chilean authorities. The same day we attended a meeting at the Ministry of Foreign Affairs in Santiago during which preparations were made for the final negotiations of the Supplementary Agreement.

Later that day we met with Mr. J.M. Insulza, Under-Secretary of Foreign Affairs, for a further exchange of views on all related matters. We were pleased to feel again the very positive attitude of the Under-Secretary personally and also the sincere desire of the Chilean Government to see the VLT installed in Chile. Mr. Insulza is going to visit Europe later this year, and we took the opportunity to extend a warm invitation to him to visit the ESO Headquarters in Garching during his stay in Germany.

Finally, as many of the administrative and scientific activities have now been transferred from La Silla to Santiago, we decided to inaugurate the Vitacura offices on this occasion. The brief ceremony was attended by many Chilean astronomers and related scientific authorities. I took this opportunity to express again the importance of clear support for ESO's case from the scientific community in Chile.

TELESCOPES AND INSTRUMENTATION

VLT Progress Report

M. TARENGHI, ESO-Garching

The following series of pictures best illustrates the enormous progress made in the VLT Project which is now in a new and dynamic phase of construction. The recent decision by the Council to continue with the erection is the natural consequence of the major progress made in the construction of the first unit telescope in Europe. The first 8.2-m mirror is currently undergoing the polishing process at REOSC, and the first interferogram was taken successfully. Blank no. 2 is now ready and Schott will deliver it to REOSC in October. Blank no. 3 has successfully completed the ceramization phase. In Milan, the foundations for the pre-erection in Europe are ready to receive the azimuth track, 16 m in diameter, which was machined at Ansaldo in Genova.

Figure 1 shows the azimuth track on the turning table supported by the special tool (the blue part) which was de-signed and manufactured for the VLT Project.

Elements of the fork structure have been welded and machined as shown in Figure 2. In addition, many of the subsystems of the tube are in the advanced

Figure 1.

Figure 2.

Figure 3.

Figure 4.

phase of manufacture, as can be seen in Figures 3 and 4.

In the course of the first half of 1995, with the full integration of the telescope in Milan, we will be able to see the VLT resembling Figure 5 which shows a graphic presentation of the unit telescope prepared by J. Quebatte.

While telescope no. 1 is ready to be assembled in Milan, enclosure no. 1 is ready to be assembled in Chile. The civil engineering activities on Paranal are proceeding as planned and will be reported in greater detail in an article in the next *Messenger*. It is expected to start the erection of the first enclosure in December 1994.

The first elements of the enclosure, the mini-seismic supports embedded in the foundations, are already in Chile (Figure 6 on page 4). In a few weeks they will be placed at their final location.

All structural elements of enclosure no. 1 have been machined, and for a few critical sub-assemblies there will be a pre-erection in Europe to test performances and interfaces. Figure 7 (page 4) shows the upper ring of the fixed structure on which the boogies will be

Figure 5.

3

mounted, a part of the enclosure platform that will give access to the Nasmyth platform.

In the last week of September, the first shipment of more than 100 tons of steel will leave Europe for the journey to Chile.
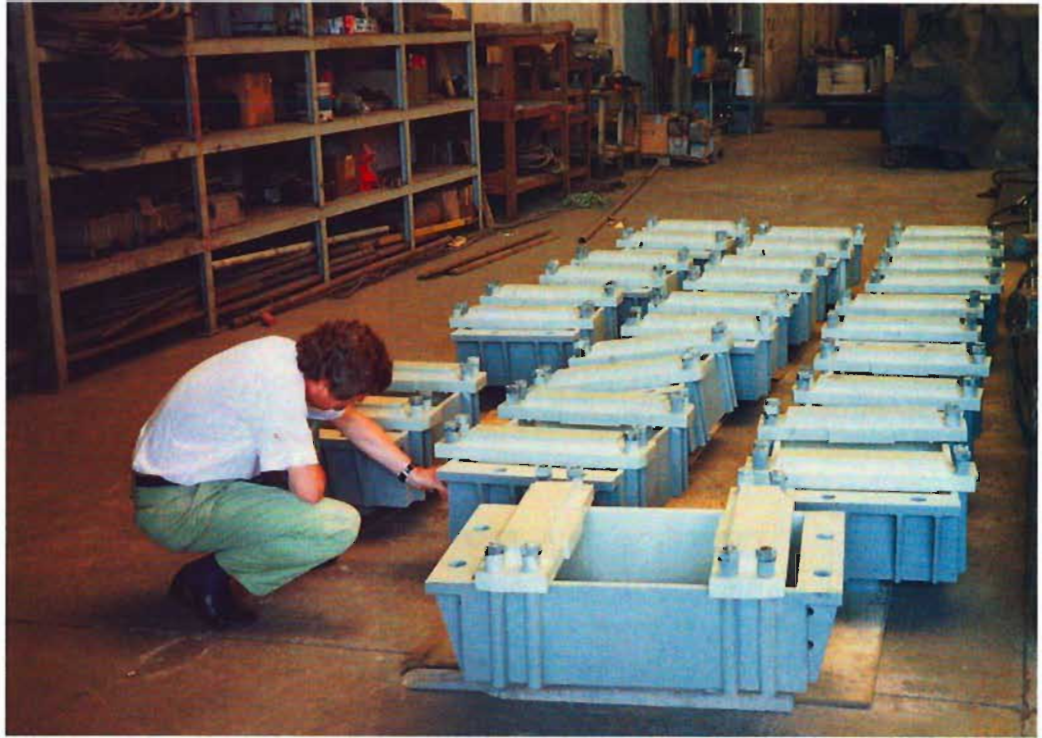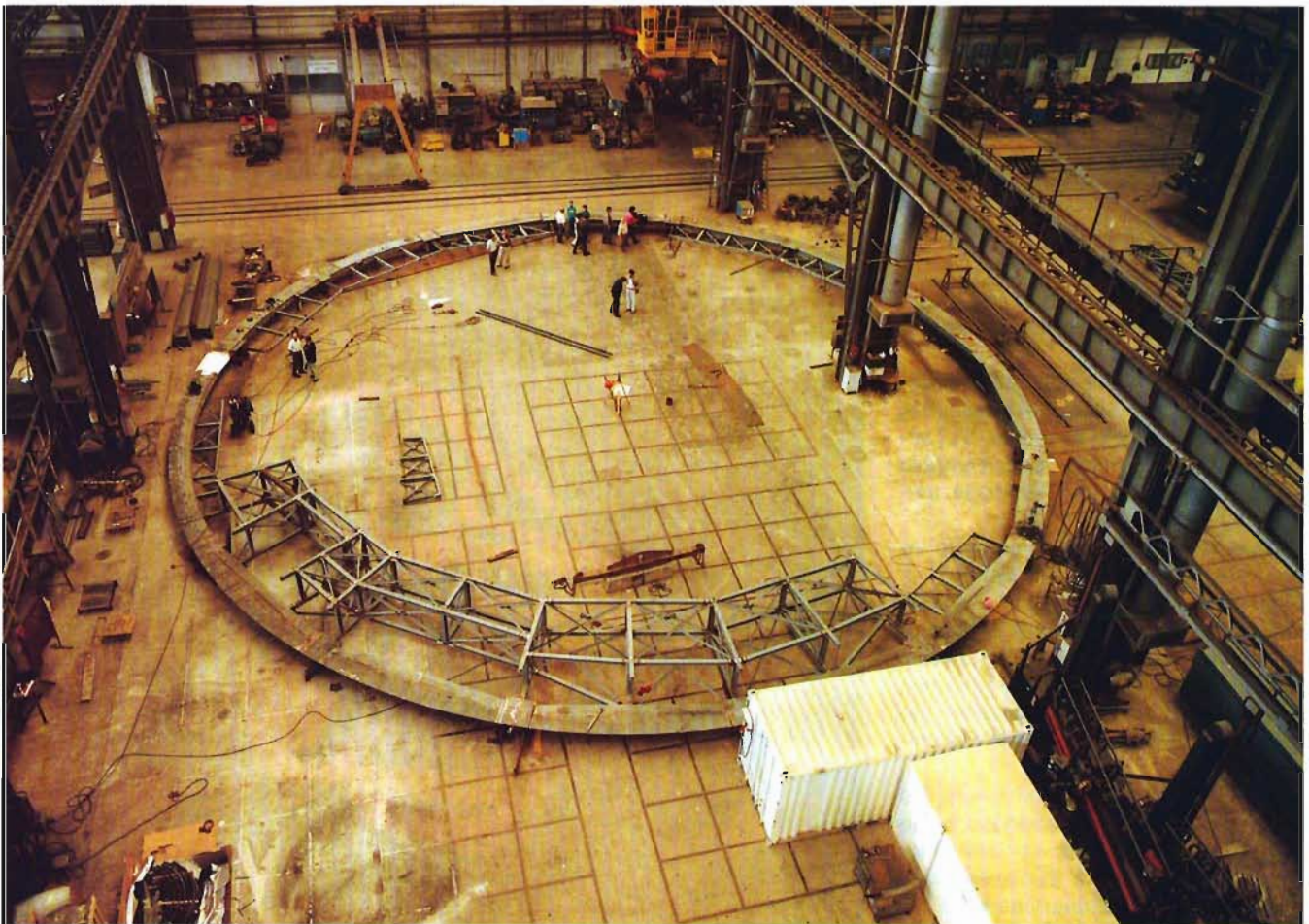

Figure 6.

Figure 7.

A New High-Resolution Holographic Grating for the Blue Arm of EMMI

L. PASQUINI, J. STORM, ESO-La Silla, and H. DEKKER, ESO-Garching

1. Introduction

A high-resolution capability for the blue arm of EMMI has been high on the list of wishes of many astronomers. As cross-dispersion is not possible in the blue arm, S. D'Odorico and H. Dekker explored the possibilities and found that the best solution would be a holographic grating with a very high groove density. Previously the highest groove density grating was Grating #3 with 1200 g/mm, but the new grating (hereinafter Grating #11) with 3000 g/mm pushes the resolution limit down from 0.1 nm to 0.03 nm entering the domain of the echelle in the red arm.

Grating #11 is produced with holographic techniques: i.e. the grating grooves are not manufactured with the conventional process of diamond ruling, but with the chemical treatment of a blank coated with photoresist and impressed by interference fringes from a stabilized laser (Hutley 1976). The advantages of holographic gratings with respect to the conventional ones can be summarized in two main points (Dravins 1978):

(1) The holographic process permits a higher density of grooves with respect to the conventional ruling, therefore allowing a higher spectral resolution for a given slit width and beam dimensions.

(2) The ruling process is extremely clean. The surface of each groove does not present the (even small) imperfections (microroughness) present in the conventional gratings. These imperfections are the main source of grating scattered light. Also, the very precise groove spacing eliminates the possible periodical errors in the inter-groove spacing, which is the major cause of ghosts.

As a consequence, holographic gratings produce very pure instrumental profiles and a very low level of stray light

(see for example Dravins 1978, Gilliotte and Mendes de Oliveira 1994).

On the other hand, low groove density holographic gratings have a lower efficiency than blazed ruled gratings due to the fact that their symmetrical groove profiles diffract light in the + and − orders with about equal efficiency. Only recently has it become possible to obtain blazed holographic gratings by the combination of ion etching and interferometric techniques.

However, if the grating is used at a high angle of incidence the grating equation $\sin\alpha + \sin\beta = m\lambda n$ [1] permits only diffraction in the zeroth and first order as the other orders have $|\sin\beta| = |m\lambda n - \sin\alpha| > 1$. For a 3000 g/mm grating in the 300–500 nm range, the value of λn ranges from 0.9 to 1.5. In this domain the diffraction efficiency of a holographic grating reaches acceptable values whereas stray light is much better than that of ruled gratings.

Many spectral lines of astrophysical interest are located in the spectral region from 300 to 520 nm covered by EMMI blue, and it is important to have the capability to study these lines in detail. Grat-

---

[1] α and β are the angles of incidence and exit, respectively, with respect to the grating normal, m is the order number, λ the wavelength and n the number of grooves per mm.

ing #11 will therefore provide the ESO user community with a configuration with a resolution intermediate between that of the low-resolution spectrographs present at La Silla (Boller & Chivens, EFOSC's, and EMMI) and that of the high-resolution spectrographs (CASPEC, CES, EMMI Echelle). Thanks to the absence of a cross-dispersing element, it is possible to approach high-resolution capabilities with an efficiency close to that of low-resolution spectrographs.

The Grating

The grating characteristics are summarized in Table 1 and the efficiency curve is shown in Figure 1.

Although the efficiency curve strongly depends on the polarization of the light, the average efficiency is quite good, as it may be deduced by comparing Figure 1 with the efficiency of the classical gratings available at the NTT (Giraud 1994). This comparison is even more favourable considering that the groove density is more than doubled with respect to the conventional gratings.

Grating #11 is mounted on a standard EMMI support, and the central wavelength can be changed by the user using the standard EMMI user interface software.

TABLE 1.

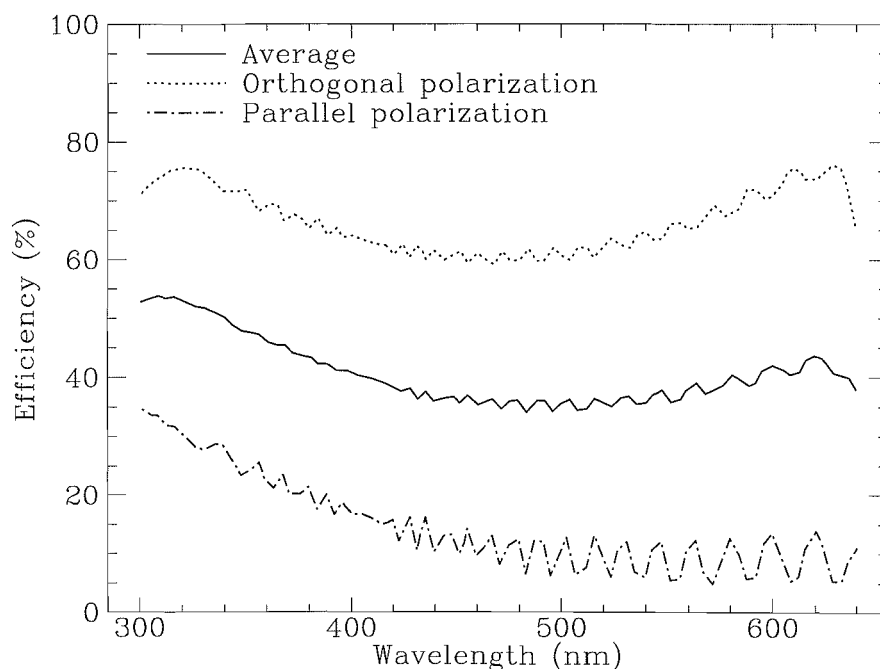| Grating #11 specifications	
Type	Holographic plane grating
Grooves/mm	3000
Wavelength range	300–500 nm
Stray light	1×10^{-10} (measured by Jobin-Yvon)
Size	$180 \times 135 \times 30$ mm
Blank Material	Silica
Manufacturer	Jobin-Yvon

Figure 1: *The efficiency of Grating #11 as measured in the laboratory by B. Buzzoni. Note the very strong dependence on polarization, especially towards the red.*

Results of the Tests

After some small modifications to its original housing, Grating #11 was successfully mounted for the first time in November 1993. The first astronomical tests were performed in December 1993.

The dispersion, as measured directly on Th-Ar spectra, is 0.64 nm/mm at 390 nm. Considering the pixel size (24 μm) of the Tektronix CCD mounted on the blue arm of EMMI and the non-cross-dispersed format, this translates into a spectral range of 15 nm. The slit resolving power product R_s is about 9000 at 400 nm (1" slit) but the maximum resolving power (considering two pixels FWHM) is almost 13,000 at 400 nm. This resolving power can only be realized with a 0.7" slit but it is not at all unreasonable to use such a narrow slit at the NTT. Tests with the internal Th-Ar lamp have shown that two pixels FWHM can also be obtained in practice with this grating, if the instrument focus is kept under very good control. These tests also showed that the resolution was uniform within $\pm$ 0.2 pixels over the covered spectral range without any obvious trends with wavelength.

No ghosts were found, even in very high S/N observations. Note here that ghosts are quite common with high-density groove conventional gratings.

The efficiency of the whole system (NTT + EMMI + Grating #11 + CCD #31) was measured with 4 different wavelength settings, observing two high-resolution spectrophotometric standard stars (Hamuy et al. 1992). One star was observed at low and one at high airmass. The results are summarized in Figure 2, where the measured efficiency is given as a function of wavelength. The error bars indicate the position of the individual measurements for the two stars. For the wavelengths shorter than 390 nm the high airmass measurements were only given half weight as mean extinction coefficients were used for the reduction.

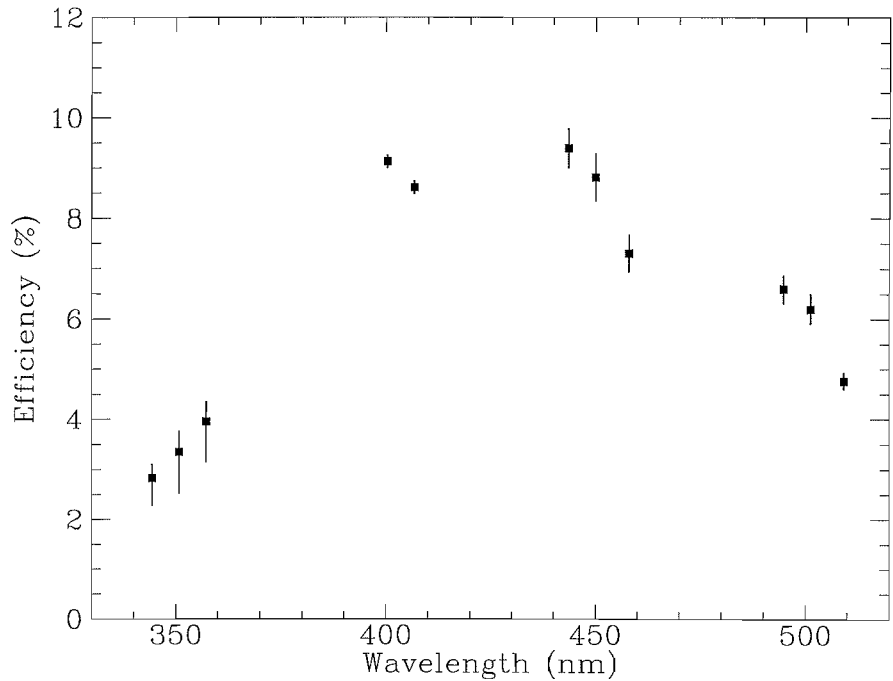The curve matches very well the efficiency expected from the grating effi-

Figure 2: *The total efficiency of the NTT, EMMI blue with Grating #11 and CCD#31 as a function of wavelength. The error bars indicate the actually measured values for the two stars observed.*

ciency curve of Figure 1, together with the CCD #31 response and the transmission of the EMMI blue optics (Giraud 1994).

The efficiency peaks at more than 9% in the B pass band, a value which compares very well with state-of-the-art high-resolution spectrographs in this spectral region.

An obvious use of the grating will be in the dichroic mode (DIMD) with one of the echelle gratings mounted in the red arm of EMMI. In this configuration the new grating will, simultaneously, provide a complementary blue spectrum at a comparable resolution to the one achieved in the red arm. The light loss due to the dichroic beamsplitter in the wavelength range 385 to 400 nm ranges from about 15 to 25% but this should be considered an upper limit as the dichroic prism and the wide-band mirror are performing better at bluer wavelengths.

Grating #11 is offered to the users starting the next period.

Acknowledgements

References

Dravins, D. 1978: *Applied Optics*, Vol. **17**, No. 3, 404.
Gilliotte, A., Mendes de Oliveira, C., Tighe, R. 1994: *The Messenger* No. 77, p. 6.
Giraud, E. (Ed.) 1994: EMMI and SUSI. *ESO Operating Manual* No. **5**, Vers. 2.0.
Hamuy, M. et al. 1992: *PASP* **104**, 533.
Hutley, 1976: *J. Phys.* E **9**, 513.

New Holographic Grating for the B&C on the ESO 1.52-m Telescope

C.M. DE OLIVEIRA, A. GILLIOTTE and R. TIGHE, ESO-La Silla

There are 31 ruled gratings currently available for the Boller and Chivens spectrograph (B&C) on the ESO 1.52-m telescope. These have dispersions ranging from 3.2 to 51 nm/mm. Recently, a new holographic blazed grating has become available from the Jobin-Yvon manufacturer and successfully tested at La Silla. This grating is designated #32. Its main characteristics are given in Table 1.

In first order, grating #32 gives the

TABLE 1.

Specifications of Grating #32 for the B&C	
Type	Holographic blazed grating
Grooves/mm	2400
Blaze wavelength	400 nm
Wavelength range	320-470 nm
Dispersion	3.2 nm/mm
Size	110 × 110 mm

same dispersion as the second order of the ruled gratings #11, 12, 20 and 22. A comparison of the efficiency of grating #32 with that of one of the ruled gratings (#20) of same dispersion is given in Figure 1. As can be seen from the curves given by the manufacturer, grating #32 is 1.9 and 1.6 times more efficient than grating #20 at 350 and 450 nm respectively.

In addition to greater efficiency, the holographic grating also produces significantly less stray-light contamination than any of the ruled gratings. This will be an important consideration for any programmes in which high-precision placement of the continuum is important, e.g. abundance measurements, and for spectrophotometry.

The superior performance of the holographic grating can be seen in the spectra shown in Figure 2. These spectra were taken with grating #32, in first order, and with grating #20, in second order (using CCD #24). Both grating set-ups give a dispersion of ∼ 3.2 nm/pixel.

In Figure 2 we show a cut around the Ca II H and K lines in the spectrum of the star HR 3459. The effects of the lower stray-light contamination for the holographic grating are well exemplified here. For the spectrum taken with grating #32 the doublet Ca II lines are clearly more detailed. Also, the small absorption features on the wings of the Ca II lines are deeper. This figure also demonstrates the higher efficiency of grating #32, as compared to #20 with a significantly higher signal-to-noise ratio in the spectrum obtained with the former.

The new holographic grating for the B&C on the ESO 1.52-m, grating #32, is offered to the astronomical community starting October 1994.

Figure 1: *The efficiency curves for the ruled grating #20 (RG), in second order and the new grating #32 (HG), in first order, as measured by the manufacturer, Jobin-Yvon.*

Figure 2: *A comparison between two spectra taken with equivalent set-ups using a classical ruled grating (grating #20, in second order) and the new holographic grating (grating #32 in first order). The top spectrum was arbitrarily shifted upwards by 10 units, to allow a comparison. The grating #32 spectrum has less stray light contamination and thus it shows a cleaner stellar line profile, in which more details of the lines can be detected.*
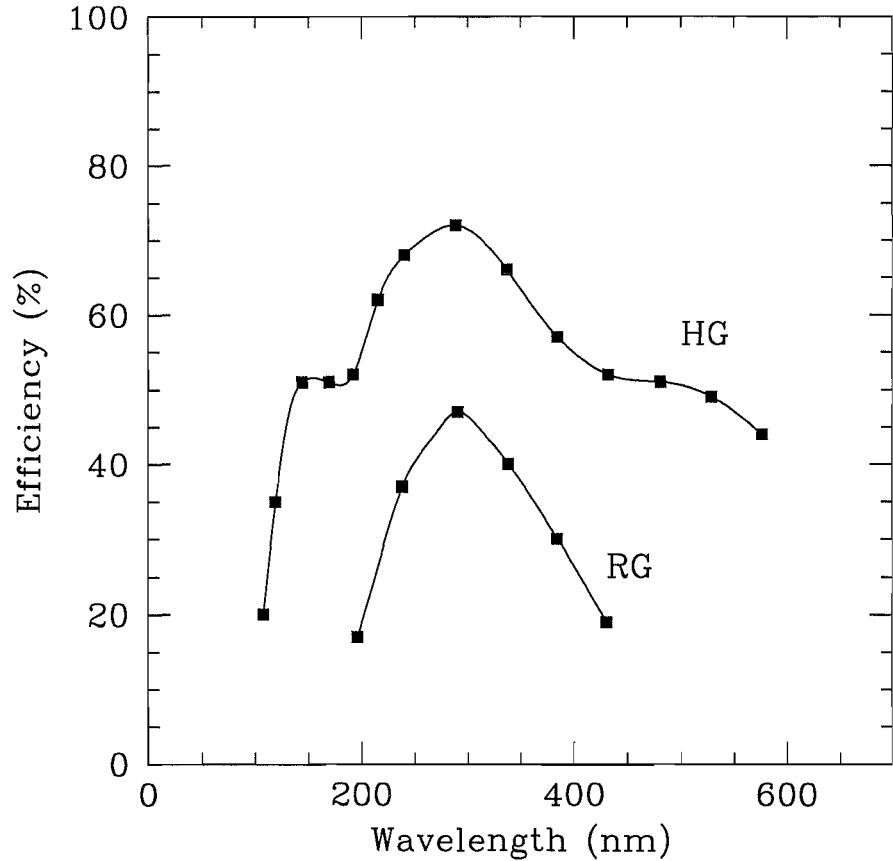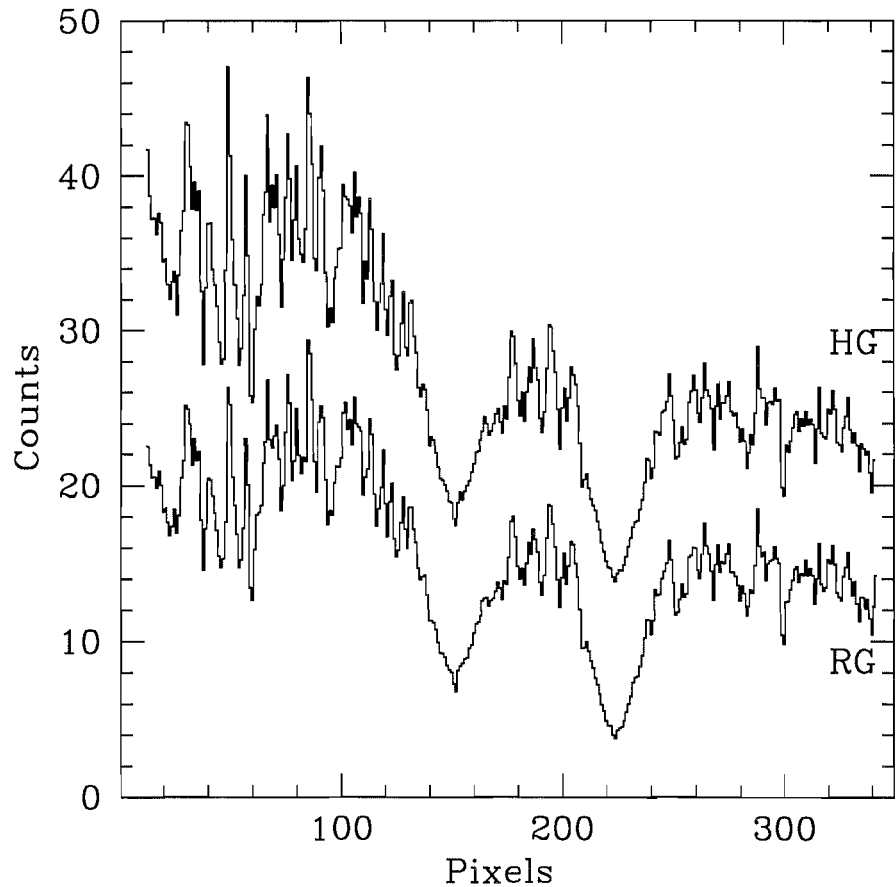
7

Test of the Upgraded IRAC1 Camera for 1–5 μm Imaging

A. MOORWOOD, G. FINGER, ESO-Garching, and H. GEMPERLEIN, ESO-La Silla

1. Status

IRAC1 has been upgraded with an SBRC 58 × 62 pixel InSb array sensitive from 1 to 5.4 μm and was reinstalled and tested at the F/35 infrared focus of the 2.2-m telescope in May 1994. It is now being offered primarily (i) to complement IRAC2 (1–2.5 μm) at the 2.2-m and TIMMI (8–17 μm) at the 3.6-m by providing for L(3.8 μm) and M(4.7 μm) band and 3–4.5 μm CVF (Circular Variable Filter) narrow-band (R ~ 50) imaging and (ii) to replace the decommissioned infrared photometers for 1–2.5 μm photometry of objects too bright for IRAC2 (K ≤ 6). It also provides the capability for obtaining photometry of objects over the complete 1–5 μm range without switching cameras. Using solid-nitrogen cooling for which this camera was originally designed, however, its performance is background limited in the thermal infrared but detector dark current limited at the shorter wavelengths with the new array. Although we have confirmed that this problem can be overcome with liquid-helium cooling, we have not managed to achieve a holding time sufficient to avoid refilling during the night thus increasing the operational overhead on La Silla. As IRAC2 is still expected to remain the instrument of choice for most 1–2.5 μm imaging applications due to its larger array (256 × 256) and superior sensitivity over this range, it is currently foreseen that nitrogen cooling will be considered the norm unless there are scientifically justifiable reasons for enhanced short-wavelength performance with IRAC1.

2. Observing Modes

IRAC1 provides for imaging through broad-band, narrow-band and Circular Variable (CVF) filters between 1 and 5 μm at two selectable pixel scales as summarized in Table 1.

Observations can be made in DC (staring) mode or with secondary-mirror sky chopping, and both modes can be combined with telescope nodding. Tests at the telescope (see below) confirmed that optimum performance in the broad/narrow-band filters at > 3 μm requires sky chopping while observations in the shorter wavelength filters and the CVFs are generally best made in the *dither* mode. In the latter case, a sequence of images recorded at different telescope positions is used to construct both the final object and sky frames. Such sequences can now be executed automatically using the IRAC sequencer and the combined telescope/guide probe offset feature introduced in May which maintains the TV autoguiding without manual intervention.

3. Test Results

3.1 Emissivity

Telescope emission is expected to dominate the background and hence set the performance limits in the thermal infrared. Measurements of the total background at the 2.2-m with the photometer have implied a relatively high emissivity of ~ 0.2 compared e.g with ~ 0.13 at the 3.6-m and have led to some speculation regarding a possible additional, unidentified source of thermal background emission. In order to investigate this further, we included a series of measurements designed to separate the various background contributions. These included measurements with the camera viewing (i) a liquid-nitrogen-cooled blackbody, (ii) the sky directly with the camera located outside the telescope dome, (iii) the telescope + sky, and (iv) a black plate at ambient temperature. The results indicate that the camera entrance window contributes a few per cent and yielded the sky and telescope emissivities summarized in Table 2.

TABLE 1. *IRAC1 Camera Characteristics*

Image Scales and Fields		
Objective	arcsec/pix	arcsec
L4	0.45	26×28
S3	0.8	46×49

Filters		
Name	$\lambda(\mu$m)	$\Delta\lambda(\mu$m)
J	1.25	0.3
H	1.65	0.3
K	2.2	0.4
PAH	3.3	0.16
PAH ref.	3.3	0.8
L′	3.75	0.7
LN1	3.7	0.1
LN2	3.83	0.2
MN1	4.7	0.1
MN2	4.7	0.17
CVF 1	1.5–2.5 μm	$\lambda/\Delta\lambda$ ~ 50
CVF 2	2.5–4.5 μm	$\lambda/\Delta\lambda$ ~ 50

TABLE 2. *Sky and Telescope Emissivities*

Filter	Sky	Telescope
L′ (3.75 μm)	0.03	0.15
LN1 (3.7 μm)	0.007	0.16
MN1 (4.7 μm)	0.09	0.13

In assessing the telescope emissivity values it should be noted that the absolute minimum that could be expected is ~ 0.08 from the telescope mirrors, spider and adapter dichroic assuming the mirrors are clean. In addition, however, the 2.2-m telescope has a large central primary hole which could contribute up to ~ 0.08 additionally and which we have attempted to minimize by mounting a mirror, which views the cold camera, at the centre of the secondary. Given the uncertainties in estimating the individual sources of telescope emissivity, however, it appears that the measured values are consistent with assuming more realistic operational values for the mirrors and incomplete rejection of thermal radiation from the central obstruction without invoking additional unidentified sources. At the longest wavelengths, in the M band, the sky contribution becomes comparable to that of the telescope even in the narrow-band filter centred in the best part of the atmospheric window.

3.2 Sky chopping

The question as to whether or not sky chopping with array detectors is necessary in the thermal infrared and, if so, at what frequency, has become a much debated issue and one of particular importance for the design of the next-generation large telescopes where chopping the secondary mirrors presents a considerable technical challenge. Both to optimize the performance of IRAC1 at the 2.2-m and with an eye also to the VLT, we have investigated this aspect by measuring noise as a function of frequency in the L′(3.75 μm) band. The results are shown plotted in Figure 1 where the "high" frequency points were obtained with secondary-mirror chopping and the low-frequency ones by nodding the telescope and the total measurement time is the same at each frequency.

The result clearly shows a rapid decrease in noise with increasing chopping frequency up to ~ 2 Hz where it flattens
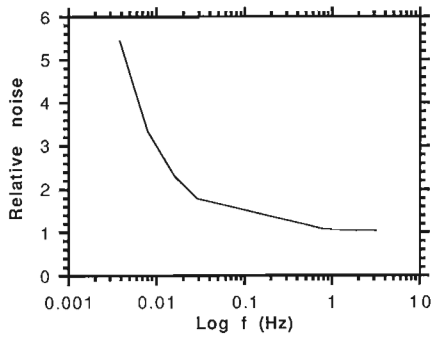
Figure 1: *Relative noise versus chopping frequency using the L'(3.75 μm) filter and the same total measurement time.*

off at the value to which this curve is normalized and which was found to correspond to the expected shot noise on the measured background. At this background level (which is very similar to that in MN1 also) the detector half full well capacity is reached in ~0.075 s so there is no conflict with the chopping requirement. At the much lower backgrounds experienced at wavelengths < 3 μm and when using the CVFs, however, it is necessary to utilize longer detector integration times (up to DIT ~60 s) together with telescope nodding or "dithering" every ~1 minute, rather than chopping to reach the backround limits.

3.3 Detection limits

Due to poor weather during the telescope tests, the performance could not be measured in all modes and the magnitude limits given below are therefore a mixture of directly measured and derived values as specified.

Table 3 summarizes the 3σ detection limits in the 3–5 μm range expressed as mag/sq. arcsec obtained in 2×60 s total measurement time. They are background limited and the values given were measured with a relatively high telescope temperature ~13 C. These are also worst-case values in the sense that the chopping amplitude was larger than the field, i.e the object integration time was only half the total measurement time. By chopping within the field and combining the images, these limits should be ~0.4 magnitude fainter. The values quoted are based on measurements with objective L4 and should be ~0.1 mag fainter in S3 based on their relative efficiencies. Extrapolation to other s/n ratios and integration times can be made assuming s/n $\alpha\, t^{1/2}$ where t is the total integration time.

Table 4 summarizes the 1–2.5 μm limits as defined above achievable using N_2 (dark-current-limited) and He (background/read-noise-limited) cooling. The IRAC2 limits have also been included for comparison.
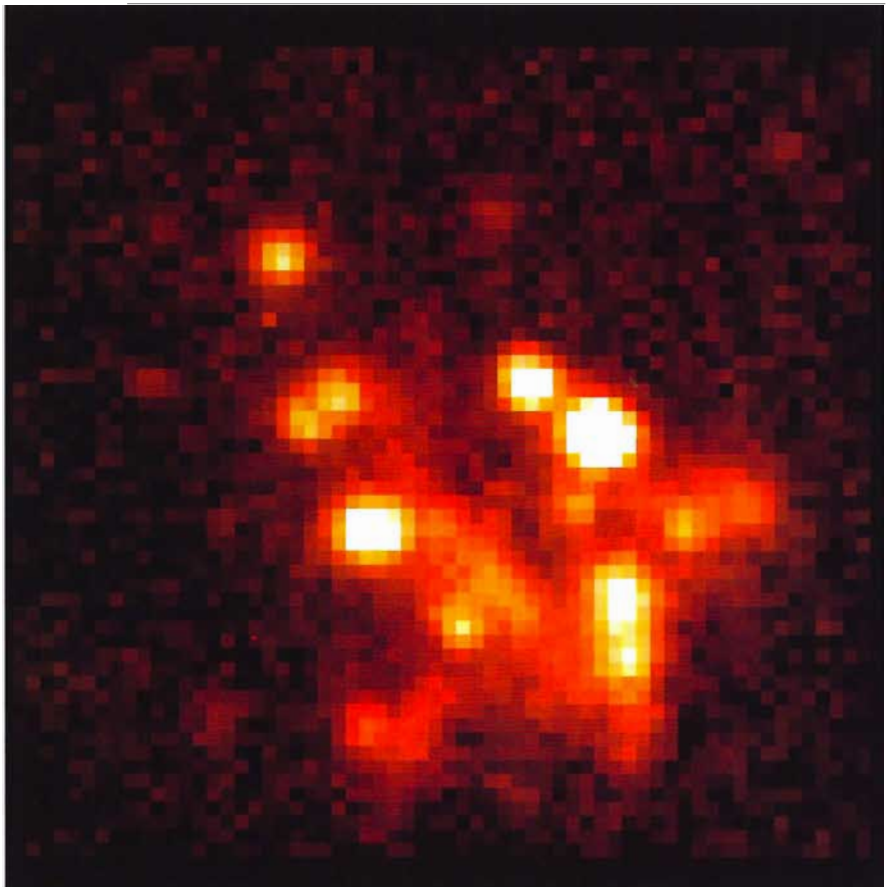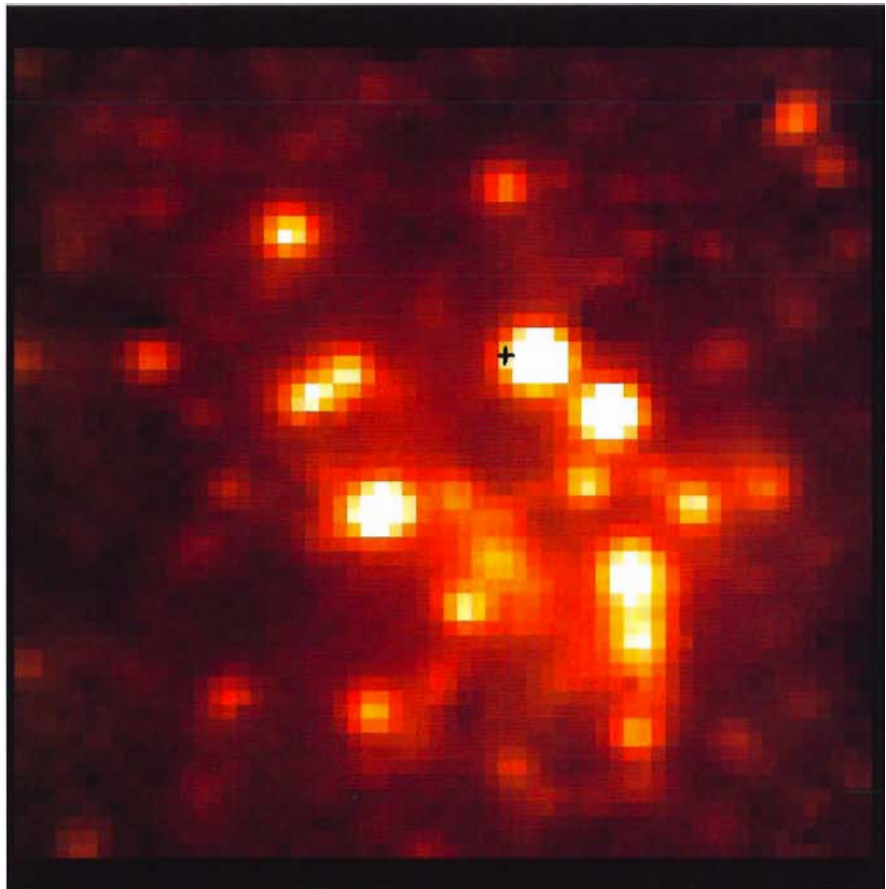

Figure 2: *Images of the Galactic centre in the L'(3.75 μm) (upper) and MN1(4.7 μm) bands obtained using sky chopping and a total measurement time of 2 minutes. The cross on the L' image just to the E of the brightest source marks the position of SgrA*. The relatively faint source to the N is IRS7 which is the brightest object in the region at 2 μm.*

9

TABLE 3. *3–5 μm Detection Limits (mag/sq. arcsec at s/n = 3 in 2 × 60 s)*

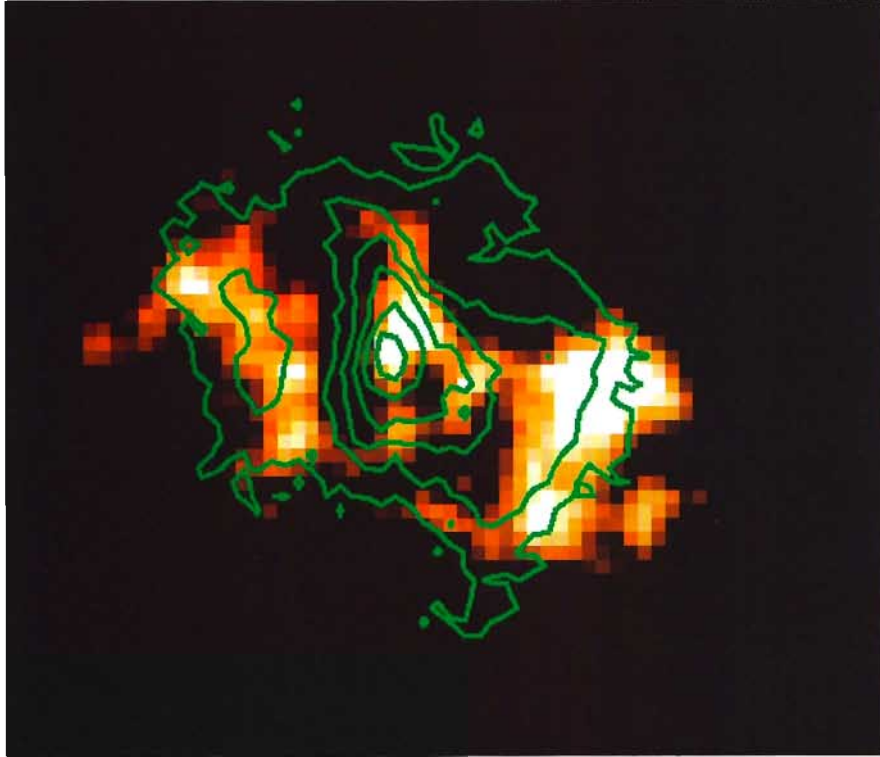| Filter	DIT (s)	NDIT	Cycles	Chopping	Mag/sq. arsec
L	0.075	2	2 × 400	yes	12.3
MN1	0.075	2	2 × 400	yes	9.5
PAH	0.075	2	2 × 400	yes	11
PAHREF	0.075	2	2 × 400	yes	12.5
CVF 3.28	3	2 × 20	1	no	11
CVF 4.05	1	2 × 60	1	no	10.3

Figure 3: *Image of the Galactic H II region G333.6-0.2 in the 3.28 μm PAH feature with Brα(4.05 μm) hydrogen recombination line contours superimposed. Both features were measured in DC mode using the CVF. The final images in each case were both sky subtracted and continuum subtracted using the mean of images measured on either side of the feature wavelength. Observation times at each CVF position were 60 s and 30 s respectively on both the object and sky positions. Of particular interest is the fact that the PAH feature emission appears brightest at the ionization front to the SW traced by the Brα emission.*

Figure 4: *L' (3.75 μm)-band image of the starburst ring in the nuclear region of the galaxy NGC 7552 using sky chopping and a total measurement time of 8 minutes. The spatially resolved bright spots correspond to particularly active star forming regions.*
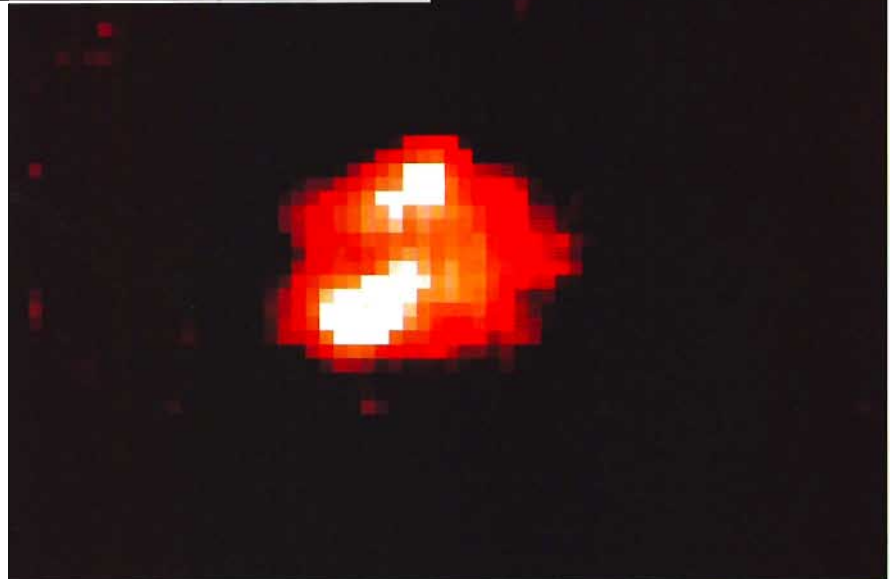
3.4 Saturation limits

The brightest objects observable depend on seeing and whether or not defocusing is allowed. As a guide, a point source with integrated magnitudes $\sim J = 2$, $H = 2$, $K = 1.5$ measured at the highest frame rate ~ 50 Hz should just

saturate in the brightest pixel assuming it contains 20 % of the light.

3.5 Sample images

Figures 2–4 show L' and MN1-band images of the Galactic centre; CVF images of the 3.28-μm PAH feature and Brα-line emission in G333.6-0.2 and an L'-band image of the starburst galaxy NGC 7552 which illustrate some of the main capabilities of IRAC1 in the thermal infrared. All images are oriented with N at the top and E to the left and have a scale of 0.45"/pixel. Additional specific information is given in the figure captions.

TABLE 4. *1–2.5 μm Detection Limits (mag/sq. arcsec at s/n = 3 in 2 × 60 s)*

Filter	mag/sq. arcsec (N_2)	mag/sq. arcsec (He)	mag/sq. arcsec
	Lens S3/L4	Lens S3/L4	IRAC2
J	17.3/16.7	19.2/18.8	20.5
H	17.2/16.6	18.6/18.4	19.2
K	16.7/16.1	17.8/17.6	18.3
CVF 1.6	14.5/14.0	16.9/16.3	
CVF 2.166	14.2/13.6	16.6/16.0	

> *With this periodically compiled collection of short notes, the NTT team intends to keep the community informed about changes in performances, configuration, and operation of the NTT and its subsystems.*

More Software Support

On June 16 and July 1, we could welcome Thanh Phan Duc and Marco Chiesa, respectively, as new members of the NTT Team. They are reinforcing our software development capacity and are working on the new control system for the NTT. With the beginning of the final implementation phase around the end of 1995, both Thanh and Marco will be transferred to La Silla.

First Field Tests of New Control System

In May, an important milestone was reached for the development of the VLT control system. For the first time, part of it has been tested with a working telescope. The objective was to use VLT-standard hardware, operating system, drivers, and the Local Control Common (LCC) Software to control the NTT enclosure (Work Components Nos. 1 and 2 of the NTT Upgrade Plan).
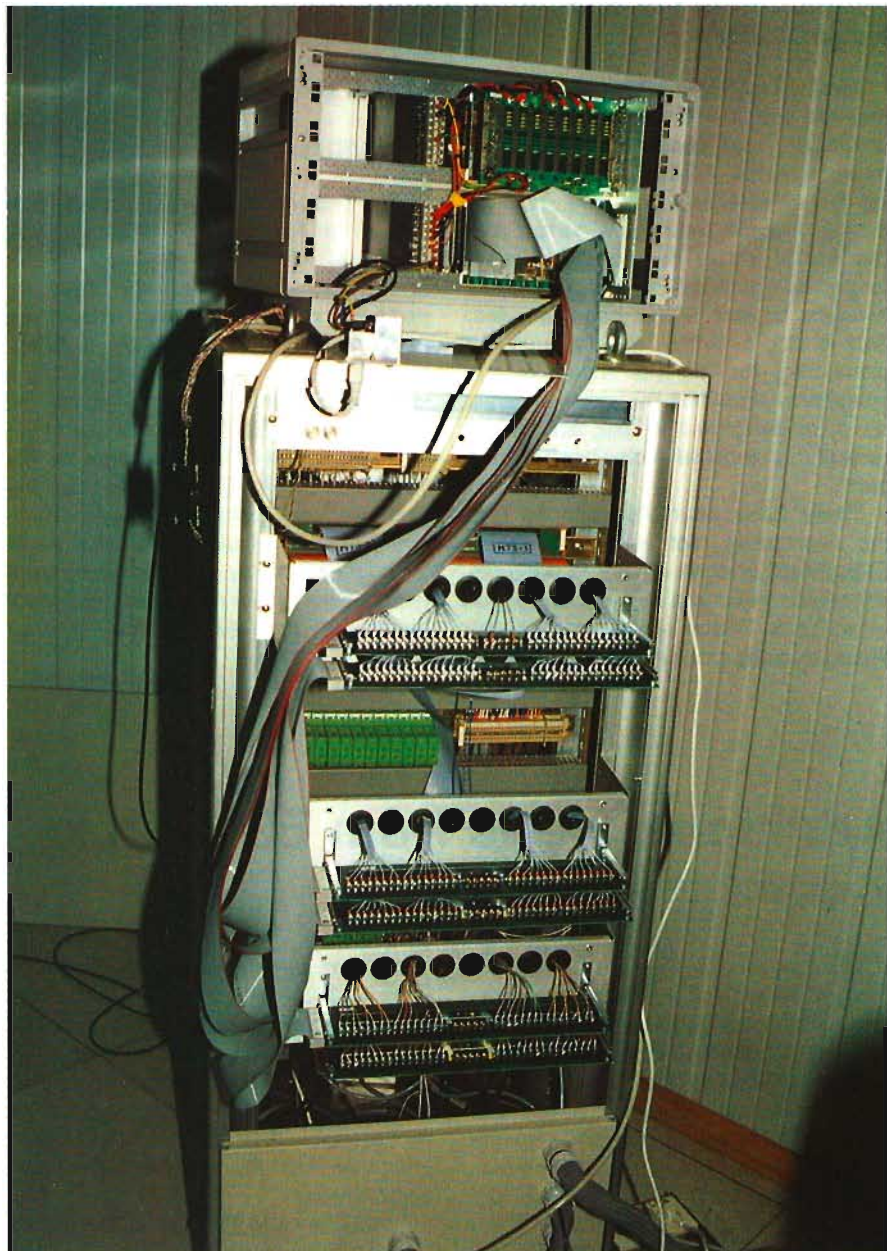
Figure 1 shows the VLT-type VME crate, with standard VLT VME boards, installed on top of the existing NTT enclosure cabinet. The field electronics have been connected to the new VME crate. Using standard VLT software and a new application developed for the NTT, the NTT enclosure functions were controlled and monitored from the LCC Engineering User Interface running on an HP700 workstation. Some early experiments could also be made with a pre-release version of the VLT Central Control Software (CCS).

The installation went so smoothly that major parts of the three nights allocated to the tests could be used for the taking of further calibration data for EMMI. The NTT enclosure application has been adopted as an example of an LCU application by the VLT Software Group and is being distributed together with the VLT Software Release 1 to VLT consortia and contractors. The complete test report is available by anonymous ftp from *ftphost.hq.eso.org* in file `./pub/NTT/testReportWC1.ps`. Tests of Work Components Nos. 3 (M2 and M3), 4 (autoguider and adapter), and 5 (hydraulics/console) are scheduled for October 1994, February, and March 1995, respectively.

Improved Pointing Models

New pointing models have been established for both foci. On side A (IRSPEC, SUSI) the all-sky rms is 1.1 arcsec. On side B it was found to be as low as 0.85 arcsec and stable over at least one month. This is comparable to the results obtained at the time of commissioning.

The most critical zone for any telescope with alt-az mounting is around the zenith where the telescope turns around very quickly during the meridian passage of the objects. At the moment the pointing is not yet as good here as over the rest of the sky. Extensions of the present pointing models to this region will be attempted in August with a special measuring technique.

Using the NTT as a testbed for the VLT control system. The VLT-type VME crate, with standard VLT VME boards, installed on top of the existing NTT enclosure cabinet.

Tracking of Moving Targets

Special efforts were undertaken to better support the tracking of moving targets. In autoguiding mode, the guideprobe was stepwise offset as to compensate for the differential motion of the target. But because there is no servo in the control loop, the errors tended to accumulate with time. On the other hand, the improvement of the pointing model automatically enhanced the tracking accuracy (both functions use one and the same software), and it was concluded that within certain limits the freely tracking telescope would in this case give a better performance. A special pointing model was built, therefore, to enable observations of the impact of comet SL-9 on Jupiter down to elevations of just 10 degrees (with an rms of 1.7 arcsec).

Image Quality

A careful mapping of the field astigmatism has been performed on side B. The results are very consistent with similar measurements obtained on side A during the commissioning period. This indicates that the results are correct and that the NTT has been stable over a long period of time. The image analysis software for side B has been updated. This is also a further step towards implementing the parallel mode of the image analysis where the image analysis has to be performed off-axis. Successful tests of this mode have also been carried out.

There have been suggestions that the elongation sometimes seen in EMMI/SUSI images is due to astigmatism. A more in-depth analysis kindly provided by R. Wilson shows that for any plausible assumptions field astigmatism

cannot explain this effect, even if not corrected at all. Additional tests will be made in August.

IRSPEC

Following the solution (by B. Gilli) last year of a problem with the recovery from synchronization losses of the various real-time VME nodes controlled by the NTT computer, the operation of IRSPEC has now been very smooth for several months. Especially beam switching has no longer been a nightmare.

Even better news is that the software to transfer IRSPEC data directly to the workstation is now almost ready to use. There, the data can be reduced with the IRSPEC package in MIDAS. A graphical user interface to this package has been developed by C. Levín and is now being offered on an experimental basis.

The manual was updated a few months ago. It is offered via anonymous ftp only (node ftp.hq.eso.org, subdirectory pub/NTT.

EMMI/SUSI

The Optical Detector Group has performed a full test of CCD No. 36 (red arm of EMMI); No. 25 (SUSI) is scheduled for August. Test reports are available via anonymous ftp from node lw5.ls.eso.org, subdirectory pub/CCD/new_noise_tests. It is recommended to always check file /pub/CCD/README first because structure and scope of the database are not yet final. CCD No. 31 (blue arm of EMMI) was this year tested only partly. However, the control electronics was carefully fine-tuned by P. Sinclaire, which resulted in a further reduction of the read-noise level from 6.6 to 4.3 e⁻ in slow mode.

Following a design by T. Abbott, R. Warmels has implemented a set of MIDAS commands which will enable Visiting Astronomers to evaluate CCD test data at the telescope or their home institutes. It is expected that after further testing, this software will be distributed with the 94NOV release of MIDAS as an extension of the present CCD reduction package. In addition, the EMMI/SUSI control software has been modified such that sets of exposure definitions can be saved to and restored from disk. This should also facilitate the taking of test data by Visiting Astronomers according to a fixed standard. For the same purpose a LED assembly was prepared by S. Deiries which should eventually replace the radioactive β lights as stable standard light sources.

A new, intermediate version of the EMMI/SUSI manual can be requested from the Visiting Astronomers Section in Garching (visas@eso.org).

More Disk Space and Computing Power for Observers

With the advent of the 2k×2k CCDs at the NTT, many observers have strongly felt the shortage of disk space. The computer group at La Silla has now installed a new 4 Gbyte SCSI-2 disk which triples the previous capacity. A further increase to 6 Gbytes is envisaged. For the same reason, the computer group at La Silla replaced the Sun Sparc 10 workstation with an HP 735 workstation with 96 Mbytes of RAM. This gives significantly improved throughput, especially for operations involving several large frames.

Because especially in the afternoon observers and technical staff were competing for the keyboard and screen of the workstation, an additional X-terminal has been installed for the technical staff.

Additional News from ESO-Chile

J. MELNICK, ESO-La Silla

The weekend of August 19 was extremely hectic on La Silla. The movers arrived to transport the material of the Astronomy Support Department to our new base in the Vitacura office. The computer network had previously been divided into two subnets, both of which were kept running for about 10 days before the move. Then the Santiago subnet was disconnected and packed for Santiago. Thus, computer service was maintained with minimal interruption throughout the process. Service was started in Santiago

about one week after the material was unpacked, a mere 10 days after packing started on the mountain, and in fact much of the delay was due to the upgrade of the Sun Servers from Sparc10 to Sparc20. I would like to congratulate our two systems managers, Cristián Levin and José Méndez for this remarkable achievement!

The library was also moved in a record time. Packing started on August 18, and the library was ready in Vitacura on August 25. The initiation of activities on

Vitacura was celebrated that day with a cocktail offered by the Director General and attended by ESO staff and Chilean scientists and educational authorities. Congratulations to our librarian, Maria Eugenia Gómez, for this success.

The Santiago-Based Model

For already more than one year before the move we had been experimenting and fine-tuning the so-called Santiago-based model. This means that science

operations on the mountain are handled by a multi-disciplinary team, the *Telescope Team*, composed of astronomers, operations staff, systems managers, and night assistants, who from Tuesday to Tuesday are on duty. Astronomers are on duty one week every three. The rest of the time is used for compensatory leave and scientific research.

La Silla and Vitacura are linked with a dedicated 64 k digital line which carries computer communications and two voice channels. Thus, any telephone in the Santiago base can be reached by dialling a code and the extension (just like the tie line from La Silla and Garching). The computer network is in fact one network divided into two subnets, and computer communications between the two sites are remarkably fluid. We expect to upgrade the link to 256 k in order to accommodate multi-media communications.

We are pleased to report that, with the exception of changes in the Library, visiting astronomers have hardly noticed the change!

The Library

The Library from La Silla was almost completely moved to Vitacura (with the exception of some engineering books and journals), and the Library in the old ESO office in La Serena was moved to La Silla. Thus, while the Library on La Silla now contains most journal collections, most colloquia and symposia series, all catalogues, and about 1000 books, it is still not as complete as the old Library.

The reduced Library contains most of what we consider to be necessary to support observers on the mountain. We are aware, however, that for some requirements this may not be enough and, starting in October, together with the end-of-mission reports, observers will be kindly asked to fill a questionnaire concerning the Library which we will use, to decide on the purchase of books, journals and collections deemed necessary on the mountain by a significant number of observers.

Seminars

The traditional seminars will from now on take place in Santiago. We hope that our colleagues coming to observe at La Silla will continue to be so generous with their time, and agree to give talks in Santiago, and all visiting astronomers are strongly encouraged to come to the office on the way to or from La Silla to talk about science, attend the seminars, check their e-mail, discuss the instrumentation, or simply to say hello!

Computers

The computer systems on Vitacura and La Silla are actually very similar. Both are X-terminal nets served by 2 SparcServers each. There is plenty of disk space at both places to allow efficient data reduction by staff and visitors. The number of X-terminals in the La Silla computer room has also been increased to provide off-line computing services for visiting astronomers. The workstations at the telescopes are being upgraded to HP735 and equipped with about 4 Gby of disk to be used for on-line data reduction. At the beginning of next year the off-line nets will be upgraded by increasing substantially the computing and disk-storage capacity. Visiting astronomers who have a gap between observing runs may think of spending some of that time at Vitacura reducing their data.

3.6-m Seeing Improvement Programme

We are still struggling with the Air Conditioning system (AirCo). The tests we have done so far show that under most conditions it should be possible to eliminate most of the dome seeing if we operate the AirCo properly. So far, these tests have been done thanks to the co-operation of visiting astronomers on "stolen" time. A number of nights have been scheduled for the next period which should allow us to reach firm conclusions and develop an operational scheme for the system.

Globular Clusters with the VLT

F. FUSI PECCI, C. CACCIARI and F.R. FERRARO, Osservatorio Astronomico di Bologna, Italy
R. GRATTON, Osservatorio Astronomico di Padova, Italy
L. ORIGLIA, Osservatorio Astronomico di Torino, Pino Torinese, Italy

1. Introduction

Globular clusters are the best example of a "simple" stellar population, i.e. a group of stars with the same age and chemical composition (with a few exceptions) where the only varying parameter is mass. Therefore, they are ideal laboratories to study stellar astrophysical problems such as the evolution of Population II stars and the phenomena related to the environmental conditions (e.g. internal cluster dynamics, binary formation and evolution, star interactions, captures, mergers, X-ray sources, pulsars, etc.). Moreover, considering their integrated properties, they can be used as test particles to study the formation, evolution and dynamics, and the stellar populations of the parent galaxies.

Given the extent of the subject and its possible connections to many astrophysical fields, we shall present and discuss briefly only some topics of major scientific interest involving globular clusters, with some evaluation on the most efficient telescope/instrument combination to reach the desired results. The telescopes we have considered are the 4-m-class (NTT-like), 8-m-class (VLT-like), HST and ISO. The specific cases where the VLT is the best choice with respect to the other telescopes will be treated in some more detail, and the most suitable instruments will be suggested.

2. Cosmological Tests

Cosmological models can be tested using two main aspects of globular cluster properties, namely absolute ages which are related to the age of the universe, and dark matter content which is related to the baryonic matter in the universe.

2.1 Absolute ages

Globular clusters (GC) are nearly the first objects that formed at the time of the galaxy formation. The oldest metal-poor clusters set thus a lower limit to the age of the universe. The better the accuracy of globular cluster dating, the more stringent will be the cosmological implications. In the Colour-Magnitude Diagram (CMD), the optimal *clock* is the Main Sequence (MS) turn-off (TO). The absolute age of a globular cluster is obtained by linking the TO observable parameters (i.e. magnitude and colours) to the corresponding quantities (i.e. luminosity and temperature) in the theoretical isochrone with the same chemical composition. Since stellar clocks are intrinsically based on stellar models, the *verification* of the validity of these models is both *complementary* and *necessary* to any dating procedure.

A few rough estimates may be useful before proceeding. Assuming an absolute age of 15 Gyr, an uncertainty of ± 1 Gyr is given formally by an error of 0.07 mag in the TO luminosity, or 0.30 dex in the metallicity [m/H], or 0.03 dex in the helium content Y.

The errors currently obtained on TO absolute luminosity (~ 0.2 mag), metallicity (~ 0.2 dex), and helium abundance (~ 0.02) lead to an error on the absolute age not smaller than 3 Gyr.

Therefore the problem, from the observational point of view, is four-fold:
• Test the evolutionary models (assumptions, input physics, approximations, etc.) to ensure a proper *clock running*. See Section 4 which is devoted to the discussion of this item.
• Derive the TO apparent magnitude and colour as accurately as possible from the observations, to ensure a proper *clock reading*. The TO luminosity level is a quantity of intrinsically difficult sharp definition, as the TO region is almost vertical in the V-(B-V) plane. Alternative filter combinations should probably be devised. The required photometric accuracy (~ 0.01–0.02 mag for the individual stars at the TO) can be obtained if the observations reach at least 2–3 mag below the TO (V $\sim$ 20–27, depending on the cluster distance).

This can already be done with good CCD equipment and 4-m-class telescopes on sufficiently well-populated external zones of the clusters.
• Estimate accurate chemical abundances (not only overall metallicity, [m/H], and helium abundance, Y, but also the relative abundances of elements such as Fe,C,N,O, etc. which are very important for the determination of the correct theoretical model), with an accuracy of at least 0.1 dex. The bright red giant branch (RGB) stars can be used for this purpose, although some tests to verify that these abundances do not differ from those of the MS stars are recommended. The spectroscopic observations of the RGB stars can be obtained with 4-m-class telescopes, the MS stars are much fainter (V > 17) and require the use of an 8-m-class telescope and high-resolution spectrographs (MFAS, UVES).
• Estimate accurate distances to the clusters, as the *absolute* magnitude of the TO is needed to determine the age. This relies upon the use of various types of "standard candles", for example:

– The RR Lyrae variables. Absolute magnitudes can be obtained using the Baade-Wesselink method which requires accurate V(RI)K light and radial velocity curves. The accuracy presently attained on individual field stars is about 0.15 mag using 1.5-m telescopes with CORAVEL and 1-m telescopes for the photometry (Cacciari *et al.* 1992). A few stars in three among the nearest GCs have been analysed with considerable better accuracy. This programme is feasible with 4-m-class telescopes, and by averaging the results on several stars in a cluster, a sufficiently high *internal* accuracy can be obtained.

– The HB luminosity level, applied to globular clusters in M31. Given the large distance to M31, its globular clusters can be considered all at the same distance. Therefore, the apparent magnitude level of the HBs as a function of metallicity provides directly the slope of the HB luminosity-metallicity relation, whereas the zero-point of this relation has to be set by other methods (see above). This needs accurate photometry (~ 0.1 mag) of individual stars at V = 25–26 in crowded fields where the spatial resolution is essential. The HST is presently the only instrument capable of this performance.

– The RGB tip. This method needs accurate and complete luminosity functions of all bright stars ($M_V \sim -3$, V $\sim$ 10–17) in very populous clusters to reduce the impact of statistical fluctuations. It can be done with small/medium-size telescopes.

– The field subdwarfs with known accurate parallaxes (e.g. from Hipparcos) and metallicity determinations. These stars are used to match the MS stars in a globular cluster with the same metallicity, and thus derive their absolute magnitudes. All the necessary photometric and spectroscopic observations can be done with small/medium-size telescopes.

– The White Dwarfs (WDs). According to theoretical predictions (Fusi Pecci and Renzini 1979, Renzini 1985) the WD cooling sequence is well defined in the $\log L$–$\log T_e$ plane (to within $\pm$ 0.03 mag) and could be used in Galactic GC distance determination. Since very accurate photometry and medium-low resolution spectroscopy (to confirm the WD nature and to distinguish between DA and DB types) of very faint stars is needed, the use of an 8-m-class telescope is required. However, the very high space resolution and the possibility to observe in the UV wavelength range make HST a better suited instrument for this purpose. Nonetheless, the VLT can be used profitably on certain aspects of this programme (e.g. spectroscopy), and also to search for WD candidates in the more external regions.

As an example, for a WD star at approximately 25,000° K ($M_V \sim 10$ $\Rightarrow m_V \sim 23$–30) an error in the temperature of 1000°K (corresponding to $\Delta(1800$-V$) = 0.078$, Δ(U-B)$ = 0.025$ and Δ(B-V)$ = 0.005$) produces an error in the absolute bolometric magnitude of 0.234 mag. Accurate UV photometry of many very faint stars is therefore very important in order to define a reliable distance modulus. To avoid using UV data, not accessible from the ground, one can try to detect and measure cooler WDs, which are however fainter (a temperature difference of 10,000°K corresponds to a magnitude difference of about 1.5 mag). At magnitudes $m_V \sim 25$–32 the same error in temperature and luminosity as above corresponds to photometric errors Δ(U-B)$ = 0.06$ and Δ(B-V)$ = 0.02$, and by observing 10–20 WDs significant results can be obtained. The major problems will be crowding and field decontamination, and a sufficiently wide population sampling.

• *GC Peak Luminosity Function*

Some further impact of the GCs on the distance-scale determination is offered by the study of globular clusters in external galaxies (after proper calibration on Local Group clusters). This method does not intend to find the distance and age of globular clusters, but uses the brightest globular clusters as standard candles to derive the distance to external galaxies. The zero-level assumption is that the Luminosity Functions (LFs) of GCs are described by the same law everywhere or,

at least, that it is possibile to know in detail how the LFs vary with varying galaxy morphological types and masses.

This method needs very deep imaging over quite large fields for magnitudes and colours (and possibly photometric metallicity indices), and medium-low resolution spectroscopy for testing the GC nature and membership and for abundance determinations. Depending on how far one wants to reach (M81, NGC 5128, Virgo, etc.), a transition from 4-m-class telescopes to HST is necessary for imaging. Similarly, 8-m-class telescopes with MOS capability are necessary for an effective spectroscopic investigation (MFAS, FORS).

2.2 Very Low Mass (VLM) stars, Brown Dwarfs (BD) and dark matter

Many candidates exist for baryonic dark matter, with masses ranging from black holes down to comets. Among the most popular candidates are the stars at the low-mass end of the Initial Mass Function (IMF). These degenerate dwarfs are commonly roughly divided into two sub-groups, i.e. the very low mass stars (VLM) above the hydrogen-burning limit (~ 0.08 M$_\odot$), and the brown dwarfs (BD) with M < 0.08 M$_\odot$.

The latest results on microlensing of LMC stars presented by Alcock et al. (1993) and Aubourg et al. (1993) add support to the existence and importance of these very low luminosity degenerate objects. However, to provide a significant quantity of baryonic dark matter to the Galactic halo, a steepening of the IMF slope at very faint limits, well into the VLM and BD regions, is absolutely necessary.

The main challenging problems are (a) constructing a statistically complete and uncontaminated sample of these very faint stars, (b) transforming the observed MS Luminosity Function into a Present-Day Mass Function (PDMF) via a theoretical mass-luminosity relation and known bolometric corrections, and (c) understanding the relationship between the PDMF and the IMF.

Globular clusters offer the environment where a sufficiently homogeneous group of VLM and BD objects could still live unless dynamical evolution and stripping have totally depleted the clusters. Though the clusters' low metallicity makes the VLM and BD brighter than expected in the solar neighbourhood and in the Galactic disk, these objects in the typical Galactic globulars (even in the closest ones) are very faint, V > 25–27, and securing statistically complete and uncontaminated LFs is extremely difficult with the available tools.

By measuring deep I-band LFs in six GCs, Fahlman et al. (1989) and Richer et al. (1991) have claimed that most GCs probably have very steep IMFs (slope $x > 2.5$, with Salpeter IMF $x = 2.35$), implying a large number of low-mass Pop II stars in the halo. On the other hand, Piotto and collaborators (see Piotto 1993) have found that the PDMFs measured in the mass range $0.5 <$ M/M$_\odot$ < 0.8 in about 20 GGCs correlate with position in the Galaxy.

Recently, Paresce et al. (1994) using deep HST-WFPC2 images have obtained the LF for the MS of NGC 6397 down to $m_I \sim 25$. Their corresponding PDMF rises to a plateau between ~ 0.25 and ~ 0.15 M$_\odot$, but drops towards the expected mass limit of the hydrogen-burning MS at about 0.1 M$_\odot$. As they note, this result is in clear contrast to that obtained from the ground for the same cluster by Fahlman et al. (1989) and may alter strongly the possible implications on dark matter problems.

According to the Wide Field Direct Visual Camera specifications (Wampler 1994), this imager at the VLT would be capable of providing a space resolution of 0.1 arcsec FWHM (almost comparable with HST), a larger field of view and 10 times the HST collecting area. Assuming the limiting magnitude I ~ 28.5 (for S/N ~ 2 in 10 hours) one could for instance extend the LF obtained in NGC 6397 by Paresce et al. (1994) by at least two magnitudes.

On the other hand, VLMs and BDs have high density and cool atmospheres ($T_{eff} < 3000$°K) dominated by H$_2$ molecules, hence they emit predominantly in the red and IR bands. Both ISAAC and NIRMOS would thus be most suitable for both detection and low-resolution spectroscopy of very faint candidates. For example, NIRMOS can provide unique LFs as faint as J = 25 and H = 24 with S/N = 10 in 1 hour with pixel scale 0.3 arcsec, and also low-resolution spectroscopy (R = 200) for candidates as faint as J = 22 and H = 21 with S/N = 10 in 4 hours (Le Fèvre 1994).

3. Tests of Galactic Formation and Evolution

The various models of galactic formation and chemical evolution (see Majewski 1993 for references) can be tested by investigating three main aspects of the globular cluster system, namely: (i) the age spread, (ii) the relation between location within the Milky Way, kinematics, dynamics, metallicity and age, which provides also the galaxy total mass and its distribution out to distances of ~ 100 Kpc, and (iii) the abundance ratios, which are a signature of the initial chemical composition of the protocluster stars and

hence of their origin. This can be done by studying an adequate sample of individual stars in each cluster to derive the average properties of the cluster itself, or by investigating the integrated properties directly.

Globular clusters in our own Galaxy (GGCs) and in the other galaxies of the Local Group (including the dwarf spheroidals) represent the best template stellar populations for this purpose, as they cover the requested wide range in ages and metallicities, provided they can be assumed as reliable representatives of the halo and bulge stellar population. A similar complementary approach has to be pursued with field stars, but we shall not discuss them here.

3.1 Age spread and the HB "second parameter" problem

In order to distinguish between different models of galaxy formation, an accuracy not worse than $\pm$ 0.5 Gyr is necessary in the *relative* ages (coupled with complementary data on abundances and kinematics). Relative ages with respect to a given reference cluster can be derived more easily and accurately than absolute ages, after proper calibration of suitable photometric and spectroscopic features.

In a resolved cluster, the two basic methods presently used are the so-called *vertical method*, which measures the magnitude difference ΔV_{HB}^{TO} between the Turnoff (TO) and the Horizontal Branch (HB) (see Buonanno *et al.* 1989, Sandage and Cacciari 1990), and the *horizontal method*, based on the colour difference between the TO and the RGB (VandenBerg *et al.* 1990, Sarajedini and Demarque 1990). To achieve the error in age of $\pm$ 0.5 Gyr, the errors in magnitudes and colours must be smaller than 0.03–0.04 mag and 0.01 mag, respectively. The chemical abundances must be known at the level of accuracy requested for the absolute age determination. These requirements can be met using (V,B-V) or (V,V-I) photometry and spectroscopy, both currently feasible with 4-m-class telescopes for most of the galactic halo and Magellanic Cloud GCs. Globular clusters in the bulge, however, need IR (K,V-K or K,J-K) observations because of the very large extinction in that region of the Galaxy, and 8-m-class telescopes are necessary to obtain accurate magnitudes at least 2–3 mag fainter than the TO (K(TO) $\geq$ 16) and properly define the unevolved MS. Moreover, since the required space resolution is very high, Adaptive Optics techniques are crucial. The scheduled VLT instruments ISAAC and CONICA, equipped with large-format arrays and AO facility, can satisfy these requirements, al-

lowing deep and both high (for the central regions) and medium (for the external zones) space resolution imaging in various near-IR filters.

In non-resolved clusters, ages could be estimated by means of integrated colours and spectroscopic indices, after proper calibration on the local template clusters, for which age and metallicity are known. For the clusters in M31, where the TO region for direct age estimate is not accessible even to HST, a multiobject spectrograph on a 4-m-class telescope is sufficient for the purpose. For more distant clusters, FORS and MFAS on the VLT are the ideal instruments thanks to the size of the field of view, the number of slits or fibers, and the spectral resolution.

The use of the VLT opens a new window to this type of studies as deep imaging and spectroscopy can be extended into the IR. In fact, in the near-IR region there are many interesting stellar absorption features due to atomic (neutral metals such as Si, Mg, Al, etc.) and molecular (CO, OH, H_2O, CN, etc.) species which are very sensitive to the variation of the fundamental stellar parameters of cool stars. In fact, young stellar systems are characterized by the presence of cool and red M supergiants, while in older stellar populations the integrated luminosity is dominated by less massive and hotter giants.

For this purpose an 8-m-class telescope is necessary to take IR spectroscopy at different resolving powers (depending on the intrinsic broadening of the selected atomic and molecular lines) of a complete sample of globular clusters in our Galaxy and in the Local Group. Only the $\sim$ 20 brightest clusters both in our Galaxy and in the Magellanic Clouds are presently observable in the IR at medium-low resolution with a 4-m telescope, having K < 16 mag per square arcsec. An instrument like ISAAC can provide these fundamental data. A multifiber imager-spectrometer (like NIRMOS) is crucial, especially to observe globular cluster systems in the Local Group galaxies, which are spatially separated by a few tens of arcsec, depending on the galaxy distance.

Another possible approach to deal with relative characteristics between GGCs is to study their HB morphologies, in particular the so-called "HB second parameter effect", i.e. the occurrence of extremely blue or red HBs in clusters having the same (intermediate) metallicity.

In the Galaxy the "second parameter" morphology seems to be related with the Galactocentric distance (Zinn 1986). Differences in age up to 3–5 Gyr have been detected among globular clusters (see Buonanno *et al.* 1994, for references), and age is presently the most favoured second parameter candidate. However,

the dynamical and structural conditions of the clusters (stellar density, concentration, kinematics, etc. see Section 4) could play a rôle (Fusi Pecci *et al.* 1993).

HBs in GGCs are sufficiently bright (including the faintest part of the extended BHB) to allow very accurate photometry with medium-size telescopes (apart from the highly crowded central regions which require the use of HST). As mentioned below, spectroscopic measurements necessary to disentangle basic evolutionary problems related to HB stars require very high resolution, hence the use of the VLT.

Photometry of HBs in the Magellanic Clouds and in the Fornax dSph galaxy is also feasible with 4-m-class telescopes, and would possibly need HST only in order to achieve sufficient space resolution in the central regions. Useful spectroscopy of individual HB stars in the MCs and beyond, however, cannot be done without 8-m-class telescopes and instruments like FORS, MFAS, NIRMOS, etc. to yield abundances and velocities as accurate as those presently obtained in the Galactic GCs.

For the globular clusters in M31 and beyond, the use of HST or of the VLT with highly sophisticated Adaptive Optics devices is indispensable to detect individual HB stars because of the faintness of the stars and the spatial resolution necessary to resolve them.

In unresolved clusters the best (possibly only?) way to detect "second parameter" HB morphologies is probably in the UV (with HST), after proper calibration with local clusters, but there are problems with the possible dominant impact of just a few UV-bright stars. Useful information on the HB morphologies can be obtained also using visual and near IR photometry (UVK) once the metallicity effects have been estimated with low resolution spectroscopy in the red,
where the major contribution is due to cool stars.

3.2 Dynamics of the GC system and the parent-galaxy total mass

The necessary data for a comprehensive study of the dynamics and kinematics of the GC system are radial velocities, spatial motions and knowledge of orbit type and possible interactions with the parent galaxy. In turn, globular clusters themselves can be used as test particles to study the radial mass distribution and the total mass of the parent galaxy.

For the Galactic GCs, radial velocities can be obtained with the highest accuracy from the analysis of a large number of individual cluster stars, and the use of 4-m-class telescopes is adequate to this purpose. Obtaining space motions

and orbital shapes is however the crucial item. According to the latest estimates (Tinney, 1994) important progress can be made using CCD devices and 8-m-class telescopes, as accurate proper motions could be obtained using a relatively short baseline (5–10 years).

Spectroscopic observations of extragalactic cluster candidates in very distant galaxies require typical integration times of several hours per cluster. In addition, since clusters beyond ~ 2 Mpc can hardly be distinguished from foreground stars and background galaxies, the observing efficiency will be considerably lowered by the contamination from spurious objects. The use of Multi Object Spectroscopy on the VLT is therefore essential to make these programmes feasible and efficient.

3.3 Chemical abundances and abundance ratios

The surface composition of unevolved stars reflects that of the ISM at the epoch of their formation. Therefore, in a simple, closed-box model of the galactic chemical evolution, the element-to-element abundance ratios are determined by the interplay between the timescales of star formation and evolution, because the yields of production of different elements are a function of stellar mass. Since the star formation rate is usually related to the density of the ISM from which the stars form, it is important to study stars at various locations corresponding to different densities of the ISM, in particular in the galactic halo and bulge. Since globular clusters as such do not play a specific rôle in this issue, we refer the interested reader for instance to Larson (1974), Gratton and Sneden (1989) and McWilliam and Rich (1994) for the latest results.

4. Stellar Evolution Tests

Globular clusters in the Galaxy or in the MCs where different age-metallicity combinations can be found, are excellent laboratories to test the assumptions and results of the stellar evolution theory. Many basic quantities (e.g. age, primordial helium abundance, etc.) can be determined once the model validity is verified and guaranteed (see for discussion and references Renzini and Fusi Pecci 1988, Chiosi et al. 1992). Some of these tests use photometric techniques on relatively bright stars (e.g. luminosity functions of post-MS stars) and can be carried out satisfactorily with 4-m-class telescopes (or HST if high space resolution is required). Other tests, which are based on high-resolution spectroscopy of bright and faint stars, are more relevant for the present discussion.

4.1 Spectroscopic tests of stellar evolution

The original surface composition of stars is altered during their evolution by various mechanisms. Therefore, the study of abundances of stars in different stages of their evolution, but likely with the same original composition, provide basic and sensitive tests of stellar evolution. We will now consider separately different phenomena which have been observed, or are likely to be important, for old (small-mass) stars and which can be excellent programmes for an 8-m-class telescope.

● Diffusion and Lithium abundances in main-sequence and turn-off stars

Diffusion on the Main-Sequence may affect the abundance of Li for stars in the Turn-Off region of globular clusters. Li abundance in metal-poor stars provides a basic constraint on cosmological models. A significant fraction of the present Li may have been formed during the Big Bang; once this fraction is determined, it should severely constrain the baryonic density in the universe.

In this respect, a very important result was achieved by Spite et al. (1984), who found a constant Li content (LogN(Li) = 2.05 ± 0.2) among a large group of unevolved, metal-poor, old stars, that is likely to be the Big Bang signature. However, Li is manufactured also by other processes: the most important contribution is spallation by cosmic rays on interstellar grains, but a significant fraction may come from intermediate-mass stars during their AGB phase. On the other hand, Li is easily destroyed in stars and a careful discussion of these mechanisms (which depend on details in the internal structure of MS and TO stars) requires a comparison with stars having an appropriate range in mass, ages, metallicity, and luminosity. Stars in globular clusters are thus very important, since these parameters are known with much better accuracy than for field stars.

A determination of the Li abundance for a star at the turn-off of NGC 6397 (the closest cluster, V(TO) $\sim$ 16) has been obtained recently by Pasquini and Molaro (1994) using EMMI at the ESO NTT. However, these observations (R = 28,000, 4×90 min) are clearly at the limit of a 4-m-class telescope's possibilities, and a systematic study of stars of different luminosity in various clusters can only be done using an 8-m-class telescope. UVES at the VLT is very well suited for these studies.

● Mixing and environment

Dredge up of CNO-processed material is expected to occur in GC stars at the base of the RGB (first dredge up) and perhaps during the latest stages of AGB evolution (third dredge up). Classical theory predicts a moderate mixing (with depletion of ^{12}C, and enhancement of the surface abundances of ^{13}C and ^{14}N) during the first dredge up (Vanden-Berg and Smith 1988). No alteration is predicted for other observed elements, including O, Na and Al.

These predictions are generally rather well satisfied for most metal-poor field stars, which show a well-defined trend of C and N abundances and isotopic ratios with luminosity, and no clear indication of O depletion. The low $^{12}C/^{13}C$ ratios observed in the brightest field halo giants could be explained by a slightly more severe mixing, which could be due to meridional circulation activated by core rotation (Sweigart and Mengel 1979). The only rare exceptions (Ba stars, CH stars, N-rich dwarfs) can probably be explained by pollution from an evolved companion, presently a white dwarf; Ba stars and CH stars are in fact known to be members of spectroscopic binary systems.

Observations of stars in GGCs show a far more complex picture (Smith 1987). Only in a few clusters (like M92 and NGC 6397) there is a quite good correlation of C and N abundances with star luminosity; in most clusters stars with weak and strong CN bands (both sharing a similar fraction of the overall population and sometimes exhibiting bimodal distributions in CN band strengths) stand side-by-side in all regions of the CMD, even at the TO level. These anomalies are correlated with variations of strength of the O, Na and Al lines: there is a clear anticorrelation between O and Na overabundances (Kraft et al. 1992), while the sum of CNO abundances is probably constant. Finally, several authors found very low $^{12}C/^{13}C$ ratios.

There are strong indications that a dense environment plays an important rôle in causing these anomalies: however, the responsible mechanism has not been identified yet, candidates being enhanced core rotation (perhaps due to close encounters between protostars), pollution by (possibly temporary) companions or even by other cluster members, and/or some still unknown mechanism (mixing?) at work during evolution.

The dependence of these mechanisms on evolutionary phases and cluster dynamical parameters is different, and a systematic study of large samples of stars at different luminosities and positions in several clusters is decisive.

While specific observations for a few bright giants may be carried out with a 4-m-class telescope, a fiber instrument like MFAS (both in the Medusa and Argus mode) at an 8-m-class telescope is

required for a systematic and complete study of fainter stars.

• *Mass loss and intracluster matter*

Stellar evolution models predict a mass loss of ~ 0.2 M$_\odot$ prior to the HB phase and ~ 0.1 M$_\odot$ on the asymptotic giant branch (AGB) (e.g. Fusi Pecci and Renzini 1976, Renzini 1977). This mass loss is required to explain the morphology of the HB observed in the GC colour-magnitude diagrams and the lack of any significant population of AGB stars brighter than the RGB tip.

Quantitative direct information on mass-loss rates can hardly be obtained so far for any star, and especially for globular cluster stars no reliable data are available. The basic features related to stellar mass loss are the lines in the UV domain, OH masers (1612 MHz), CO lines (in the microwave range), dust-induced features in the IR, and Ca H+K or H$_\alpha$ lines (but these can be contaminated by other contributions). As an example, with the VLT + UVES one could extend to GC stars the type of studies carried out by Reimers (1975) on field stars, based on the detailed analysis of high-resolution Ca H+K line profiles.

Assuming a constant gas-to-dust ratio and typical expansion velocities (Skinner and Whitmore 1988) useful data could be obtained using VLT + MIIS by observing the brightest GC stars for instance at 9.7, 11.5 and 18.0 μm, typical features already observed in bright nearby objects with high mass-loss rates.

As a result of stellar mass loss, some amount of interstellar matter should also be present in GCs. A typical GGC population of $\sim 10^3$ post-TO stars is expected to release about 10^2–10^3 M$_\odot$ of intracluster matter during the $\sim 10^8$-yr periods between each cluster passage through the galactic plane. This matter should be present if no "cleaning" mechanism is at work. A significant amount of gas and dust could then be accumulated in the central regions of the most massive and concentrated clusters (i.e. those with large central escape velocity).

The intracluster gas could be in the form of atomic (neutral or ionized) hydrogen and/or molecular H$_2$ and CO. Searches for HI and H$_\alpha$ emission (Smith et al. 1990, Roberts 1988, for a general review) in the central region of a few GGCs resulted only in marginal detections which would be incompatible with a total mass loss per star of ~ 0.3 M$_\odot$, if the cluster is "closed". A few explanations for this apparent lack of gas have been suggested, and invoke for instance high gas velocities (e.g. winds driven by novae or flare stars) but the details are not well understood yet.

Searches for CO performed so far in the central regions of GGCs (Schneps et al. 1978) have been unsuccessful, but no firm conclusions can be derived from these observations because of the low sensitivity and the small beam of the employed receivers.

On the contrary, some evidence of cold dust was found in the intracluster medium of GGCs (Forte and Mendez 1989). Its origin is probably related to the processes of mass ejection during the RGB and AGB phases, which would imply the presence of dusty envelopes around red variables, as also suggested by the IR excess that has been measured around luminous giants and long-period variables in 47 Tuc (Frogel and Elias, 1988; Gillet et al. 1988). Multicolour polarization and CCD photometry of some clusters with P $\leq 2\%$ and scattered polarized light detected at a few core radii suggest that the dust distribution may be considerably extended within the central region of the observed GGCs.

In many clusters IRAS point sources have also been detected within their tidal field (integrated fluxes in a 30" aperture between 0.2 and 1 Jy, Lynch and Rossano 1990). For some of them this far-IR emission might indeed be due to dusty structures in the intracluster medium, because the IRAS sources are located in the cluster core. A few of them are extended at 12 μm, with typical sizes of 2–4 arcmin, and this could be a significant indication of the presence of cold dust in the intracluster medium. A mid-IR Imager/Spectrometer would allow to investigate the presence and the chemical composition of these dusty features in the circumstellar envelopes of the coolest giant stars and/or in the intracluster medium.

ISO observations can provide a deep survey (0.1–1 mJ) of the cluster central regions with low spatial resolution and small field of view, due to the small-format arrays. The use of an 8-m-class telescope and large-format arrays would allow to make almost as deep surveys (down to ~ 1 mJy per square arcsec) on a much larger field of view (a few arc-minutes) and with high spatial resolution (0.1"/pixel and an Airy disk of 0.6" at 10 μm). A complete mapping of the emission regions would thus be possible, even for quite extended and low surface brightness areas. Note that the high spatial resolution available only with the VLT will allow to distinguish between diffuse emission (dust) and point sources (very cool stars, e.g. brown dwarfs or carbon stars). An instrument like MIIS could satisfy these requirements.

• *Gravitational settling, diffusion and rotation for HB stars*

As mentioned above, the distribution of stars on and their evolution off the ZAHB of GCs is not yet completely understood. However, it is known that the combined action of gravitational settling and outward diffusion by radiation pressure observed in Pop-I B8-F2 stars may change significantly the surface abundances of He and metals in the outer radiative envelope of hot HB stars, since the typical timescale of these phenomena (10^8 yr) is close to the HB lifetime. On the other hand, diffusion might be inhibited by rotation.

Observations of lines of He and heavier elements might then provide the age of stars on the HB, and then be used to distinguish between ZAHB and evolved stars once additional information on rotational velocities is available (see below). With proper modeling, one could get information on the direction of evolution off and along the HB. Earlier explorative observations of He lines have been done by Crocker and Rood (1988); however, an 8-m-class instrument is required for extensive observations of different elements as quite high spectral resolutions (UVES with R > 40,000) are necessary and the stars are faint (V $\sim 14 \Rightarrow 20$).

Spectroscopic observations of HB stars are also important to better understand the mass-loss mechanisms, since the colour distribution of these stars is controlled, for fixed core mass and composition, by the residual mass of the H-rich envelope. For instance, Renzini (1977) predicts that stars with fast core rotation evolve into blue HB stars, since the helium flash would occur at a higher luminosity and, in turn, the total amount of mass lost while experiencing the RGB phase would be larger.

Peterson (1983) found a high frequency of larger-than-normal rotational velocities in BHB stars of M13. While the relation between surface and core rotation is not clear yet, these relatively high rotational velocities could help explain the very blue horizontal branch of M13, a typical example of the second-parameter phenomenon. A confirmation of Peterson's result would thus be of paramount importance as one could eventually get direct hints on both rotation and mass loss. However, these observations are very difficult and uncertain as the blue HB stars are faint and reliable rotational velocities require high-resolution spectra with high S/N ratios. The use of an 8-m-telescope with a MOS capability is thus highly desirable.

4.2. Binaries: Blue Stragglers, CVs, X-ray sources, MSP, etc.

It is common belief that any object which does not fit into the "standard evolution theory" of normal stars could somehow be related to a binary system. Though it seems unlikely that binarity is

responsible for so many different types of stars, it may be interesting at least to mention several categories of "unusual" cluster members: objects include for instance:

- blue stragglers
- subdwarfs O and B
- cataclysmic variables
- dwarf Cepheids
- extremely blue HB stars
- novae
- Ba, CH stars, etc.
- UV-bright objects
- "naked" or "nude" very blue stars
- X-ray source
- millisecond pulsars (MSP)

Since until recently there was even some doubt whether binaries might exist at all in globular clusters, the questions to answer are: how many binaries are present in GGCs? and how do they form, survive, evolve, interact with the environment?

To study these variegated classes of objects different techniques have been successfully used in the optical, X-ray, and radio bands. Several interesting programmes could easily be carried on with the VLT, for the sake of example we list here a few of them:

1. Detection of radial velocity variables. Systematic surveys with MFAS aimed at checking velocities of individual cluster stars ($\sigma \sim 1$ km s^{-1}) may reveal a number of candidate binaries starting from the bright giants down to the faint MS.

2. Detection of photometric variables. A survey using both MFAS and FRISPI could lead to detect eclipsing binaries and to study their periods. In particular, the study of variability could be focused on blue stragglers as about 25% of them have been found to vary (Stryker 1993). Moreover, one could also use the properties of spectrophotometric binaries to yield distances.

3. Detection and study of cataclysmic variables and novae. Though the total number of such objects detected so far in GGCs is low and, moreover, their membership is frequently uncertain, one could use high-resolution spectra in the UV region taken with UVES to study in detail their properties. Since these stars are faint (V > 18 even in the closest clusters), the VLT is absolutely necessary.

4. Detection of a "second" MS. If binaries are still present in the MS of a cluster and if they are formed by approximately equal mass components, one expects to detect some spread in the intrinsic MS colour or even the existence of a second "binary MS" parallel to that of single stars. Preliminary detections of such an effect have been presented for instance by Bolte (1992), but more accurate data and a spectroscopic follow-up is neces-

sary to confirm the evidence. The use of spectra obtained with MFAS may allow the detection of radial velocity variations in the candidates found via very deep imaging.

5. Study of X-ray sources and Millisecond Pulsars. This topic is so wide and the possible observations so many that we simply mention it. In this respect, especially spectrophotometry with MFAS and FRISPI are crucial to both identify and study the optical counterparts.

We wish to discuss here in some more detail the study of the blue straggler stars (BSS) and of their possible descendants. BSS can be formed via several mechanisms mostly involving the interaction and merging of stars in binary systems (both primordial and formed through subsequent encounters in dense cluster cores). These BSS have similar photometric characteristics but different physical properties, and are expected to have a mass in the range 0.8–1.6 M$_\odot$ (Nemec 1991; Fusi Pecci et al. 1992; Bailyn 1992). When they evolve off the MS and into the He-core burning phase, they are expected to be located on the red extreme of the HB due to their large mass (Seidl et al. 1987). Therefore, although their location on the HB looks *normal*, their mass distribution is very different from typical (single) red HB and RGB stars.

Metal-poor clusters with blue HBs are the ideal place where these candidate BSS descendants could be better detected, as they would be the only stars located at the red HB extreme. On the other hand, these stars might display some different characteristics if they had not been able to lose a substantial fraction of the large angular momentum acquired with the merging.

In this case, a large rotational velocity should be expected, the presence of a large convective envelope would probably cause a strong dynamo effect, and hence a rather strong activity (analogous to that observed in FK Com objects). These effects should be detectable with appropriate spectroscopic observations. Finally, He, CNO (mainly O isotopic ratios) and Li abundance anomalies might be present, even though the theoretical background is not well defined at present (Bailyn 1992; Pritchet and Glaspey, 1991).

While adequate observations of a few very bright BSS descendants in some clusters are feasible with a 4-m-class telescope, an 8-m telescope is absolutely required for most BSS progeny, as well as for the direct observation of BSS themselves. The need of a quite high spectral resolution (R = 30,000) and a statistically significant sample of stars requires the use of a fiber-fed, optical and IR medium/high-resolution spectrograph

(the determination of the O isotopic ratio can best be done with high-resolution observations of the CO bands in the K wavelength region).

5. Cluster Internal Dynamics

Globular clusters are ideal sites to test dynamical models of stellar systems, since they are relatively simple structures where large samples of individual objects can be observed.

Early dynamical models of globular clusters as a population of spherically distributed point-like single-mass objects were constructed by King (1966). These models predict a rather simple dynamical evolution of a cluster, with the formation of a dense core which finally collapses (gravothermal instability: Antonov 1962), while the outer parts of the cluster are dispersed (evaporation: Ambartsumian 1938, Spitzer 1940).

With later (multi-mass) modifications, King's models describe rather well the properties of the majority of GGCs, allowing to derive important global parameters like the mass-to-light ratios, total mass, etc. However, there is a substantial fraction of clusters whose light profiles clearly deviate from King's model predictions, since they do not exhibit the expected central plateau; these clusters have been identified (Djorgowsky and King 1986) as post-core collapse clusters, since it has been recognized long ago that formation of close binary systems and stellar evolution in very dense cluster cores may provide an energy source able to prevent the final collapse of the cluster core (Henon, 1961). However, numerical simulations of the dynamical behaviour of post-core collapse clusters are rather uncertain, due to the presence of large instabilities (gravo-thermal oscillations: Bettwieser and Sugimoto 1984, Goodman 1987).

Furthermore, since there are now strong arguments supporting significant modifications of stellar surface abundances and even stellar evolution itself in very dense environments, a systematic study of the dynamical properties of a very large cluster sample would be highly welcome.

These programmes require high precision measures of radial velocities (error < 1 km s^{-1}) for a large sample of stars in various cluster regions.

On a 4-m-class telescope, these observations are limited to a few bright giants, whereas MFAS is very well suited for these programmes, the Argus mode being useful for the cluster core and the Medusa mode for the outer regions.

Finally, it is natural to conclude by mentioning one of the most obvious dreams of anyone working on globular

clusters, i.e. to observe the very central regions (a few fractions of a parsec) with the maximum possible spatial resolution. To this aim, the VLT in its interferometric configuration is the *only* instrument capable of achieving the necessary resolution. If one could reach the nominal resolution of about 0.004 arcsec, one could really make an incredible step forward even compared to the best results one could possibly obtain from HST in its best configuration ($\sim$ 0.02 arcsec).

6. Conclusions

In conclusion, it is quite evident even from our schematic and incomplete review of globular cluster studies that the VLT will be an extremely important tool for yielding a better insight into most of the current hot problems. A fruitful complementarity exists between the results uniquely achievable from space (with HST, ISO, etc.) and those one can better obtain from the ground with the VLT and its many detectors. In this respect, it is important to note that (i) there are crucial observing programmes which require not only the use of the already planned VLT instruments (i.e. FORS, ISAAC, CONICA, UVES, and MFAS) but also of some instruments presently under study or just proposed like MIIS, NIRMOS, FRISPI, and WFDVC; and (ii) several extremely important issues in the study of globular cluster problems can best be addressed in the IR wavelength range, and since neither HST nor ISO for various different reasons are able to carry out the necessary observations, IR instruments for the VLT (especially in the near and intermediate IR) should have a very high priority in the selection, construction and commissioning.

References

Alcock C., *et al.* 1993, *Nature*, **365**, 621.
Ambartsumian V.A. 1938, Ann. Leningr. State Univ. No. 22.
Antonov V.A., 1962, Vestn. Leningr. Gros. Univ. **7**, 135.

Auburg E., *et al.* 1993, *Nature*, **365**, 623.
Bailyn C.D. 1992, *ApJ*, **392**, 519.
Bettwieser E., Sugimoto D. 1984, *MNRAS*, **208**, 439.
Bolte M. 1992, *ApJ*, **376**, 514.
Buonanno R., Corsi C.E., Fusi Pecci F. 1989, *A&A*, **216**, 80.
Buonanno R., Corsi C.E., Fusi Pecci F., Richer H.B., Fahlman G.G. 1994, *AJ*, in press.
Cacciari C, Clementini G., Fernley J.A. 1992, *ApJ*, **396**, 219.
Chiosi C., Bertelli G., Bressan A. 1992, *ARA&A*, **30**, 235.
Crocker D.A., Rood R.T. 1988, in *Globular Cluster Systems in Galaxies*, IAU Symp. No. 126, eds. J.E. Grindlay and A.G.D. Philip, Kluwer, Dordrecht, p. 509.
Djorgowsky S.G., King I.R. 1986, *ApJL*, **305**, L61.
Fahlman G.G., Richer H.B., Searle, L., Thompson I.B. 1989, *ApJ*, **343**, L49.
Forte J.C., Mendez M., 1989, *ApJ*, **354**, 222.
Frogel J.A., Elias J.H. 1988, ApJ, **324**, 823.
Fusi Pecci F., Renzini A. 1976, *A&A*, **46**, 447.
Fusi Pecci F., Renzini A. 1979 in *Astronomical Uses of the Space Telescope*, eds. F. Macchetto, F. Pacini, M. Tarenghi (ESO), p. 181.
Fusi Pecci F., Ferraro F.R., Corsi C.E., Cacciari C., Buonanno R. 1992, *AJ*, **104**, 1831.
Fusi Pecci F., Ferraro F.R., Bellazzini M., Djorgovski S.G., Piotto G., Buonanno R. 1993, *AJ*, **105**, 1145.
Gillet F.C., deJong T., Neugebauer G., Rice W.L., Emerson J.P. 1988, *AJ*, **96**, 116.
Goodman J. 1987, *ApJ*, **313**, 576.
Gratton R.G., Sneden, C. 1989, *A&A*, **234**, 366
Helou, G. and Walker, D.W., 1986, *IRAS Small Scale Structure Catalog*, U.S. GPO, Washington D.C.
Henon M. 1961, *Ann. d'Ap.*, **24**, 369.
Hodge, P.W., 1983, *ApJ* **264**, 470.
Käufl, H.U., Jouan, R., Lagage, P.O., Masse, P., Mestreau, P. and Tarrius, A., 1992, *The Messenger* **70**, 67.
King I.R. 1966, *ApJ*, **71**, 64.
Kraft R.P., *et al.* 1992, *AJ*, **104**, 645.
Larson R.B., 1974, *MNRAS* **166**, 585.
Le Fèvre O. 1994, in *Instruments for the ESO-VLT booklet*.
Lynch D.K., Rossano G.S. 1990, *AJ*, **100**, 719.
Majevski S.R. 1993, *ARA&A*, **31**, 575.
McWilliam A., Rich R.M., 1994, preprint.
Nemec J. 1991, *Nature*, **352**, 286.
Molaro P., Pasquini L., 1994, *A&A*, **281**, L77.

Paresce F., De Marchi G., Romaniello M., 1994, preprint.
Peterson R.C. 1983, *ApJ*, **275**, 737.
Piotto G. 1993, in *Structure and Dynamics of Globular Clusters*, ASP Conf. Ser. 50, eds. S. Djorgovski & G. Meylan, p. 233.
Pritchet C.J., Glaspey J.W. 1991, *ApJ*, **373**, 105.
Reimers D., 1975, *Mem. Soc. R. Sci. Liège*, **6**(8), 369.
Renzini A. 1977, in *Advanced Stages of Stellar Evolution*, eds. P. Bouvier and A. Maeder, Geneva Obs., Geneva, p. 151.
Renzini, A., 1977, in *Advanced Stellar Evolution*, P. Buovier and A. Maeder eds., Saas-Fee, Geneva Obs., p. 149.
Renzini A. 1985, *Astronomy Express*, **1**, 127.
Renzini, A., Fusi Pecci F. 1988, *ARA&A*, **26**, 199.
Richer H.B., Fahlman G.G., Buonanno, R., Fusi Pecci F., Searle, L., Thompson I.B. 1991, *ApJ*, **381**, 147.
Roberts M.S. 1988, in *Globular Cluster Systems in Galaxies*, IAU Symp. 126, J.E. Grindlay and A.G.D. Philip eds., Kluwer, Dordrecht, p.411.
Sandage A.R., Cacciari, C. 1990, *ApJ*, **350**, 645.
Sarajedini A., Demarque P. 1990, *ApJ*, **365**, 219.
Schneps M.H., Ho P.T.P., Barrett A.H., Buxton R.B., Myers P.C. 1978, *ApJ*, **225**, 808.
Seidl E., Demarque P., Weinberg D. 1987, *ApJS*, **63**, 917.
Skinner C.J., Whitmore B. 1988, *MNRAS*, **231**, 169.
Smith G.H. 1987, *PASP*, **99**, 67.
Smith G.H., Wood, P.R., Faulkner, D.J., Wright, A.E. 1990, *ApJ*, **353**, 168.
Spite M., Maillard J.P., Spite F. 1984, *A&A*, **141**, 56.
Spitzer L. 1940, *MNRAS*, **100**, 396.
Stryker L.L. 1993, *PASP*, **105**, 1081.
Sweigart A.V., Mengel, J.G. 1979, *ApJ*, **229**, 624.
Tinney C.G. 1994, in *Science with the VLT*, ESO-Garching.
VandenBerg D.A., Bolte M., Stetson P.B. 1990, *AJ*, **100**, 445.
VandenBerg D.A., Smith G.H. 1988, *PASP*, **100**, 314.
Wampler E.J. 1994, in *Instruments for the ESO-VLT booklet*
Zinn R.J. 1986, in *Stellar Populations*, Norman C.A., Renzini A. and Tosi M., eds., Cambridge University Press, Cambridge, p. 73.

Scientific Capabilities of the VLT Adaptive Optics System

B. THÉODORE[1]*, P. PETITJEAN*[2] *and N. HUBIN*[1]

[1] *ESO-Garching;* [2] *Institut d'Astrophysique de Paris, France*

1. Introduction

The theoretical angular resolution power of a telescope of diameter D is limited by diffraction and is proportional to λ/D. However, atmospheric turbulence severely restricts the capabilities of astronomical telescopes. Whatever the aperture diameter, the resolving power of the telescope is limited by the seeing angle and so the image of a point source is spread most often

over more than 0.7 arcsec in the visible. A radical way to achieve the diffraction limit is to put the telescope above the atmosphere. Though this allows high-quality imaging as demonstrated by the recent breakthrough of HST, this is rather involved and expensive. Different techniques are used to approach diffraction-limited imaging using ground-based systems, like speckle, long-baseline interferometry or post-observation deconvolution. However, adaptive optics is the simplest way for observers to overcome in real time the perturbations induced by the atmosphere on ground-based telescopes without any further image processing (Merkle 1988).

This motivates the growing interest for adaptive optics systems and explains why several prototypes are being built all over the world. Up to now, the only system allowing nearly full correction of the atmospheric perturbation and offered to visiting astronomers is the COME-ON+ system at the 3.6-m telescope of ESO.

This system has obvious limitations: it requires for instance relatively bright stars ($m_V < 13$) for use as a reference by the wavefront sensor. The relatively small diameter of the telescope restricts the possibility of this instrument. But the experience acquired by using it will greatly help designing the system to be installed at the VLT. An obvious task is to assess the scientific capabilities of such a system. After describing the effect of atmospheric turbulence on the images and the way they can be compensated we will present results of calculations of the fraction of the observable sky using this technique.

2. Effect of Atmospheric Turbulence on Astronomical Images

The refractive index along a path through the atmosphere exhibits spatial and temporal variations due to atmospheric inhomogeneities. As a result, an initial plane-parallel wavefront arrives distorted at the telescope. The variations of the phase in a reference plane may be described by the *phase structure function* $\mathcal{D}_\phi$, which is the variance of the phase variations between two points of the plane. This quantity is a function of the atmospheric characteristics and is not known in general. Assuming, however, that atmospheric turbulence obeys Kolmogorov statistics, it can be shown that $\mathcal{D}_\phi$ is proportional to the five-third power of the distance r between two points.

$$\mathcal{D}_\phi(r) = 6.88 \, (r/r_0)^{5/3} \qquad (1)$$

where r_0 is the characteristic coherence length known as *Fried parameter*. The latter is related to the seeing angle $\theta_s = \lambda/r_o$ and increases with the
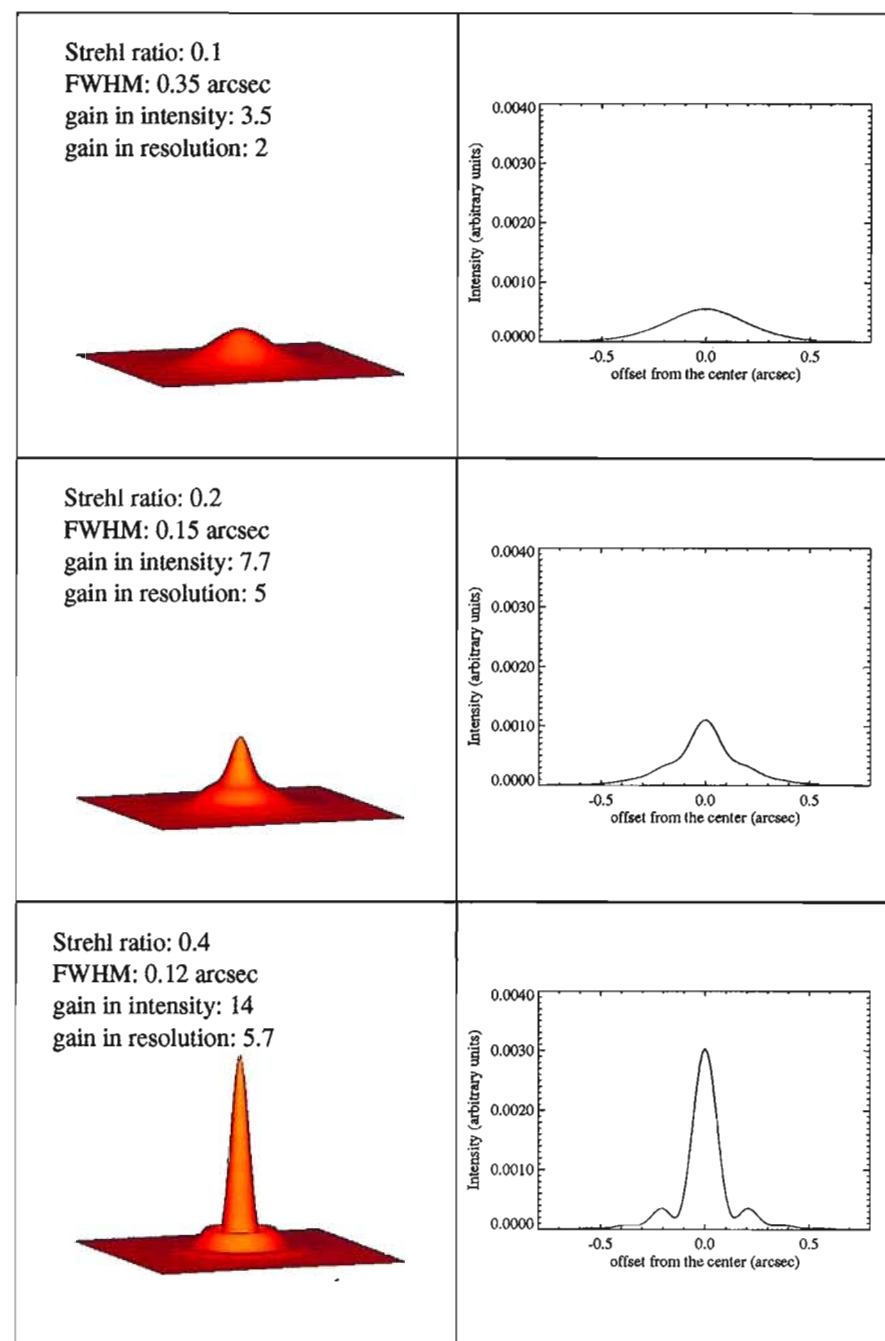

Figure 1: *Shape of the image after compensation.* **Top:** *moderate correction (Strehl ratio = 0.1): the image is Gaussian, but the compensation leads to a gain of a factor of 3.5 in intensity and 2 in resolution compared to the uncompensated image.* **Middle:** *Strehl ratio = 0.2: a coherent core appears, surrounded by a halo. The image is much sharper compared to the uncompensated one.* **Bottom:** *Strehl ratio = 0.4: the image is diffraction-limited and surrounded by a faint halo.*

wavelength as $\lambda^{6/5}$. It is also the diameter of an aperture through which, for given atmospheric and zenith angle conditions, nearly diffraction-limited images can be obtained; the images appearing to change position as the atmosphere evolves with time. This means that phase variations on such a distance are small enough so that the image profile is not altered. This means also that this is the diameter of the aperture through which

a unique phase error (the motion of the image in the field of view) may be measured and compensated by actuating a single mirror.

Overcoming the distortions induced by atmospheric turbulence on an incoming wavefront requires thus the sampling of the wavefront through areas of diameter r_0, or less, in a reference plane. This is the role of the wavefront sensor as it will be described later. For a large tele-

K band
seeing: 0.7 arcsec
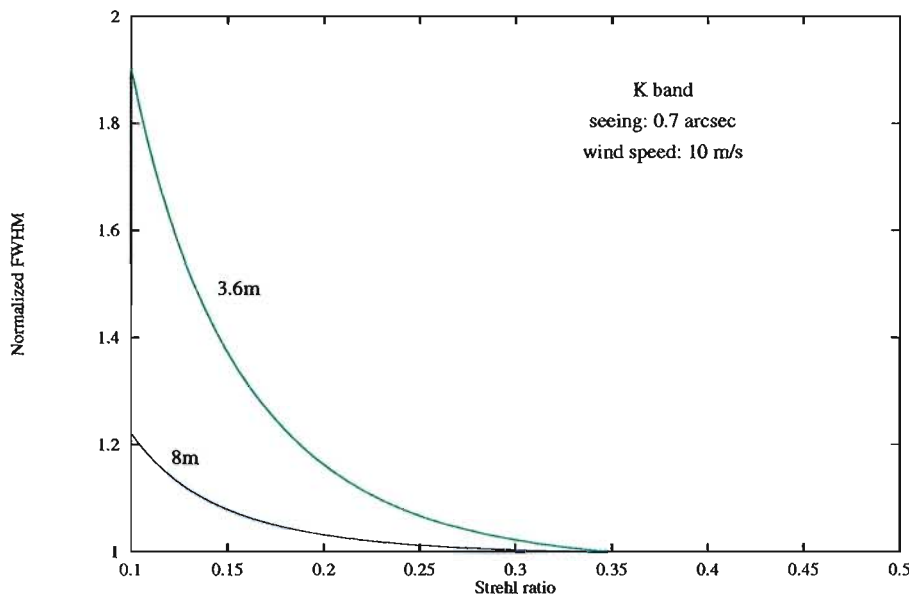wind speed: 10 m/s

3.6m

8m

Figure 2: *FWHM of the image (in units of the FWHM of the diffraction-limited image) as a function of the Strehl ratio.*

scope $(D/r_0)^2$ is thus the optimal number of actuators to be used to shape the deformable mirror of the adaptive optics system. While the average value of r_0 at La Silla is 12 cm at 0.5 μm, it is 71 cm at 2.2 μm. It is thus easier to build a system to compensate for the turbulence in the near-infrared since, for a given telescope, one needs fewer actuators in the infrared than in the visible. However, since the deformations of the wavefront do not depend on the wavelength, the wavefront sensing is performed in the visible, allowing thus the use of fainter objects as references, due to the higher performances of optical detectors.

3. Compensation of Atmospheric Turbulence

Once the phase variations on the telescope pupil are known, it is mathematically convenient to expand them on a base of orthogonal polynomials. The Zernike polynomials Z_i are often used, because they are representative of the classical optical aberrations (Noll 1976)[1]. The first order is the piston and represents a translation of the wavefront along the optical axis; thus it has no effect on the image shape. The second and third orders are the tilt in x and y directions which cause the image to move in the field of view, the fourth order is the defocus which causes the rays to cross the optical axis out of the theoretical focus

of the mirror, the eleventh order is the spherical aberration, etc...

The wavefront distortions may now be written:

$$\phi = \sum a_i Z_i \qquad (2)$$

Thus, in order to compensate for the wavefront aberrations, one must correct the wavefront in order to set the coefficients a_i of the expansion to zero or, at least, to minimize them.

It is interesting to assess the influence of a perfect compensation of the first N Zernike orders $(a_{i(i=1,...,N)} = 0)$. It is indeed possible in this case and under the usual hypothesis of a Kolmogorov turbulence to derive the residual variance of the phase on a reference plane:

$$\sigma^2 = 0.2944 N^{-0.866} \left(\frac{D}{r_0}\right)^{5/3} \qquad (3)$$

The residual is of course a decreasing function of the number of corrected modes N, since the more numerous the corrected orders the better the correction. It is also an increasing function of (D/r_0). Indeed for the same atmospheric conditions and at the same wavelength, the variation of the phase is larger on a larger distance (or here aperture) and, for the same aperture, it is larger for worse seeing (thus smaller r_0).

The residual phase variance as a way for evaluating the image quality is rather vague. A more relevant parameter is the Strehl ratio, which is the ratio of the maximum intensity of a point source image to the maximum intensity of the diffraction-limited image through the same telescope. The larger the Strehl ratio, the closer the image from the ideal case of a diffraction-limited image. Though the Strehl ratio is defined and computed from the intensity in the image, it is also a

good indicator of the image structure and sharpness. This is illustrated in Figure 1 where image profiles are drawn for different Strehl ratios. For small values, the image is almost Gaussian in profile with a width equal to the seeing angle. As the Strehl ratio increases (i.e. as the correction becomes better), the image exhibits two components: a diffraction-limited core surrounded by a halo, the importance of the latter decreasing as the Strehl ratio rises (more and more light is concentrated in the core). This is illustrated in Figure 2, which shows the normalized FWHM as a function of the Strehl ratio: it decreases very sharply for small Strehl ratios until the sharp core is dominant. Then, the image is diffraction-limited in terms of resolution and increasing the Strehl ratio only increases the intensity in the core.

For the VLT, a Strehl ratio of 0.1 corresponds to a gain in resolution and in the maximum intensity of the image of a factor of 3.2 and of a factor of 5.6 respectively. We will consider in the following, somewhat arbitrarily, that this value of the Strehl ratio is the minimum acceptable correction for any observations using adaptive optics.

4. Adaptive Optics Systems

Adaptive optics systems have been extensively described elsewhere (e.g. Rigaut 1993). We briefly review the components of the system through the constraints they put on astronomical imaging.

Figure 3 recalls the basic arrangement of an adaptive optics system and the main steps of the compensating process: the wavefront distortions are analysed by the wavefront sensor, the phase is reconstructed and the optical train of the telescope is adapted in real time. This cycle must be carried out rapidly enough so that the atmosphere has not changed between the evaluation of the phase errors and the deformation of the mirror.

As alluded to above, the wavefront sensing consists in estimating the phase variations on a reference plane. This is done by sampling the wavefront on a pupil plane by an array of lenses, each of them forming an image on a detector. Ideally (in case there are no aberrations), the image produced by each lens is aligned with its optical axis. Otherwise, the position of the image gives an estimate of the averaged slope of the wavefront over the lenslet area. Thus, the correction of the wavefront will be optimal if the wavefront can be considered as planar over each lenslet. This is the case, as a first approximation, if each lenslet corresponds to a sub-aperture of diameter r_0. Yet, since the Fried parameter is a function of the wavelength and in ad-

---

[1]Several bases may be used for the phase expansion (Rigaut, 1993), such as Karhunen–Loève functions which are more representative of the atmospheric turbulence, or the eigenmodes of the deformable mirror. We only address here the Zernike decomposition, because it is conceptually simpler.
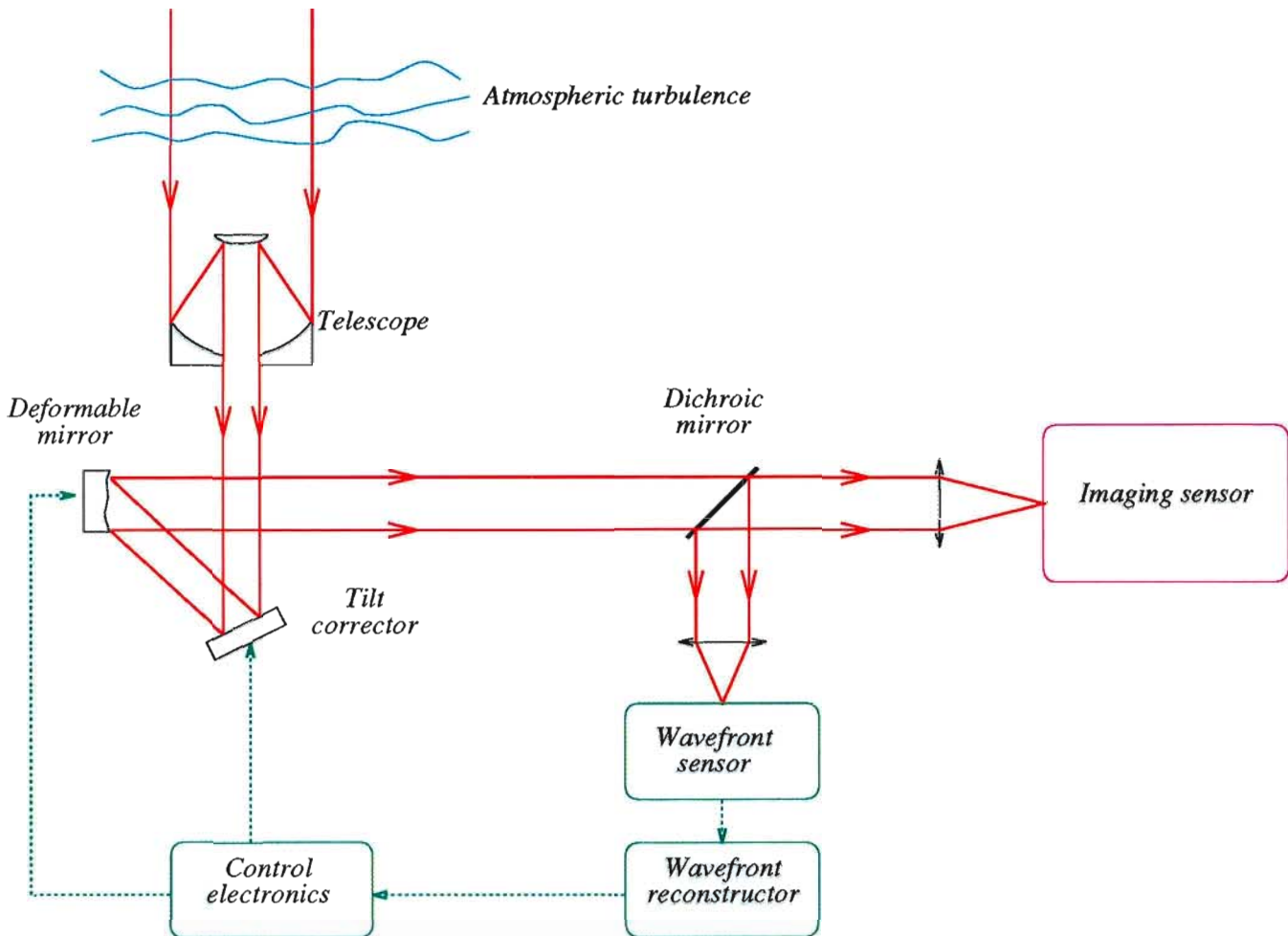
Figure 3: *Arrangement of an adaptive optics system, showing the main steps of the compensation process:* detection *of the wavefront,* reconstruction *of the phase,* adaption *of the optical train. For the latter step two distinct mirrors are used in the COME-ON+ system.*

dition exhibits a high temporal variability, the sampling cannot always be optimal since the number (and thus the diameter) of each sub-aperture is fixed by the design of the system[2].

A second constraint is that the time between two successive corrections must be shorter than the coherence time of the turbulence. The latter varies like r_0 as a function of the wavelength and is about 10 milliseconds at 2.2 μm. Consequently the integration time on the reference object must be shorter than this, which, for a reasonable S/N ratio, requires the correction to be done using a bright enough object (either the object itself or a reference star). If the S/N ratio is not large enough, the position of the image of the reference star through the sub-apertures is not well determined and the correction is bad. Thus the ability of the system to compensate for the wavefront distortions depends on the magnitude of the reference star. This is illustrated in Figure 4 which shows the expected

Strehl ratio when using the current system COME-ON+ and the future system

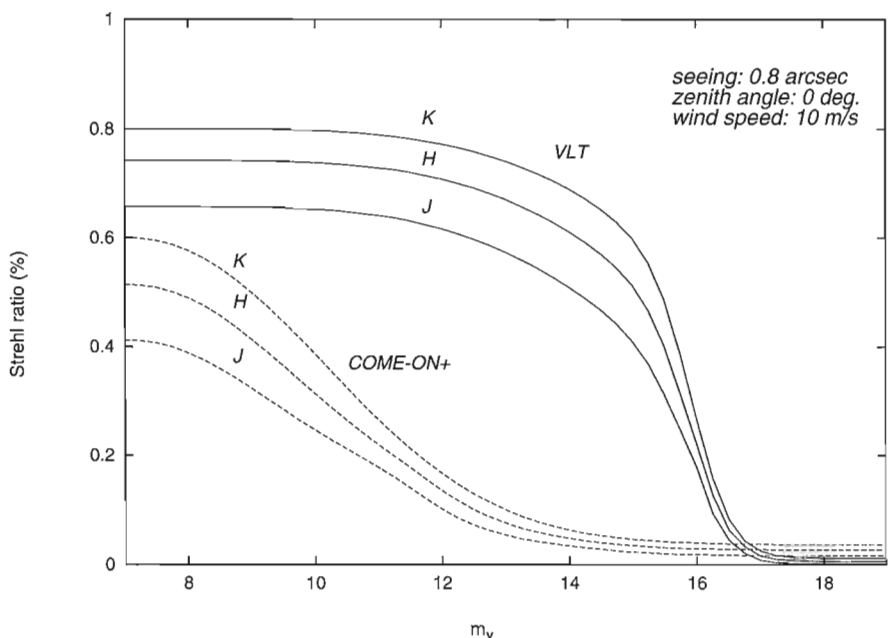for the VLT as a function of the magnitude of the reference star for various wave-

Figure 4: *The correction is a function of the magnitude of the reference object. We show here the Strehl ratio achieved in J-, H- and K-bands versus the visible magnitude m_v of the reference star.*

[2]Note that it is nevertheless possible to alleviate the problem of a super-sampling of the wavefront using, for example, modal control optimization.
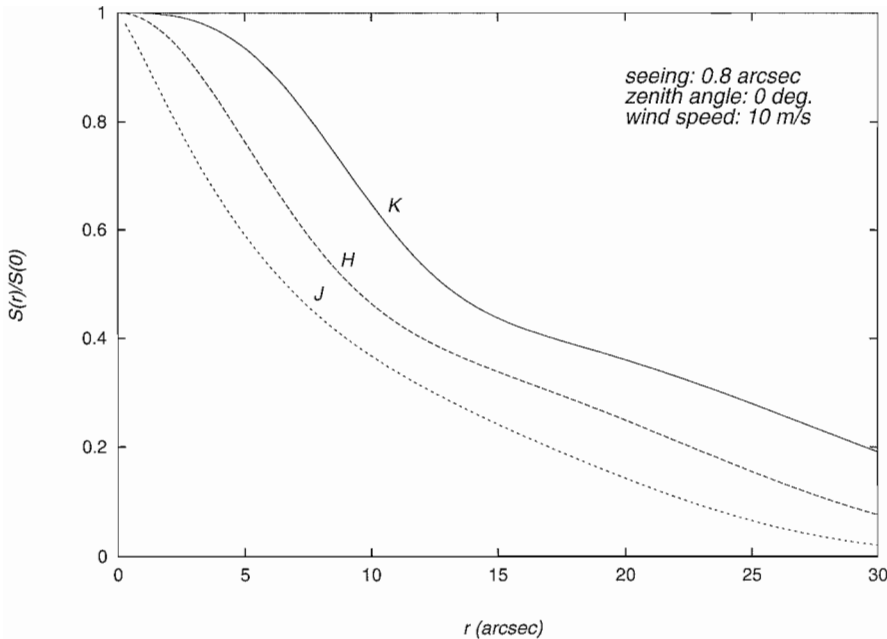
Figure 5: *Using a reference star distinct from the observed object leads to a degradation of the correction (isoplanatic effect). The ratio of the Strehl ratio achieved on an object to the one achieved on a reference star is plotted versus the separation r between the object and the star.*

bands and for a seeing of 0.8 arcsec (average value at Paranal). These curves were generated from experimental values for COME-ON+ and from a model for the VLT system (Hubin *et al.* 1993). For both systems there is a plateau up to a given magnitude (16 for the VLT and 13 for COME-ON+). Indeed, there is a minimum S/N ratio (obtained using a reference star of magnitude m_{lim}) above which the position of the images of the reference star given by each lenslet are well defined, yielding the correction to be optimal for all S/N ratios larger than this value (thus all reference stars with magnitude smaller than m_{lim}). At larger magnitudes, a rapid drop is observed because the signal of the reference star is too faint for the phase to be properly reconstructed. It may be noted also that even if the star is bright, the Strehl is not equal to one since the correction cannot be perfect due to the *de facto* discontinued sampling.

A third constraint on astronomical observation using adaptive optics is that quite a number of the objects of astronomical interest are not bright enough to achieve a proper correction ($m > m_{lim}$). In such a case a reference star is needed in the vicinity of the observed object. But since the atmosphere is not exactly the same along both lines of sight, towards the object and the reference star, the correction on the object is only partial even if the correction on the reference star is very good. This effect is called the isoplanatic angle limitation and is illustrated in Figure 5 where the ratio of the Strehl ratio achieved on the object to the one achieved on the reference star is plotted

as a function of the separation between both objects and for various wavebands. It is a rapidly decreasing function of the separation: for instance, in the K-band, if the reference star lies at 12 arcsec from the astronomical object, the Strehl ratio achieved on the latter is half the one achieved on the former.

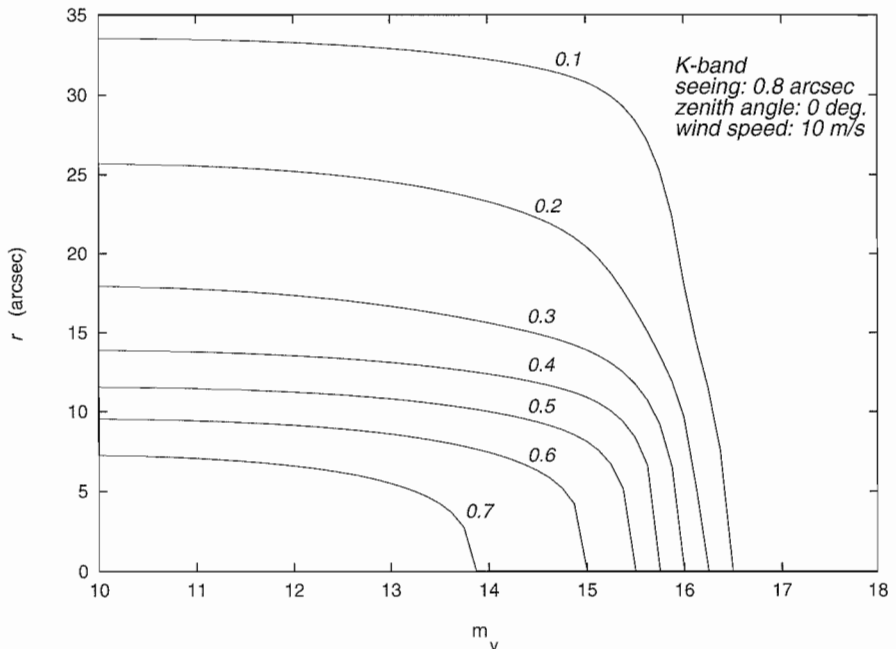Thus, the quality of the corrected image is essentially a function of two parameters: the magnitude of the reference star and its separation from the observed object. This is illustrated in Figure 6 which gives the Strehl ratio which will be achieved with the VLT system in the K-band as a function of these two parameters, the magnitude m_v and separation r. As an example, if the correction is done using a star of magnitude 15, the Strehl ratio at 30 arcsec of the object is 0.1 in the K-band for 0.8 arcsec seeing conditions and a 10 ms^{-1} averaged wind speed. On the star itself, a Strehl ratio of 0.6 could be expected.

5. Potential Observations

The necessity to find a bright reference star as close as possible (and in any case within one arcmin) from the observed object is a severe constraint and limits the possibility of the system in terms of sky coverage. Indeed, the probability of finding such a star is rather small. We have quantified this probability using two approaches: the first one is to compute the fraction of the sky which may be observed at a given level of correction. The second one is to evaluate the expected distribution of improvement level by cross-correlating catalogues of potentially interesting objects with catalogues of bright stars.

5.1 Sky coverage

Given the characteristic of an adaptive optics system, it is possible to compute the area of the sky surrounding any bright star in which the system will allow a given level of correction when using the star

Figure 6: *Strehl ratio achieved in K-band with the VLT system plotted as a function of the magnitude m_v of the reference star and of the separation r between the observed object and the reference star.*

as reference object. For a given system, this area depends on the magnitude of the star and the level of correction aimed at. Integrating over the whole sky gives the fraction of the sky that is possible to observe in those conditions:

$$\xi(S) = \int_{m_{min}}^{m_{max}} n(m)\pi r^2(m, S)\,dm$$

where m_{min} is the magnitude of the brightest reference star considered, m_{max} is the magnitude of the faintest star possibly used for correction by the system, $r(m, S)$ is the radius where the Strehl ratio is S and $n(m)$ is the density of stars of magnitude m.

The density of stars has been estimated from the Guide Star Catalogue (hereafter GSC). It is however complete up to magnitude 14.5 only and we used the Galactic models by Bahcall and Soneira (1980) for fainter stars. Actually, the distributions from the GSC and the models are in very good agreement for magnitudes smaller than 14.

The sky coverage as a function of m_{max} for regions of the sky just above the galactic plane and for various Strehl ratios is shown in Figure 7a for COME-ON+ and 7b for the VLT system. It is a steep function of the magnitude till it reaches a plateau. The latter is mainly due to the sharp drop of the performances of the system for faint reference stars (see Figure 4).

The possibilities of COME-ON+ appear to be rather restricted since even for a Strehl ratio of 0.1, the sky coverage is less than 0.35%. For the VLT, the observable fraction of the sky can reach 17% for a Strehl ratio of 0.1 with the magnitude limit $m_{lim} = 16$ for the reference star. With a magnitude limit of 17, more than a quarter of the sky could be observed with a Strehl ratio of 0.1 in the K-band for 0.8 arcsec seeing conditions and a wind speed of 10 ms^{-1}. On the other hand, about 2% of the sky is observable with a Strehl ratio of 0.4.

As shown above, both the Strehl ratio achieved on the reference star and the isoplanatic angle are wavelength dependent. These quantities vary in a similar way, leading the Strehl ratio to be larger at higher wavelengths even for large separations. However, the gain in resolution is restrained by the increase with wavelength of the FWHM of the diffraction-limited image with the wavelength. Thus, the K-band (2.2 μm) seems to be currently the best compromise for adaptive optics observations.

5.2 Specific objects

In the previous paragraph the approach was purely statistical with no consideration of the presence or absence of interesting objects in the surveyed area.
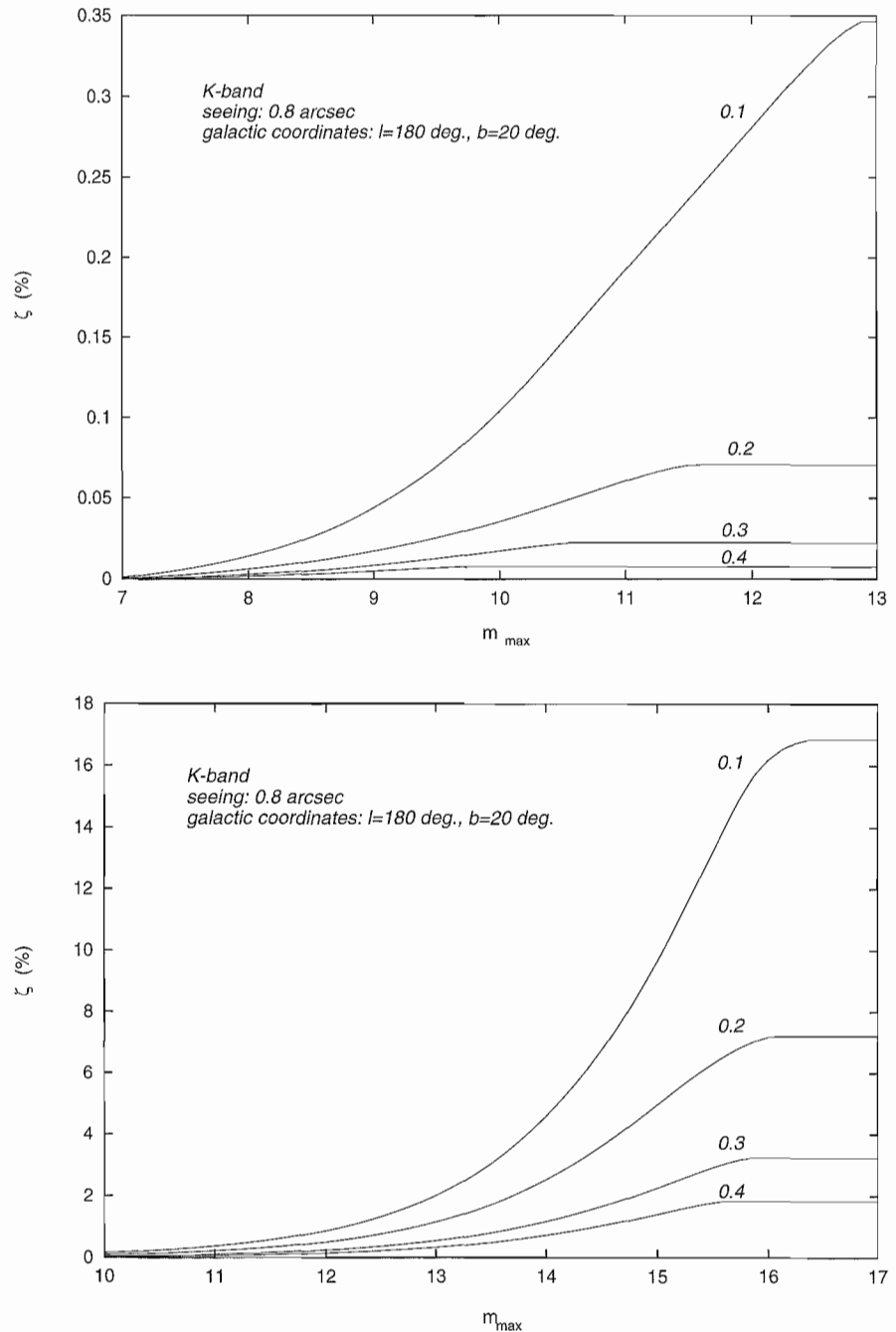

Figure 7: *Sky coverage versus the largest possible magnitude of the star used as reference* m_{max} *for several Strehl ratios (0.1, 0.2, 0.3, 0.4) achieved with COME-ON+* **(top)** *and the VLT* **(bottom)** *systems.*

A few projects will use this approach such as random search for very high redshift field galaxies. However, this is not the usual way of investigation: one aims indeed at observing a specific object. In this case, and until laser guide stars become available, the observation depends on the presence of a bright star in the vicinity of the target and this defines the correction one might expect during the observation.

Following this line one may ask for the probability to achieve a given correction when observing a sample of predefined scientific targets. This was our second approach to assess the potential of the system. To do so a catalogue of targets is cross-correlated with a bright star catalogue. Given the coordinates of the objects, the star catalogue is searched for the star that would give the best correction. A quite similar approach has been followed by Bonaccini *et al.* (1993) in the context of the Italian Galileo project. In their study, however, the image quality does not appear clearly. As an example, we use as a list of possible targets the IRAS point source catalogue, which contains about 250,000 objects, and the HST Guide Star Catalogue for the ref-
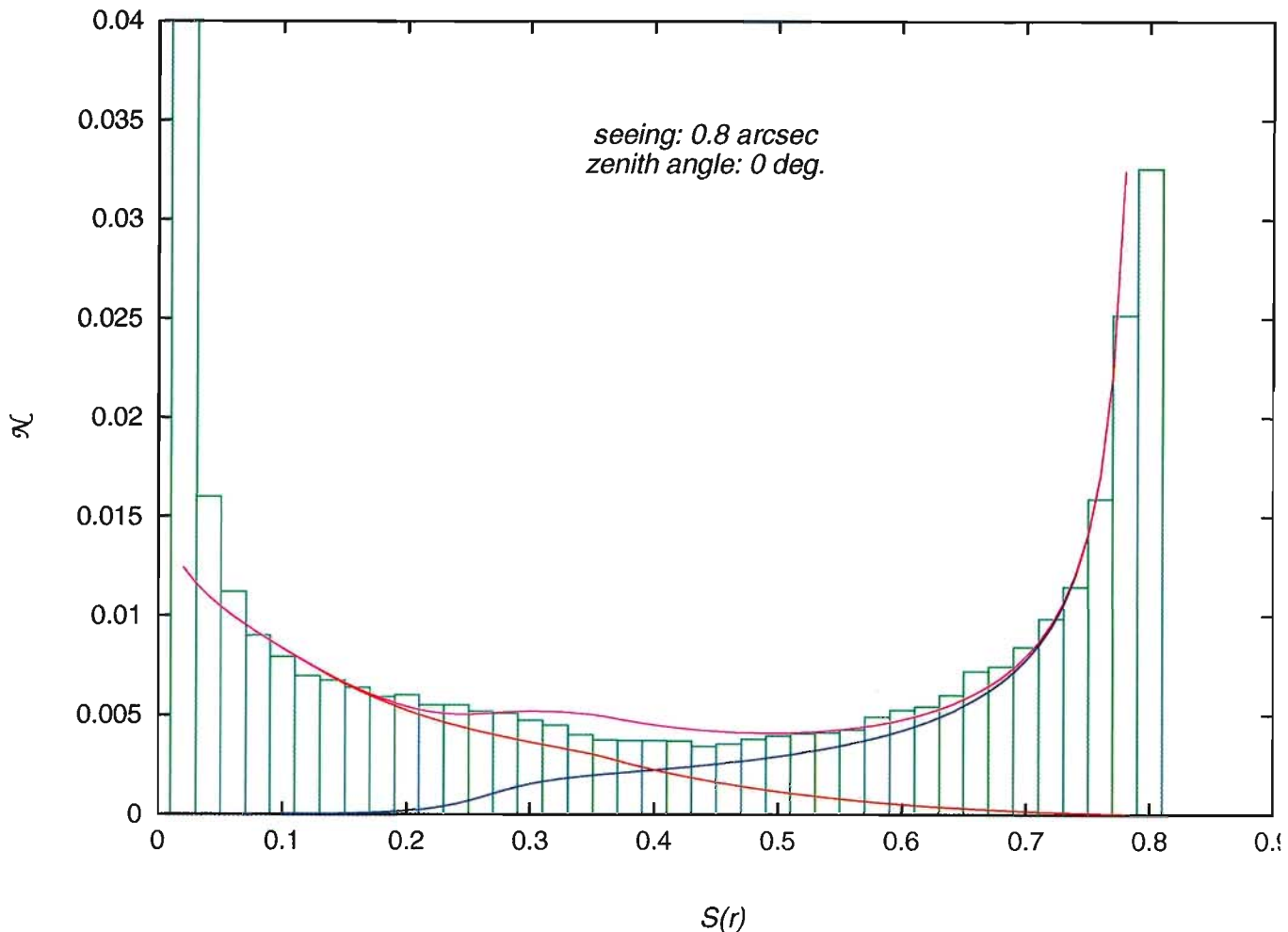
Figure 8: *Percentage of IRAS objects observable with a Strehl ratio within the range S −0.01, S +0.01, obtained from cross-correlation between the IRAS point source catalogue and the Guide Star Catalogue. Overplotted is a model (in magenta), made up with two contributions. The green curve corresponds to observations using a nearby bright star as the reference. The blue curve corresponds to objects bright enough to be used as the reference source.*

erence star catalogue. For each object, a star was searched in the GSC within 1 arcmin and, if present, the Strehl ratio was computed using the characteristics of the VLT adaptive optics system shown in Figures 3 and 4. About 89,000 objects were found to have a star lying within 1 arcmin, which holds for about one third of the catalogue. Figure 8 shows the distribution of Strehl ratios we obtained. Along the y-axis is plotted the fraction of IRAS objects (compared to the whole catalogue) observable at a given correction level. The fraction of observable objects strongly increases at both ends of the diagram. At the small Strehl ratio end, this is because the probability of finding a star in the vicinity of a given object increases as the square of the separation, and thus the probability for a small Strehl ratio increases. At the large Strehl ratio end, there is a large contribution of objects which are present in both GSC and IRAS catalogues. These objects can be used themselves as the reference source and the achieved Strehl ratio is large. Since most of the objects in the GSC have magnitudes smaller than 15, the correspond-

ing Strehl ratio should be most of the time very close to 0.8 and the distribution should be strongly peaked around this value. It can be seen however that the distribution is broad because, due to imprecision in the astrometry, the coordinates of a number of these objects differ in both catalogues.

These two contributions have been modeled. Assuming that stars are randomly distributed in the sky, the distribution of the Strehl ratios possibly achieved at given points of the sky can be computed and is shown as a red curve in Figure 8. To do this, we used the Bahcall and Soneira (1980) models. The second contribution has been computed assuming that the differences in the position of an object in IRAS and GSC obeys Gaussian statistics, with a dispersion chosen to fit the data best. This is the blue curve on Figure 8. The final distribution (in magenta on the plot) is the sum of these two contributions, and one can see that it fits reasonably well the distribution we obtained from the cross-correlation, some of the discrepancies resulting from imperfections of the star catalogue.

One of the most important limiting factors is the magnitude limit of the corrective system. This is particularly true for COME-ON+ which has a limiting magnitude of about 13 for averaged meteorological conditions, that is 0.8 arcsec seeing and 10 ms^{-1} wind speed. For the VLT system it is expected to be somewhat larger in the same conditions. It is of importance to define what would be the optimal magnitude limit. This is particularly important for extragalactic studies and can be investigated, for example, by looking at the number of QSOs as possible targets of such a system. QSOs are indeed promising reference sources since a number of extragalactic projects could use them (morphology of galaxies in clusters, absorption-line systems, host galaxies, etc.). In Figure 9a the distribution of quasars found in the Hewitt & Burbidge catalogue (Hewitt & Burbidge 1993) is plotted as a function of the redshift and the magnitude. One can see the rapid increase, whatever the redshift, of the number of quasars beyond the magnitude 16–17, that is just beyond the foreseen magnitude limit of the VLT adaptive

optics system. This is more striking in Figure 9b where the number of quasars brighter than a given magnitude is plotted, still from the Hewitt & Burbidge catalogue. While there are about 200 quasars brighter than magnitude 16, there are about 600 QSOs brighter than magnitude 17. Thus improving the capabilities of the system by one magnitude could lead to an increase by a factor of 3 in the number of observable QSOs. To achieve this, the integration time of the wavefront sensor might be increased, to the detriment of the quality of the correction, since it results in a decrease of the bandwidth of the system. To achieve a Strehl ratio of 0.1 within 15 arcsec around all QSOs brighter than magnitude 17 would be of great interest.

6. Conclusion

Adaptive optics is a promising technique to overcome the wavefront deformations induced by the atmospheric turbulence and to produce diffraction-limited quality images with ground-based telescopes. The rapid drop in quality of the correction with the distance to the reference star severely limits the fraction of the sky that is observable. This implies that the sky coverage of any adaptive optics system at a given wavelength strongly depends on the magnitude limit for the reference star. The latter should be larger than 17 so that about a quarter of the sky can be observed. This magnitude limit is also required if a copious number of QSOs (the most obvious extragalactic targets) shall become observable. The use of laser guide stars should resolve most of the above limitations (Rigaut and Gendron 1992).

To find a reference star near any potential target, a catalogue of such stars must be made available. It should be complete up to the magnitude limit of the system. At the moment the Guide Star Catalogue is complete down to magnitude 14.5.

It is clear that it is possible to build adaptive optics systems with large potentialities providing that they are able to improve the image quality in a large enough fraction of the sky. Moreover, we may expect exciting results using adaptive optics to perform very high spatial resolution spectroscopy of extended objects.

Acknowledgements
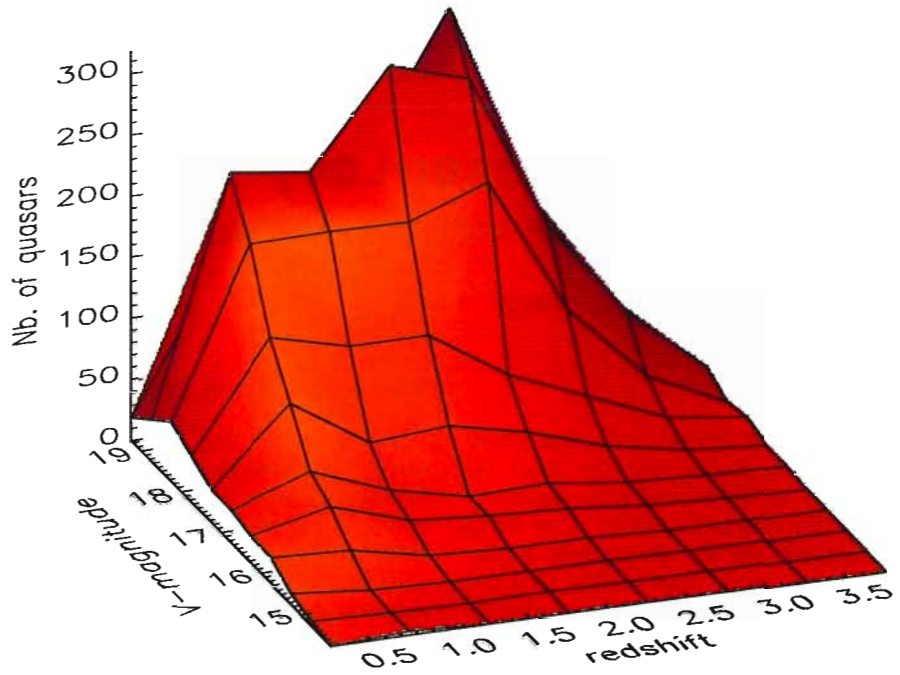
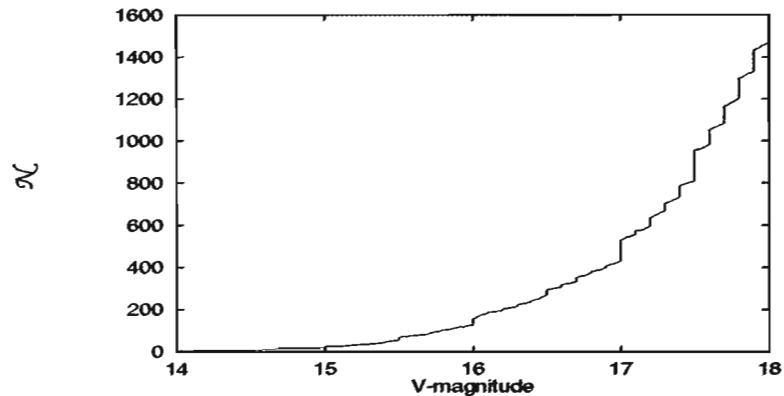### Number of quasars brighter than a magnitude m

Figure 9: **Top:** *Distribution of quasars in the Hewitt and Burbidge catalogue as a function of redshift and magnitude. Note the rapid increase of the number of quasars beyond the magnitude 16–17.* **Bottom:** *cumulative number of quasars brighter than a given magnitude as a function of the magnitude.*

References

Bahcall J., Soneira S., 1980, *ApJS* **44**, 73.
Bonaccini D., Morbidelli R., Ranfagni P. 1993, Internal report of Torino Observatory n° 27.
Hewitt A., Burbidge G., 1993, *ApJS* **87**, 451.
Hubin N., Safa F., Stoffer R., in proc. of the ESO conf. on "Active and Adaptive Optics", Garching, 2–5 August 1993.
Hubin N., Théodore B., Petitjean P., Delabre B., in proc. of the SPIE conf. on "Astronomical Telescopes and Instrumentation for the 21st Century", Kona, 13–18 March 1994.
Merkle F., 1988, *The Messenger* **52**, 5.
Noll R.J., 1976, *J. Opt. Soc. Am.* **66**, 207.
Rigaut F., 1993, PhD Thesis dissertation, Univ. Paris 7.
Rigaut F., Gendron E., 1992, *A&A* **261**, 677.

Comet Shoemaker-Levy 9 Collides with Jupiter
THE CONTINUATION OF A UNIQUE EXPERIENCE

R.M. WEST, ESO-Garching

After the Storm

The recent demise of comet Shoe-maker-Levy 9, for simplicity often referred to as "SL-9", was indeed spectacular. The dramatic collision of its many fragments with the giant planet Jupiter during six hectic days in July 1994 will pass into the annals of astronomy as one of the most incredible events ever predicted and witnessed by members of this profession. And never before has a remote astronomical event been so actively covered by the media on behalf of such a large and interested public.

Now that the impacts are over and the long and tedious work to reduce the many data has begun, time has come to look back and try to appreciate what really happened. This may be easier said than done, for few of the many actors were able to experience the full spectrum of associated events. Most of the astronomers who were directly involved in the observations hardly had time to do anything else, and the interested laymen who watched on their TV screens the frantic activity all over the world were not in the best position to get a balanced overview from all of this. At this moment, two months later, more has become known about the many observational programmes, and the first indications of the exciting science that will ultimately result from the enormous data sets have begun to emerge.

The 22nd General Assembly of the International Astronomical Union, held during the second half of August in The Hague (The Netherlands), offered the first opportunity to learn in more detail about the outcome from the very successful, world-wide observational efforts. Two four-hour sessions were ably organized at very short notice by Catherine de Bergh, David Morrison, Mike A'Hearn and Alan Harris. More recently, a meeting of the La Silla observers took place on September 12 at the ESO Headquarters in Garching.

Here follows a short and most certainly quite incomplete overview of the current status of the SL-9 observations and their great potential for new knowledge, based on the presentations during these meetings.

Six Hectic Days in July

ESO was but one of many professional observatories where observations had been planned long before the critical period of the "SL-9" event, July 16–22, 1994. It is now clear that practically all major observatories in the world were involved in some way, via their telescopes, their scientists or both. The only exceptions may have been a few observing sites at the northernmost latitudes where the bright summer nights and the very short evening visibility of Jupiter just over the western horizon made such observations next to impossible. In addition, it is most gratifying that legions of amateur astronomers immediately went into action when it became known that the changes on Jupiter could be perceived even with very small telescopes.

During the week of the impacts, press conferences were held at many observatories; ESO arranged a series of very well attended media events in Garching and in Santiago de Chile. A day-to-day chronicle of what happened during this period may be found in the "ESO SL-9 News Bulletin" of which a total of 14 issues were prepared between July 10 and 26. The full text, as well as many images and graphics may still be obtained from the ESO WWW Portal (http://http.hq.eso.org/eso-homepage.html) or via anonymous ftp (ecf.hq.eso.org; directory: pub/sl9-eso-images).

The observing possibilities were best from the southern hemisphere and, by good fortune, the weather in South Africa and Australia was very co-operative during the critical week. It was less so in Chile, where La Silla, Cerro Tololo and Las Campanas were effectively clouded out during the latter part of the impact period. Long series of excellent observations were also made from La Palma and Calar Alto (Spain), as well as from Hawaii and observatories in Japan. Although details are still lacking, it is apparent that the programmes at many observatories in other countries were also very successful. However, a complete list of all SL-9 observations has yet to be compiled.

At ESO, ten telescopes were in op-eration during the first nights and, as in other places, an extremely rich data material was secured. It quickly became evident that infrared observations, especially imaging with the far-IR instrument TIMMI at the 3.6-metre telescope, were perfectly feasible also during daytime, and in the end more than 120,000 images were obtained with this facility. The programmes at most of the other La Silla telescopes were also successful, and many more Gigabytes of data were recorded with them. Brief reports from some of these programmes are brought in this *Messenger* issue. The fact that a significant amount of observing time was allocated after the main event was over, turned out to be a major blessing, and some of the most interesting data were obtained during the period immediately following the last impact on July 22.

It is not yet possible to estimate the total amount of SL-9 observational data now available at observatories all over the world, but it may well run into many tens, perhaps hundreds of Gigabytes. One of the most urgent problems is now to get an overview of all these data so that observers from different sites will be able to establish effective collaborations. It has also become evident that in order to understand the very complex processes around the impacts, in particular the detailed evolution of the plumes ("fireballs") that rose above the impact sites, it will be necessary to intercompare data from many different instruments with a variety of techniques, ranging from the high-resolution, extremely detailed UV and visual images of the Hubble Space Telescope, to "movie-like" image sequences obtained with infrared instruments like TIMMI, and long-exposure, high-dispersion spectra of these plumes obtained with more classical spectroscopic equipment.

Much Hard Work Ahead

The observed effects were extremely spectacular, from the incredibly bright "fireballs" (or "plumes") which rose above the limb of the planet, to the intricate and changing forms of the resulting "pancake" clouds, of which several – to the greatest surprise of many astronomers –

are still visible at the end of September, although less prominent than before.

Until now, most observational programmes have not progressed much beyond a purely phenomenological description of what was seen. However, it is also the task of all astronomical research to progress far beyond such a simple description; the ultimate goal is of course to understand the physical processes behind the event. This calls for "reduction" and "interpretation" of the data. The first is a long and complicated procedure, involving different types of calibrations in order to "clean" the raw data from all possible, extraneous effects and to extract the quantitative information that is needed to arrive finally at a global understanding of what really happened.

For this reason, most observers have so far only been able to answer a few of the many questions which are now being eagerly asked from all sides. Having been treated to real fireworks of "real-time science" and "quick-shot guesstimates" (greatly facilitated by the incredibly successful initiation during this event of the "astronomy information superhighway", especially via *internet*), and having been confronted (not to say "spoiled"!) with hundreds of impressive pictures of mushroom clouds in the southern hemisphere of Jupiter, the media and the public now keep asking when we will finally know what all of this means.

In this connection, it is sometimes difficult to explain that while modern astronomical observing techniques have become extremely efficient – and this is the main reason that it was possible to respond to the unique challenge of the SL-9 event in such an impressive way and to obtain such a rich data material – this does not mean that this science has also progressed to the point where the data reduction and the astrophysical interpretation can follow at the same pace. On the contrary, I think that a major lesson of this event is that more resources than before must now be directed towards this area – otherwise we are at high risk to drown in the future data floods from the new giant telescopes like the VLT and its hosts of incredibly effective instruments.

The Comet Fragments

So what have we learned so far about the comet, about Jupiter and about the impact process itself? As expected, unique observations like these have led to important new knowledge, but at the same time they do not fail to raise a host of new and difficult questions.

First of all, the comet was obviously a complex body. From the diversity of the impacts and their observed effects, it seems that there were important differences between the individual frag-

Impact Times for Fragments of Comet Shoemaker-Levy 9

The following list of impact times (UTC times received at Earth, i.e. light-time corrected) was prepared by Don Yeomans and Paul Chodas (JPL) in early August 1994.

Fragment	Date	Prediction (h:m:s)	Accepted impact time and 1 σ error
A	July 16	20:00:40	20:11:00 (3 min)
B	July 17	02:54:13	02:50:00 (6 min)
C	July 17	07:02:14	07:12:00 (4 min)
D	July 17	11:47:00	11:54:00 (3 min)
E	July 17	15:05:31	15:11:00 (3 min)
F	July 18	00:29:21	00:33:00 (5 min)
G	July 18	07:28:32	07:32:00 (2 min)
H	July 18	19:25:53	19:31:59 (1 min)
J	July 19	02:40	Missing since 12/93
K	July 19	10:18:32	10:21:00 (4 min)
L	July 19	22:08:53	22:16:48 (1 min)
M	July 20	05:45	Missing since 7/93
N	July 20	10:20:02	10:31:00 (4 min)
P2	July 20	15:16:20	15:23:00 (7 min)
P1	July 20	16:30	Missing since 3/94
Q2	July 20	19:47:11	19:44:00 (6 min)
Q1	July 20	20:04:09	20:12:00 (4 min)
R	July 21	05:28:50	05:33:00 (3 min)
S	July 21	15:12:49	15:15:00 (5 min)
T	July 21	18:03:45	18:10:00 (7 min)
U	July 21	21:48:30	21:55:00 (7 min)
V	July 22	04:16:53	04:22:00 (5 min)
W	July 22	07:59:45	08:05:30 (3 min)

In setting forth the accepted impact times given in the final column, the priority of the various available techniques is as follows:

1. GLL PPR timing (fragments H and L).

2. When definitive flash times are available, with subsequent plume observations noted about 6 minutes later), we generally took the impact time as one minute before the flash time since the PPR instrument recorded its first signals about one minute before the reported flash times (fragments D, G, Q1, Q2, R, S, V, and W).

3. Estimates determined from HST longitudes.

4. Estimates determined from first plume observation minus 6.2 minutes.

5. Chodas/Yeomans prediction with empirical adjustment of + 7 minutes.

The impact times for fragments A, C, E, K, and N were determined by considering the ephemeris prediction error (about 7 minutes early for most fragments), the times determined from the HST longitude estimates (uncertainty = 3–4 minutes or more) and the times determined from plume observation times (impact time = plume observation time less 5–8 minutes). An effort was made to consider and balance these three factors and the uncertainties on the estimated impact times reflect our confidence level. For fragment F, the impact time was determined using the ephemeris prediction and the Lowell Observatory estimate of when the F spot was seen on the terminator. In the absence of any quantitative impact time observations for fragments P2, T, and U, only the ephemeris prediction was used (plus 7 minutes). The impact time estimate for fragment B is based upon observatory reports and is relatively uncertain because the impact time occurs before the ephemeris prediction and well before the estimate determined from the HST longitude estimate.

ments; this provides an indication that the cometary parent body must have been an inhomogeneous object. On the other hand, polarimetric measurements of the dust clouds around the individual nuclei do not show any perceptible differences, so the dust produced by them appears to have been rather similar. Some nuclei, which were thought to be "large" because they were surrounded by much dust and were relatively bright, turned out to produce comparatively small effects during impact, and in other cases, it was just the opposite. The famous example is the first fragment (A) that took everybody by

surprise with its unexpectedly violent impact effects, while the second (B), although twice as bright, showed no observable effects at the moment of impact, although the corresponding atmospheric "hole" was later seen.

No gas was ever observed in the comet, despite extreme efforts to detect at least the usually strong cometary CN lines with the ESO NTT. So the fragments apparently produced only dust comae and tails. Is this reasonable? Would not the break-up process have been accompanied by the escape of at least some gas, and would not the later release of

dust have shown a small amount of gas at some time? Could it be that the comet, after all, was of an unusual type, or was the dust production in this case not driven by gas, as is commonly thought? Or does this imply that we are mistaken in our present assumptions about how a "normal" comet ought to behave under the present circumstances? It was most probably not an asteroid though, as has also been surmised, the disappearance from view of some of the fragments makes this very unlikely. Another strange and unexplained effect is the elongation of the images of the fragments in the direction of Jupiter that was clearly observed during the last few days before the impacts. We obviously do not yet fully understand the dynamics of the dust in Jupiter's vicinity.

The Impact Process

It appears that the "meteoric" phase of the impacts, that is the entry of the fragments into the Jovian atmosphere and the expected heating of their surfaces by the associated friction, was not observed from the ground in reflection from the Jovian moons as predicted. The Galileo images of the W event which have now been transferred do show a light flash that lasted a few seconds, but it was not particularly strong and would probably not have been detected in reflection from a Jovian moon by the available ground-based instruments. Why didn't the cometary fragments glow stronger during their encounter with the upper atmosphere? The reports of a possible colour change of the moon Io during the time of some of the impacts are still unexplained. And there are no obvious detections of IR reflections from Jupiter's dust ring.

It does appear that the total energies liberated were larger than anticipated, but it will not be possible to make accurate estimates, before the processes in and around the resulting plumes are better understood. From the amount of measured infrared emission alone, it seems that the cometary fragments must have been at least several hundred metres across in order to provide enough kinetical energy, but this is most certainly a lower limit only. Other estimates point towards the release of perhaps 1 million Megatons of energy or even more during the larger impacts – this would then correspond to diameters well over one kilometre for the largest fragments.

It appears that it may already now be possible to determine the approximate depth of the penetration by the fragments into the atmosphere. The observations of large amounts of NH_3 and relatively little H_2O in some of the plumes (see below) indicate that the most energetic ex-

plosions most likely took place between the second (assumed to contain NH_4SH aerosol) and the third (H_2O) cloud layers.

The Fireballs and the Plumes

The detailed circumstances of the final explosions and the resulting fireballs pose one of the greatest interpretative problems of the SL-9 event. Several ground-based infrared instruments detected "precursors" in the form of small and bright, rapidly expanding clouds appearing above the limb within about one minute after the presumed impact times as determined by the all-disk photometer onboard Galileo. The Hubble Space Telescope high-spatial-resolution near-IR and visual images show the same phenomenon.

It is not at all obvious what this signifies, but it is now generally believed that this is the image of a rising fireball (during its continued development also referred to as "mushroom cloud" and "plume"), still in Jupiter's shadow and shining in the optical region by its own light because of its very high temperature (values in excess of 10,000 degrees have been mentioned). Rising ever higher while it rapidly cools, the total intensity of the plume above the impact site first decreases, but as it continues to grow and the upper parts move into sunlight, the optical brightness again increases as more and more sunlight is reflected.

The cooling process leads to a sharp maximum of radiation in the infrared spectral region, some 10–15 minutes after the impact – the moment of maximum and the overall shape of the light curve is determined by a complex combination of temperature, size of the plume and visibility (geometry), into which enters the effect of the rapid Jovian rotation that quickly brings more and more of the plume into view from the Earth. It will be very difficult to untangle these effects from each other and to arrive at a consistent description of the plume development. Moreover, some pronounced humps in several of the IR light curves point towards multiple impacts, e.g., at the L- and R events, adding yet another formal difficulty to this procedure.

The Long-Term Atmospheric Features

The further development of the plumes is also not entirely unambiguous, although there is now a general consensus that the debris from the explosion in the end settles into "pancake"-shaped clouds at an altitude high above the visible clouds that corresponds to about the 1 millibar level in the atmosphere. Several types of observations indicate that these clouds are made up of "haze"

(aerosols) and not by molecules (e.g., their IUE UV spectra are rather flat). In the IR spectral region, they look bright because of reflected sunlight and they hide the features below. In the visible spectral region, they are transparent at many wavelengths. They are generally darker than the Jovian cloud layer, except when viewed at the wavelengths that correspond to the strongly absorbing methane bands; here the clouds again appear bright on the very dark background.

The excellent HST images, for instance those obtained of the G impact site just after its appearance at the limb, show a very complex structure near the impact sites. In the middle is a "black" hole, which probably represents the material around the "funnel" excavated by the impacting fragment. To begin with, it is surrounded by several, partly incomplete "rings" of rather short lifetime. The inner ones are possibly shock waves in the atmosphere moving outward from the impact site, while the outer, broad horseshoe-shaped features appear to represent the resettling debris that was lifted to very high altitudes before coming back down. When compared to impact experiments in the laboratory, this pattern fits quite well with the direction and the 45° angle of entry of the cometary fragments.

It is in this connection also interesting to note that the very bright sky observed in Europe and Asia during the night following the Tunguska impact on July 30, 1908, may now be explained by a similar effect, namely the very rapid deposition over a large area of debris (dust) that moves along high, ballistic orbits from the impact site. Moreover, the trail of the Tunguska object was described as a large smoke column. This would seem to strengthen the interpretation of this terrestrial event as being of a basically similar nature.

Many of the later impacts hit the sites of earlier ones and the resulting geometric configurations soon became very complex. The further development of the cloud patterns has since been followed at many observatories. While the smaller clouds have (almost) disappeared in the meantime, the larger complexes are still visible, also in smaller telescopes. Diffusion in longitude because of the wind in the Jovian atmosphere set in early, and after some time, spreading in the north-south direction was also observed. Two months after the last impact, the cloud contours continue to be gradually washed out and there is an increased degree of mutual overlap. Nobody knows at this moment how long these features will continue to be visible. It is unfortunate that the monitoring of these changes will soon be interrupted for some time while

Jupiter moves behind the Sun as seen from the Earth.

The Composition

The composition of the plumes was investigated by spectroscopy in many different wavebands. While no entirely new molecules have been found during quick-looks at the very large data material, it is expected that further analysis will eventually make it possible to document in some detail the complex chemical processes that took place during the early phases of expansion and subsequent collapse. The following elements and molecules have been seen in the spectra: Li, Na, Mg, Mn, Fe, Si and S; NH_3, CO, H_2O, HCN; H_2S, CS, CS_2, S_2; CH_4, C_2H_2, C_2H_6, and possibly others.

Of particular interest is here the detection of the strong Li line at 6708 Å in emission: from where does this element come, the comet, Jupiter or both? I am not aware that Lithium has ever been observed in any comet. Enormous quantities of molecular sulphur (S_2) were seen in high-dispersion UV spectra obtained with the HST. A very first estimate indicates no less than $\sim 10^{15}$ g in one fireball, or almost 1% of the estimated total mass of the nucleus of P/Halley ! Although there was surprisingly much sulphur in P/Halley (about 9% of the carbon content), this material must come mostly from Jupiter and this observation provides the first unambiguous proof of the (predicted) presence of large amounts of this element in the deeper layers of the Jovian atmosphere. One of the greatest mysteries may be the almost complete absence of water in the plumes – in 1986, P/Halley was found to consist to 80% of water ice – where did the cometary water go? Or maybe the question should be reformulated: with which elements did these hydrogen and oxygen atoms later recombine to form new molecules?

Very rapid spectral changes were seen in the plumes. For instance, while emission lines of Li, Na, K and Ca were present in the first spectrum of the L impact plume obtained at the Pic-du-Midi observatory, the next spectrum only 20 minutes later was entirely different. At ESO, the IRSPEC spectra obtained at the NTT showed highly excited CH_4 emission in the first spectra of the H impact site. The intensity decreased very rapidly until it could no longer be seen 30 minutes later. KAO far-IR observations also showed hot CH_4, and submillimetre HCN spectra obtained with the JCMT telescope at Hawaii showed line broadening in areas of several impacts.

It appears unlikely that a fully coherent picture of what happened in the plumes will ever be obtained unless an unprecedented synthesis of the complex information in all available spectra is attempted. At this moment, condensation of CO and possibly other species is thought to play an important role. Moreover, the fact that for instance the PH_3 emission did not change much indicates that the deep atmosphere of Jupiter was not altered very much by the impacts.

The Jovian Magnetosphere

Another, very interesting result is the detection of enhanced auroral activity in the Jovian atmosphere which is clearly related to the impacts. This was first seen in the UV images from the HST that showed a strong effect near the northern pole. It is assumed that this is due to the rapid motion along the magnetic field lines of charged particles created at the impact site. The unexpected detection of symmetric emission patterns in the northern hemisphere in IR lines of H_3^+ and H_2, as seen in the days after July 22 by IRSPEC, is another strange phenomenon that may possibly be contributed to the same mechanism.

The predictions about possible effects of cometary dust entering into the Jovian magnetosphere ranged from negligible to dramatic. One uncertain element was of course the amount of dust, but it was very difficult to model the physical processes. The same was true for the overall effects on the faint Jovian dust ring because of dust accumulation and so were the changes in the Io torus because of charged cometary particles.

While there have been no reports about observations of changes in the Io torus or in the Jovian dust ring, the first accounts about apparent variations in the Jovian radio emission may not have taken fully into account its inherently variable nature, due to the changing aspects of Jupiter's offset dipole field. Indeed, there were conflicting claims during the first days, ranging from no changes at all, e.g. the first summary of the observations from the Ulysses spacecraft, to very significant changes purportedly registered in some places.

However, after the firm establishment of valid baseline models it has become clear that a gradual, but significant enhancement of the radiation was actually observed, amounting to about 20 % at 13 cm wavelength. Increases were also seen at longer wavelengths, perhaps even in excess of this figure. An interesting effect was the apparent inward motion of the "radiation points", as observed at Westerbork and with the VLA. The physical reason for this is not yet established.

Seismology

What about the seismological measurements which may finally give us the first opportunity to elucidate the inner structure of Jupiter? It is still too early to say anything, except that the necessary observations, in the form of more than 100,000 infrared images, have indeed been secured and that the extremely tedious data analysis has already started. It will take a long time to eliminate all the instrumental effects and even longer to extract any faint, seismic message from these frames. Incidentally, certain reports about ring-shaped structures which were purportedly seen on some CCD frames and which were provisionally interpreted as possible waves in the Jovian atmosphere, are now believed to be instrumental and/or reduction artefacts.

Future SL-9 Meetings

The analyses of the voluminous SL-9 data continue, but it is unlikely that a coherent picture of what really happened will emerge before next year. In the meantime, the observers stay in contact and have begun to exchange information about this process. They will also meet at regular intervals. The first major presentation will take place during a one-day session at the DPS meeting in Bethesda near Washington DC on October 31, 1994. A major IAU colloquium is planned for May 1995 at the STScI in Baltimore, Maryland, USA.

The possibility of holding a smaller meeting at ESO in February 1995, mainly with the participation of observers in Europe, is now being looked into and a decision is expected to be taken by mid-October 1994. For the latest information, please consult the ESO WWW Portal (address see above).

Conclusions

SL-9 is no more. By its glorious death it has provided us with an unequalled and exciting opportunity to study the inner parts of a comet and to analyse the Jovian atmosphere. It also has enabled us to learn what they do to each other when they collide at 60 km/sec.

When asked what the preliminary information from this event can tell us about a similar one on the Earth, Mike A'Hearn, the summary speaker at the IAU General Assembly sessions on SL-9, said that there is now little doubt that a cometary impact of the same nature and dimensions would not dissipate much energy in the upper atmosphere and that it would obviously reach the Earth's solid surface and produce the associated effects. The continued study of the SL-9 observations will most certainly also cast more light on this very relevant terrestrial problem.

Imaging of Comet SL-9 in the Gunn Photometric System

G. CHERNOVA and K. JOCKERS, Max-Planck-Institut für Aeronomie, Katlenburg-Lindau, Germany

Comet Shoemaker-Levy 9 was observed with the focal reducer of the MPI for Aeronomy attached to the ESO 1-m telescope from April 25 to May 1, 1994, when the comet was very close to opposition. The aim of the study was to determine the brightness and colour distribution of the individual nuclei and their dust tails. These observations therefore did not directly address the impending collision. Instead, we wanted to study the fragments of a parent comet and the dust surrounding them, in order to compare this dust, which probably was liberated only during the break-up, with the dust of other comets observed at Jupiter's distance, e.g., comet Schwassmann-Wachmann 1. As the cometary fragments all come from the same parent nucleus, colour differences between individual nuclei would indicate an inhomogeneous nucleus.

More than 100 useful individual frames were obtained between April 27 and May 1 in the G, R, and I bands of the intermediate-band photometric system of Thuan and Gunn (unfortunately, our lens optics does not allow to use the common wide-band photometric systems). For each night, all useful images of one colour are combined into a single image, free from stars, in order to increase the signal-to-noise ratio.

The night of April 27/28 has already been evaluated and Figure 1 shows the resulting G-band image in a false colour display. Nucleus A(21) is on the top left and nucleus W(1) at bottom right. The following Gunn G magnitudes have been derived (the fluxes are taken in square boxes of 5×5 pixels, i.e. 8×8 arcsec, corresponding to $21,000 \times 21,000$ km at the comet): 20.6 ± 0.4 A(21), 20.0 ± 0.3 B(20), 20.2 ± 0.3 C(19), 19.3 ± 0.15 E(17), 19.6 ± 0.20 F(16), 18.4 ± 0.09 G(15), 18.8 ± 0.11 H(14), 18.5 ± 0.09 K(12), 18.9 ± 0.12 L(11), 19.1 ± 0.17 P2(8b), 19.3 ± 0.15 R(6), 18.9 ± 0.11 S(5), 19.5 ± 0.17 W(1). The nuclei P1, Q1 and Q2 are too close together to measure their flux individually in 8×8 arcsec boxes. The Gunn G magnitude of P1, Q1 and Q2 together, measured in a square box of 11×11 arcsec is 17.7 ± 0.08. At the time of these observations the phase angle was less than 0.2 degrees, so some opposition brightening must be present.

Within the noise limits the nuclei all have the same colour. Figure 2 shows the colour difference in magnitude per pixel, Gunn G – Gunn R, as a false-colour image. At the bottom left part of the image there is no emission and the image represents only noise. About half of the pixels have cyan colour, corresponding to zero value, given by MIDAS to the logarithm of a negative argument. The individual comet fragments have a similar colour, and there seems to be a colour trend into the tails. Such a trend is expected, as the dust particles are likely to be sorted by the solar light pressure into different sizes in different tail regions, and different dust sizes may give differ-
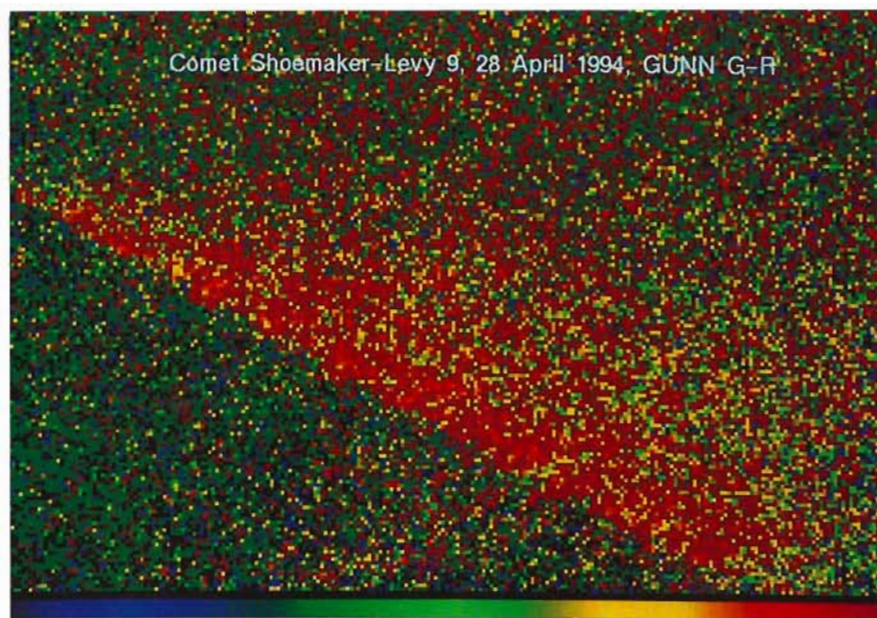

Figure 1.

Figure 2.

ent colours. Whether the observed trend is indeed real, depends on the accuracy of sky background subtraction, which still needs to be assessed.

To determine the opposition effect and obtain information on the dust size, our images must be compared with images of other observers, obtained at other times and phase angles. It is interesting to note that no significant change in the appearance and direction of the tails occurred when the comets passed opposition. This indicates that the dust particles do not move under a combined central force of solar gravitation and light pressure repulsion, but are significantly influenced by Jupiter's gravity field.

Predicting the Impacts

R.M. WEST and O. HAINAUT, ESO-Garching

Astrometry of SL-9

For several reasons, it was of importance to predict the locations and times of the impacts of the SL-9 fragments with the greatest possible precision. The first, approximate calculations were performed towards the end of 1993 by Brian Marsden at the Minor Planet Center. They were based on long observation series, in particular by Jim Scotti at Kitt Peak, and correctly showed that the impacts would all happen in the southern Jovian hemisphere, but the timings were still not very accurate.

More astrometric observations were made during the first months of 1994, and the predictions slowly gained in precision. Don Yeomans and Paul Chodas at JPL used the special orbital software available at that institution (from where the Galileo spacecraft is navigated) to further improve the accuracy and in mid-June, about one month before the event, the 1σ timing accuracy had been reduced to about 30 min for many of the fragments. This corresponded to 95% intervals of approximately ± 1 hour, i.e., not yet good enough for most purposes.

The ESO Observations

A few nights were allocated in early May at the Danish 1.5-metre telescope at La Silla to our astrometric programme for comet SL-9. In view of the need for the highest possible accuracy, we were very glad to learn at the same time that it would be possible to make unpublished Hipparcos positions available and we are very thankful to Michael Perryman (ESTEC) and Catherine Turon (Paris) for having provided us with these data.

Indeed, the first SL-9 observations showed that it would be possible to obtain a formal accuracy of about ± 0.2 arcsec in both coordinates. There was a problem, however, in that our observations appeared to be systematically offset by 0.5–0.7 arcsec from those by other observers. An analysis of this problem showed that this was most likely due to the lower astrometric accuracy of the Guide Star Catalogue (GSC) which formed the base for the other measurements. Note, however, that this catalogue was compiled to serve a different purpose and was never claimed to be of the highest perfection in astrometric terms. The offset was in the sense that the Hipparcos-based ESO positions would tend to move the times of the impacts later.

During the first 14 days of July, we provided Brian Marsden and Don Yeomans with (almost) daily positions of most of the SL-9 fragments. We wish here to acknowledge the extremely positive attitude by many La Silla observers (see below), who graciously allowed us to use their telescopes for astrometric exposures in the early evening, and some of them even did the observations for us.

The subsequent procedure was the same every day. One of us (O.H.) cleaned the exposures at La Silla and immediately transferred them to Garching over the internal link. Here the other (R.W.) measured the secondary astrometric standards on an ESO Schmidt plate, made the transfer to the CCD frame and obtained the positions of the comet fragments. They were then sent on to the orbital computers in the afternoon and new orbits became available a few hours thereafter. On several occasions, new impact predictions were also made.

It turned out that the ESO observations carried a great weight in the end, when it became more and more difficult for all observers to image the comet as it came very close to Jupiter. The last week we were pretty much alone in the field. The very last, measurable frames were obtained with the NTT on July 15.0 UT, or less than 48 hours before the first impact; the night thereafter, the strong straylight from Jupiter would have been too dangerous for the ultra-sensitive CCD array.

Still, we were not the last to see the comet. Observations of some of the latter fragments were made a few days later by the HST, just a few hours from impact, and David Jewitt at Hawaii obtained some final positions by means of the coronographic technique (covering Jupiter with a mask in the telescope) at the same time.

The Prediction Accuracy

The final predictions were believed to be good to about ± 8 minutes ($1\sigma \sim 4$ minutes). However, although there is still some uncertainty about the exact impact times for many of the fragments – the definitive values will probably have to wait until the Galileo data have all been reduced – it now appears that the predictions were generally 5 - 7 minutes too early.

It is not yet known what the real cause for this discrepancy is, but at least part of it may probably be explained by the above-mentioned GSC systematic offset. It is the intention, however, to look into this to learn whether other effects could possibly have been present.

In this connection, the hitherto unexplained observed elongation in the direction of Jupiter of most of the fragments as they came very close will also have to be studied; perhaps there is a connection between the two effects? For this, a careful morphological/photometrical study will now be made of the ESO astrometry frames.

Searching for SL-9 Impact Light Echoes – a Challenge for High-Speed Multi-Channel Photometry

H. BARWIG and O. BÄRNBANTNER, Universitäts-Sternwarte München, Germany

Shortly after the announcement of probable impacts of Comet SL-9 on the far side of Jupiter, the idea was born to use suitable Jovian moons as mirrors in order to witness the very first impact phenomena which would otherwise not be directly visible from Earth. First estimates of the energies released in the optical during the entry of the comet fragments into Jupiter's atmosphere indicated possible flash-like illuminations of the inner Jovian satellites increasing their brightness for a moment by up to a few per cent. We therefore proposed high-speed multi-colour photometry of the Gallilean moons during the predicted impact times. The aim of this programme was to derive the actual impact times at Jupiter and to estimate the flash temperature as well as the energy released in the visual wavelength range. The knowledge of the exact impact times would establish reliable reference points for the proposed studies of the propagation of impact phenomena through the Jovian atmosphere and for seismic observations. Furthermore, accurate impact times could help to select and transmit to Earth the most interesting images obtained by the Galileo spacecraft from the far side of Jupiter.

Our multi-channel multi-colour photometer (MCCP), mounted on the ESO 1-m telescope was thought to be the most suitable instrumentation for a light-echo search. This special photometer allows three light sources in the focal plane of a telescope to be selected by using optical fibers. Each of them is connected to a prism spectrograph providing UBVRI signals to photon- counting detectors. Thus, simultaneous multicolour observations, e.g., of a variable programme star, of a nearby comparison and of the sky background can be performed with a maximum time resolution of 20 ms. In particular, these measurements allow to compensate for variable atmospheric extinction by applying the so-called standard reduction procedure which computes the intensity ratio of two star channels after individual sky subtraction.

A search for impact light echoes requires simultaneous monitoring of at least two Jovian satellites and of the sky background. Due to different radial distances to Jupiter only the moon nearest to the impact site is supposed to exhibit an observable flash reflection which, even under non-photometric conditions, should become visible after data reduction. Originally, the input fibers of the

MCCP were fixed by means of acrylic masks which had to be prepared prior to observations. However, for our observing programme this method had to be replaced by computer-controlled positioning devices for each fiber since differential orbital motions of the Jovian satellites require continuous centring of the individual fibers. This difficult task could be completed after four months. The new device was then successfully tested at the Wendelstein observatory in the Bavarian Alps a few nights before

shipping the MCCP to La Silla at the end of June.

During our first observing night at La Silla on July 15, all photometer components as well as the measuring procedures were checked again (Fig. 1). A CCD camera was used to guide the ESO 1-m telescope on the rim of the Jovian disk whereas two moons were monitored through diaphragms in front of the fiber-positioning devices. For their individual tracking motions, a programme provided by O. Montenbruck (DLR) was used to
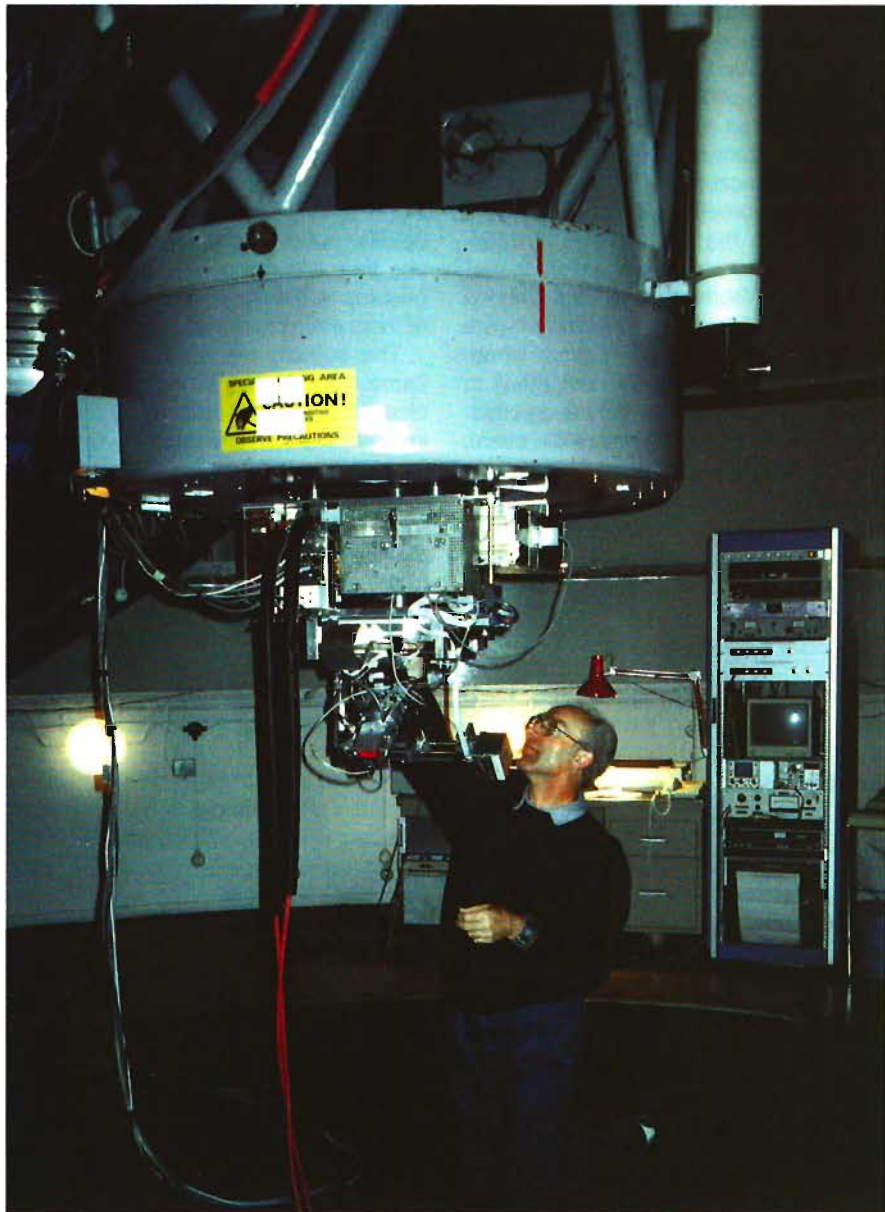

Figure 1: *The multi-channel multi-colour photometer MCCP mounted at the ESO 1-m telescope. Final fiber check by O. Bärnbantner.*

keep the satellites perfectly centred in the diaphragms for several hours.

According to the impact time predictions, only 3 events occurred during night time at La Silla (fragments B, F, V). Two additional fragments (L, U), which impacted during dawn, required of course clear skies for optical photometry. After the spectacular A impact observed in the IR from La Silla in the afternoon of July 16, we were optimistic to detect a flash signature during the impact of fragment B which was much brighter than A in images of the comet train. Half an hour before the predicted time we started to measure the surface brightness of Europa and Callisto every second. The individual data were displayed on-line on a graphic monitor to watch for any sudden brightness increase exceeding the photon noise level. Unfortunately, the observations were strongly affected by clouds which prevented on-line detection of any possible flash echo. Preliminary data reduction immediately thereafter did not reveal any significant peak in the light curves either.

The second event observable from La Silla during night time was the impact of fragment F. This time we set the fibers on Ganymede, Callisto and the sky, respectively. Though the post-impact plume caused by this SL-9 fragment was clearly detected by ESO observers in the IR, fast-moving clouds which partly reduced the visual transparency to only a few per cent, once again prevented on-line searching for an impact light echo.

As an example for the provisional data reduction performed immediately after observation, the raw I-band light curves of Ganymede(A) and Callisto(B) are displayed in Figure 2. They were increasingly affected by thick clouds during the predicted impact time interval. The reduced light curve of Ganymede(C) is plotted below. No flash signatures significantly exceeding the noise of the mean relative brightness (1 s ~ 1 %) could be detected so far.
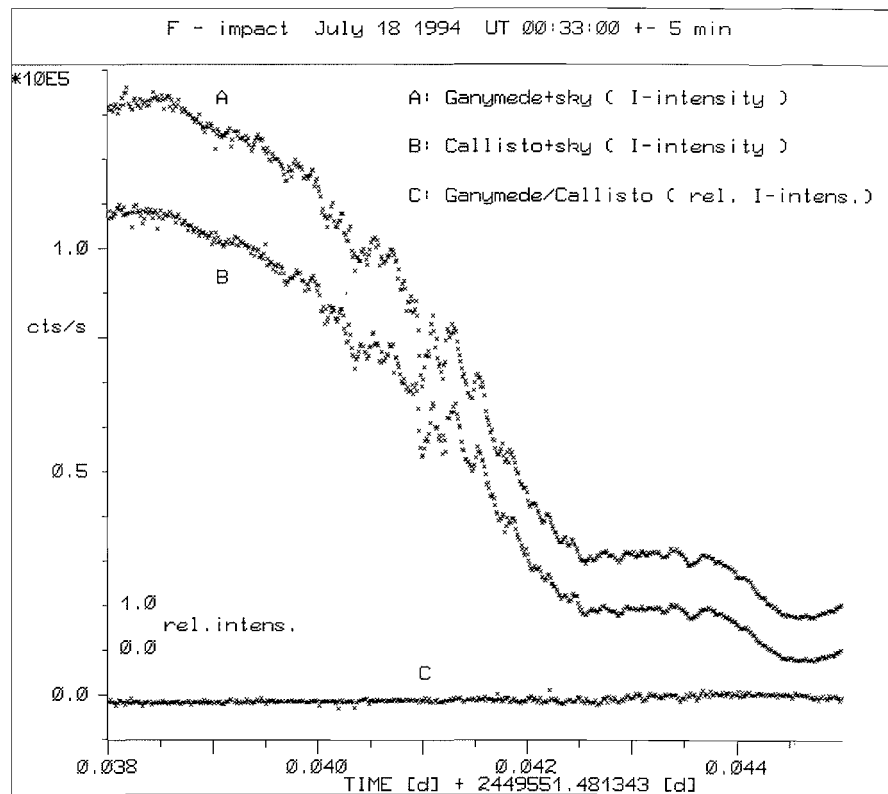

Figure 2: *Example of the standard reduction procedure: the relative brightness of Ganymede during the impact of fragment F.*

The remaining impact events observable from La Silla were much less favourable for a search for visual light-echo effects due to the low S/N during dawn and due to the fact that only the comparatively distant satellite Callisto could have been used as flash reflector. These photometric observations however failed because of unfavourable weather conditions.

Similar photometric programmes have also been performed by two other groups at La Silla using CCD cameras (PIs: K. Horne, B. Sicardy) and also by many other observers around the world. When their photometric data become available,

a concerted effort will be made to search for probably very faint, coincident flash signals, which might still be hidden in individual light curves behind features that were otherwise thought to be artefacts of the different reduction procedures.

The faintness (or even absence?) of light echoes in optical light is nevertheless an important result from our observing campaign. Together with other data obtained world-wide during the SL-9 impacts, both from Jupiter itself and its satellites, it will certainly help to better understand the physics involved in such high-energy processes.

Near-Infrared Imaging of Comet SL-9 and Jupiter's Atmosphere

K. JOCKERS, Max-Planck-Institut für Aeronomie, Katlenburg-Lindau, Germany

The Max-Planck-Institut für Astronomie in Heidelberg kindly granted observing time at the ESO 2.2-m telescope during "German" time from July 16 to 24. During this run, Jupiter was

observed with ESO's IRAC 2B near-infrared camera in the K band through interference filters and a tunable Fabry-Perot-interferometer (FPI) with resolution approximately 1000. This programme

aimed at studying the interaction of the cometary fragments with Jupiter's atmosphere.

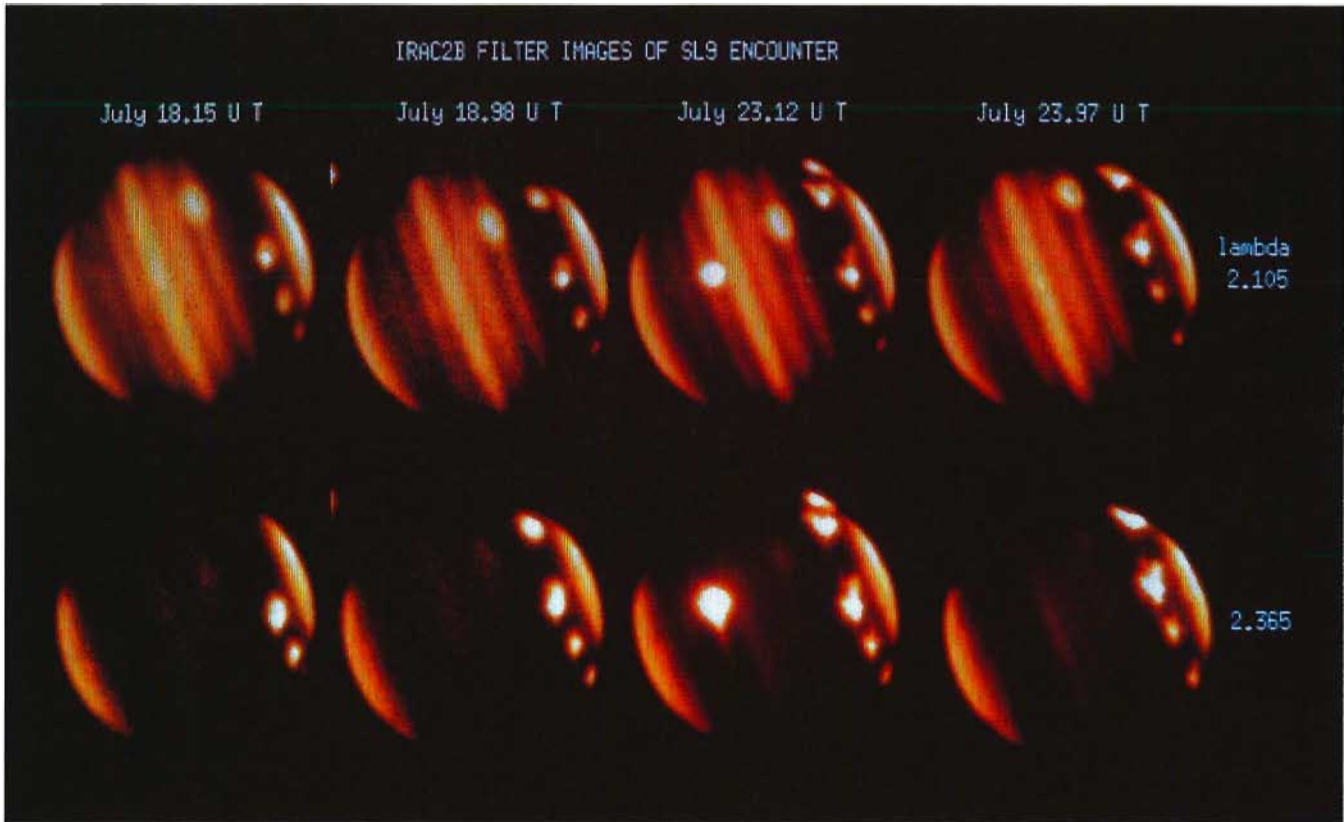Regrettably, no impacts were observed. Apart from some wide-band im-

IRAC2B FILTER IMAGES OF SL9 ENCOUNTER

July 18.15 U T   July 18.98 U T   July 23.12 U T   July 23.97 U T

lambda 2.105

2.365

Figure 1.

ages taken through the K and Ǩp filters, mainly during the time of impact B (which did not produce any observable effects), most filter images are taken through the interference filters BP4 and BP11 (central wavelengths 2.105 and 2.365 μm, and FWHM 0.037 and 0.088 μm, respectively). These wavelengths are located in the wing and in the centre of a deep methane absorption band.

While at 2.105 μm some of the Jovian clouds are still visible, Jupiter's disk is practically black at 2.365 μm, and even the Great Red Spot, which extends to great height, is barely visible at this wavelength. Figure 1 shows several frames taken at different Jovian rotations at similar aspects of Jupiter's disk. The well-known feature of the Jovian polar haze is visible in both wavelengths at nearly the same brightness, while the Jovian atmospheric clouds appear only at 2.15 μm. On July 23.1, Jupiter's satellite Io is seen to cross the disk. The impact clouds appear bright in front of the disk. As time goes on, more impacts occur, and more of these clouds appear. They

are remarkably stable, but in the course of a few days they are getting sheared by Jupiter's velocity field.

From comparison of the images in the two wavelength ranges, it is obvious that the clouds must be located in atmospheric heights that are unaffected by methane absorption. Outside of wavelengths of strong methane absorption the impact clouds appear dark in front of the bright Jovian disk. This, and the observed high stability of the clouds, makes it likely that they consist of solid material, either remains of the comet, or material from deeper layers of Jupiter's atmosphere brought into the Jovian stratosphere during or shortly after the impacts. Spectra in the infrared and visual range, as obtained by other ESO projects, are needed to investigate the nature of the cloud material.

With the Fabry-Perot interferometer the line of H_3^+ at 2.093 μm and the H_2 quadrupole line at 2.121 μm were observed. Both lines are sensitive to temperature enhancement in the outer layers of the Jovian atmosphere. The fun-

damental vibration band of H_3^+ at 3–4 μm can always be observed in Jupiter's aurora, where it is excited by heating Jupiter's ionosphere through electron precipitation caused by magnetospheric phenomena. The H_3^+ lines in the "hot" overtone band at 2 μm can be observed only when the auroral heating is particularly strong.

Because of Jupiter's rapid rotation, line images and continuum images at a wavelength of 2.108 μm were taken alternately. So far only single pairs of line and continuum images have been processed. They show that at both wavelengths the line and continuum images, apart from a factor, seem to be exactly identical. Consequently, despite the positive results obtained with the IRSPEC instrument, the FPI images so far do not show any evidence for line emission. Most likely the signal/noise ratio of individual pairs of images is not sufficient to show the line emission. To increase the signal/noise ratio many pairs of interferograms must be averaged.

Imaging of the Signatures of the Impact Events in the Thermal Infrared

H.U. KÄUFL, ESO-Garching

1. Introduction

TIMMI, ESO's 10 μm instrument (for a detailed description of TIMMI see e.g. Käufl *et al.* 1992, 1994) was mounted at ESO's 3.6-m telescope from July 15 to July 31 to provide for infrared imaging with broad- and narrow-band filters in the 5 and 10 μm atmospheric windows. The purpose of the observations was twofold:

- to investigate and monitor the atmospheric consequences of the impacts (P.I. Tim Livengood, NASA GSFC, Greenbelt, Md)
- to search for global oscillations of Jupiter resulting from the impacts (P.I. Benoît Mosser, IAP, Paris)

The observing time was shared between the two programmes and the filters were chosen strategically in such a way that the data are in principle useful for both programmes.

2. Technical Details and Calendar of Observations

Impacts covered

Impact A: Impact A was observed on July 16, starting at 20:23 UT, i.e. the first images of the impact area correspond to the peak brightness at 10 μm. Photometrically these data are not the best, but the evolution of the morphology of the impact area can be very nicely studied.

Impact B: A time window of ± 1 h around the predicted impact time was covered in good to acceptable weather conditions. Even after careful inspections of the data no signatures could be seen.

Impact F: This was the next impact visible over La Silla. A minute signature of the impact was detected.

Impact H: This impact was the one best covered by TIMMI (0.5 h before till 3 hours after impact) under good to acceptable weather conditions.

Impact L: This impact was observed marginally through heavy clouds. Few scientific valuable data are available from this impact.

All the other impacts could not be observed due to bad weather.

Other observations

February 28–March 4, 1994; pre-event observation of Jupiter.

July 22–July 31, 1994; with few interruptions constant monitoring or the Jo-

vian disk with TIMMI for atmospheric effects and seismological signatures.

Scales

0.6 arcsec/pixel (≈ 2300 km/pixel) for all observations during daytime and for all observations specialized for seismology.

0.45 arcsec/pixel (≈ 1700 km/pixel) for night-time observing when studying the effects of the impacts on the Jovian atmosphere.

Filters

9.1–10.41 μm: used for seismology and sensitive to C_2H_4 and NH_3. To be most sensitive to the signatures of the effects on the atmosphere, additional filters tailored to the IR spectrum of CH_4, NH_3, C_2H_4, C_2H_6, and the standard 5 μm (M-Band) filter were used.

Observers

The observations were carried out by Tim Livengood (NASA GSFC) and Hans Ulrich Käufl (ESO) for the atmospheric effects proposal. Benoît Mosser (IAP) and Marc Sauvage (SAP/DAPNIA, Saclay) did the observations concerning seismology of Jupiter.

3. The Selection of Data Presented Here

The data shown in this article constitute a rather arbitrary selection. The number of frames obtained exceeds 100,000! Since there is a separate article dealing with seismology, the scope of this presentation is restricted to atmospheric effects, particularly also since they exceeded all expectations of the observers. A full analysis and reduction of the data will clearly take some time.

The original idea of the Livengood *et al.* proposal was to try to trace temperature changes resulting from the impacts in the Jovian atmosphere above the cloud layer. Since the abundance of infrared trace molecules in the upper atmosphere is governed by depletion through condensation, minor changes of the temperature would be amplified via the exponential behaviour of the vapour pressure to somewhat bigger abundance changes. These would be easier observable than radiance changes introduced by the temperature increase alone for constant abundances. Nevertheless, also with this amplification it was never anticipated that the impacts would create signatures of the size and strength actually observed.

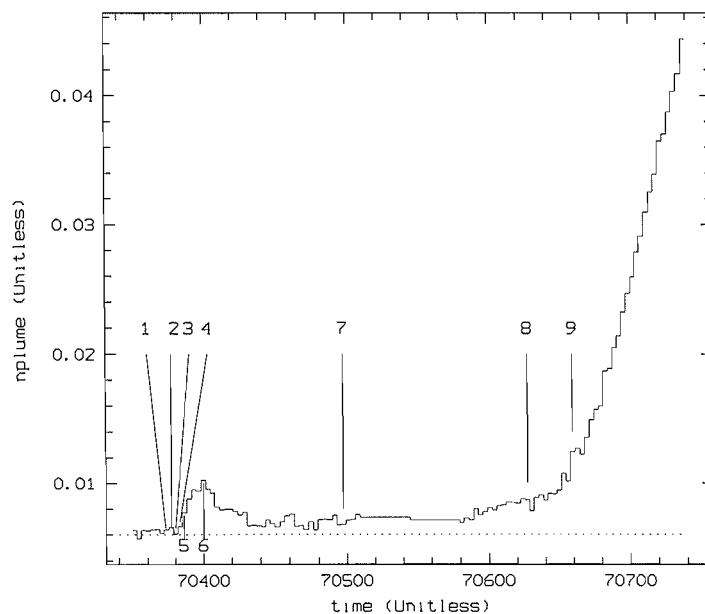In this contribution I will concentrate on

Figure 1: *Light curve for the precursor event of impact H. The time axis is in seconds since midnight (U.T.). The numbers and arrows correspond to the frames shown in Figures 2a and 2b. The light curve is normalized on Jupiter (disk-integrated), i.e. the peak of the precursor event at t = 70,400 s corresponds to ≈ 4 % of the disk-integrated signal from Jupiter in the filter pass band (9.1–10.41 μm). A dotted line shows a constant offset of the photometry. For the rapid rise on the right see Figure 3.*
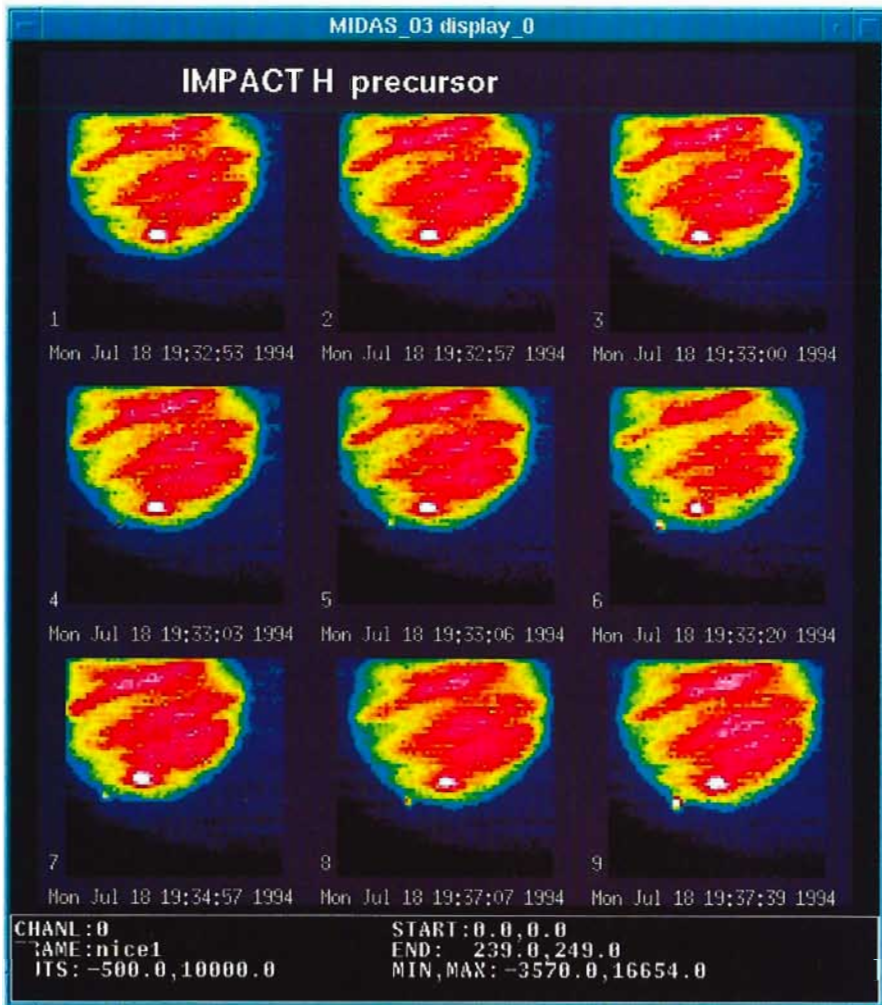
37

Figure 2a: *A sample of frames obtained with TIMMI (filter 9.1–10.41 μm) during the time interval of the section of the light curve shown in Figure 1. The projected size of one pixel on Jupiter is 2300 km. Between frame 2 and 3 the emission from the impact area becomes apparent. In all frames, the impact area is not resolved (i.e. smaller than 2 pixel). For the photometry of the frames see Figure 1. Impact area G (age 12 h) can be clearly seen in all frames on the Jovian disk.*
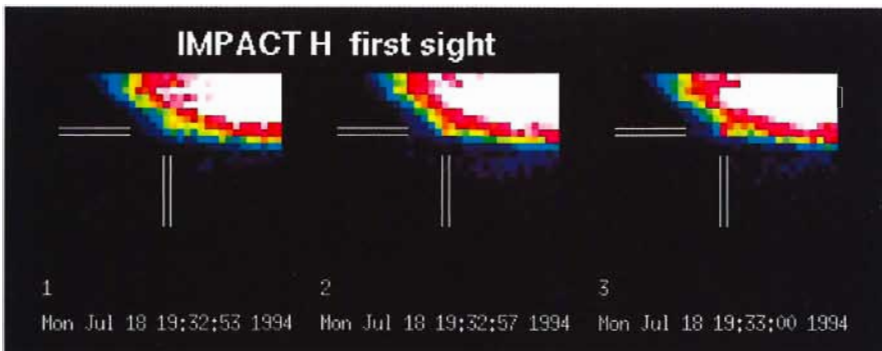

Figure 2b: *An enlargement of the first three frames obtained with TIMMI shown in Figure 2a (with compressed dynamic range). The projected size of one pixel on Jupiter is 2300 km. While subframe 1 at 19:32:53 clearly does not show an emission on the limb, subframe 2 at 19:32:57 shows a faint signature, and for subframe 3 at 19:33:00 the emission is obvious. This leads to the determination of first sighting of the impact area with an uncertainty as small as 3 seconds.*

two absolutely unexpected events: the very bright thermal emission and the very fast expansion of the impact area.

4. The Precursors of Impact H

Figure 1 shows a section of the light curve of the impact H area obtained with the 9.1–10.41 μm filter. The light curve was normalized using the Jovian disk as the photometric standard. Figures 2a and 2b give the corresponding frames. A small "blip" becomes apparent at 19:32:57 occurring typically 58 seconds after the now accepted impact time for fragment H (19:31:59 U.T., Yeo-

mans and Chodas, private communication). This value is just at the edge of the 1σ error estimated by these authors.

While a detailed analysis of the light curve would need to disentangle projection effects and refraction by the Jovian atmosphere, it seems clear that a thermal IR signature is visible either instantaneously or within seconds after the impact. Interesting to note is, that with respect to the time resolution of the observations (3.5 s), the rise of the thermal emission is not fully resolved. Extremely surprising is that this pre-flash decays rapidly and the strong emission sets on only 4 minutes later which probably coincides with the impact area rolling across the terminator for Earth-bound observers. Already the pre-flash achieves a surprising brightness: 4–5 % of the disk-integrated signal of Jupiter in the same filter.

Figures 2a and 2b show a selection of frames whose location are indicated in the light curve shown in Figure 1. It should be mentioned that all thermal IR observing of bright impact events as reported from other observatories also showed this pre-cursor behaviour. Figure 2a also shows the impact area of impact G which was by then 12 hours old.

5. The Expansion of the Impact Area

Figure 3 shows the light curve of impact H during peak and decay phase. Figure 4 shows again a selection of images whose location in time is noted in the light curve. While frame 1 and 2 show the impact plume basically as a point source, frame 3 in Figure 4 shows a slight extension parallel to the limb. Because of the projection, an expansion perpendicular to the limb cannot be observed. This extension is then more and more obvious in the other frames shown in Figure 4. As can be seen in Figure 3, the apparent expansion of the impact area is coincident with the "hump" appearing in the decay of brightness. The time elapsed between impact and frame 4 in Figure 4 is 1200 seconds. The apparent size of the impact region in frame 4 of Figure 4 on Jupiter is 10,000 km. This implies an "expansion velocity" exceeding 5 km/s and could be as large as 10 km/s, depending on the size of the impact area directly after impact.

While the propagation of an atmospheric wave with 5–10 km/s is hard to understand, another scenario would easily explain the observations. If one assumes that after the impact, secondary ejecta with 15 km/s vertical velocity are thrown out of the impact site then it takes these ejecta typically 1200 seconds until they fall back on the Jovian surface.

Figure 3: *Light curve for the brightness maximum of impact H. The time axis is in seconds since midnight (U.T.). The numbers and arrows correspond to the frames shown in Figure 4. The light curve is normalized on Jupiter (disk-integrated), i.e. the peak of the event at t = 71,000 s corresponds to ≈ 15 % of the disk-integrated signal from Jupiter in the filter pass band (9.1–10.41 μm). The rise of the light curve is probably due to the rolling in of the already cooling impact area over the terminator into the Jovian hemisphere visible from Earth. Interesting to note is the bump at t = 71,500 seconds. This could be caused by secondary heating superposing the apparently exponential cooling (see text). The spikes on the curve indicate the noise of the photometric data.*
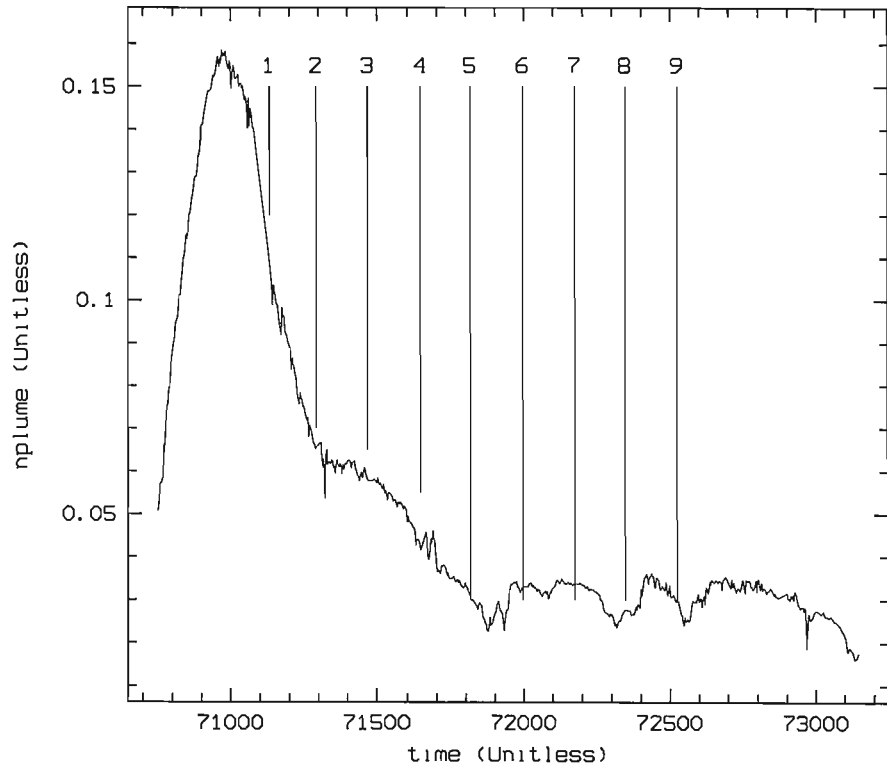
Provided these ejecta would have a tangential velocity of 5–10 km/s then the apparent expansion of the impact site could be the signature of the secondary impacts of the ejecta of the primary event. This scenario is nicely supported by the "hump" in the decay in the light curve which could be caused by the onset of a heating process (secondary impacts). If this scenario is correct, then the maximum altitude of the trajectories of the ejecta would be typically 4000–5000 km above the Jovian surface. Similar morphological behaviour was found for impact A. Additional support of the scenario sketched here comes from the fact that 30–40 minutes after the impact the rapid apparent expansion slows down appreciably.

6. Conclusion

After a very brief inspection of a minute amount of data it is already clear that these data obtained with TIMMI alone will provide substantial insight into the physical processes during the entry of the impactors. In the same way it will be possible to describe the dissipation of the energy and the depletion of the material injected into the Jovian atmosphere by the impacts. Unfortunately, the observing time allocated for the project was not sufficient to monitor the 10 μm signatures until complete fade-out.

During the last moments of observation (July 31, 3:00), nearly nine days after the last impact, the signatures of the collision were clearly observable! Following the first evaluation of the TIMMI data alone, the next step then will be to obtain a comprehensive view of the event by taking advantage of observational data obtained from other sites but especially assembling all data obtained from La Silla in a coherent way.
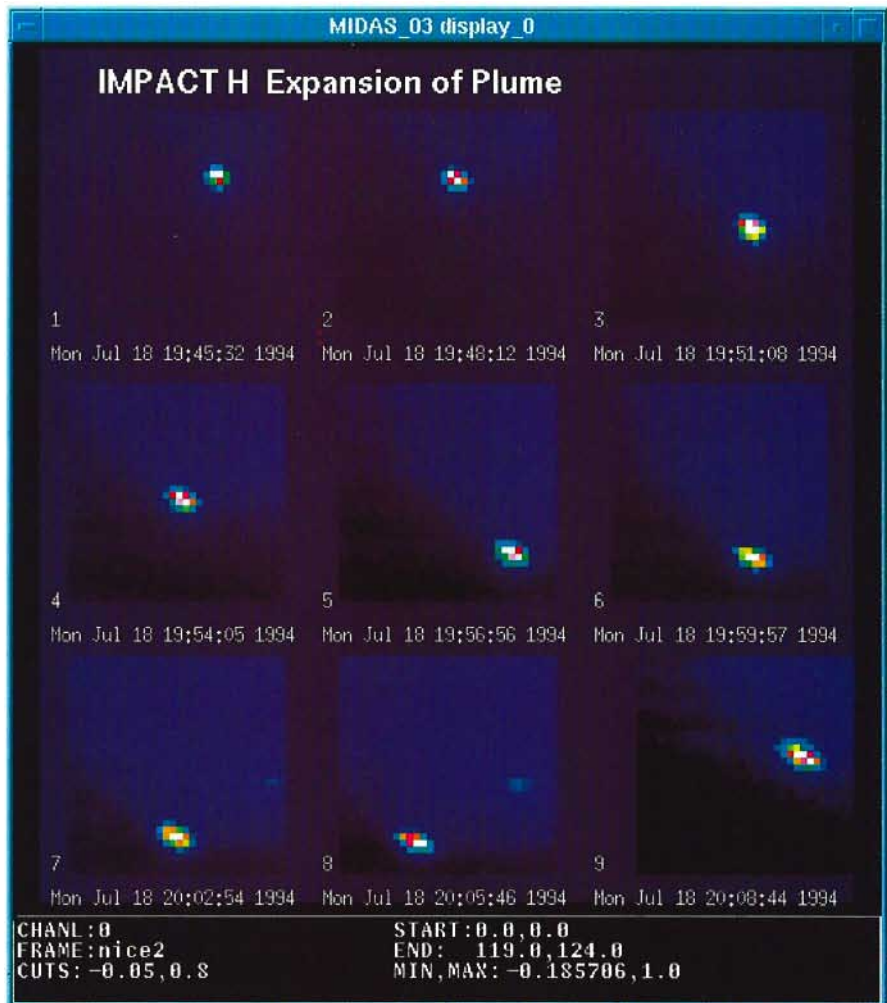
Figure 4: *A sample of frames obtained with TIMMI (filter 9.1–10.41μm) during the time interval of the section of the light curve shown in Figure 3. The projected size of one pixel on Jupiter is 2300 km. All subframes are normalized to the brightest pixel in the impact area. While frames 1 and 2 are compatible with an unresolved point source, frame 3 is not. Frames 4–9 show a further expansion of the impact site with time. For further explanations see text.*

support of ESO's La Silla staff. I would like to mention especially E. Matamoros, J. Roucher and U. Weilenmann. This campaign was particularly difficult because of day and night-time observing since TIMMI was usually observing 18 hours and more per day. The author appreciates also valuable discussions with K. Zahnle.

References

H.U. Käufl et al. 1992, *The Messenger* **70**, p. 67.

H.U. Käufl et al., 1994, *Infrared Phys. Technol.*, **35**, p. 203.

Near-IR Spectroscopy of Jupiter at the Time of SL-9 Impact Using NTT-IRSPEC: Emissions of CH_4, H_3^+ and H_2

TH. ENCRENAZ[1], R. SCHULZ[2], J.A. STUEWE[2], G. WIEDEMANN[3], P. DROSSART[1] and J. CROVISIER[4]

[1]*DESPA, Observatoire de Paris, Meudon, France;* [2]*Max-Planck-Institut für Aeronomie, Katlenburg-Lindau, Germany;* [3]*ESO-Garching;* [4]*ARPEGES, Observatoire de Paris, Meudon, France*

Near-infrared observations of the Jovian disk, using IRSPEC at the 3.5-m NTT, have been performed continuously from July 16 to July 28, 1994, with a final observing night on July 30/31. Data were recorded every night, with the exception of the three nights of July 18–22, lost because of bad weather.

The IRSPEC instrument is an imaging spectrometer working between 1 and 5 μm, with a resolving power ranging from 1300 to 3000. Its 4.4 arcsec slit was aligned along the parallel of impact sites ($l = -44°$) to monitor these sites as they were rotating with the planet. After the impacts, in the second part of the run, we monitored the entire Jovian disk by shifting the slit (still aligned with the parallels) in 9 different positions to cover the whole latitude range from pole to pole. This method allowed us to monitor systematically the impact regions and the corresponding emission regions detected at the same longitude in the northern hemi-
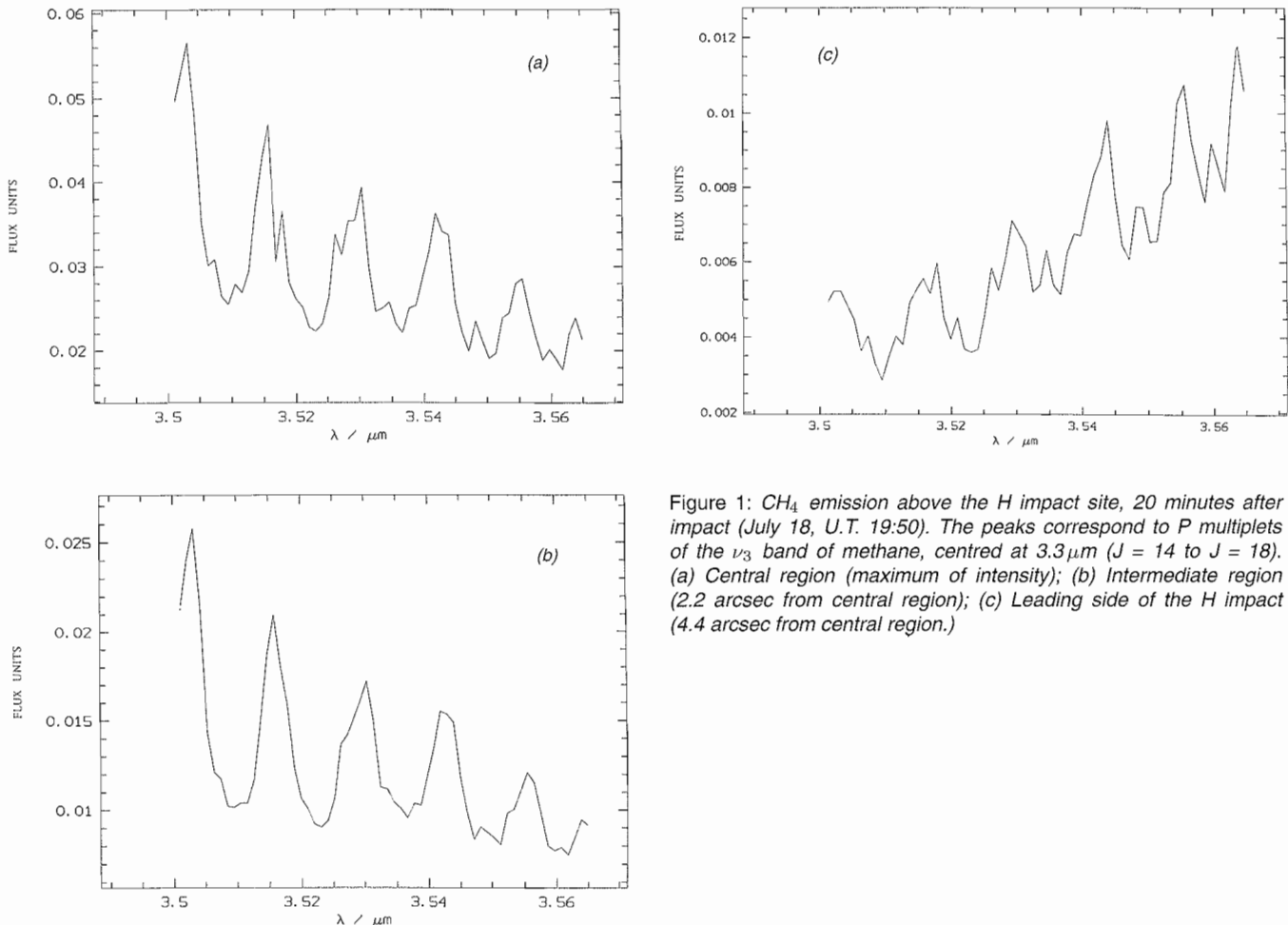

Figure 1: CH_4 emission above the H impact site, 20 minutes after impact (July 18, U.T. 19:50). The peaks correspond to P multiplets of the ν_3 band of methane, centred at 3.3μm ($J = 14$ to $J = 18$). (a) Central region (maximum of intensity); (b) Intermediate region (2.2 arcsec from central region); (c) Leading side of the H impact (4.4 arcsec from central region.)

sphere at $l = +44°$ (see the article by R. Schulz et al. in this issue) as well as the equatorial and polar regions.

In order to monitor the stratosphere of Jupiter at the time of the impacts, our observations were focused on two spectral ranges: (1) the H_2 emission at 2.12 μm and (2) the H_3^+ emission at 3.53 μm. Both emissions occur very high in the Jovian stratosphere. Under nominal conditions, the H_2 quadrupole line is formed at a pressure level of about 0.1–1 microbar, while the H_3^+ emission occurs at even higher levels (P = 10–100 nanobars). In the two spectral ranges, the expected emissions were recorded above the impact sites, and the spectra exhibited drastic differences in and out the impact regions. The most surprising result was the detection of a very strong emission of methane in the 3.53 μm range, just after impact H.

Figure 2: H_3^+ emission above impact G, measured on July 18, U.T. 19:46, i.e. about 12 hours after impact.

Methane Emission at the Time of Impact H

Our observations, covering the range 3.501–3.566 μm with a spectral resolving power of 1700, started on July 18 U.T. 19:46, i.e. 13 minutes after the impact, at a rate of 1 spectrum per minute. A very strong emission was detected over the whole spectral range; it was soon identified as high J-value multiplets of the CH_4 ν-3 band centred at 3.3 μm (J = 14 to 18). The signal intensity decreased exponentially with a time scale of about 5 minutes and was detectable for about half an hour.

A spatial analysis of the emission was performed along the slit, with a pixel size of 2.2 arcsec. At the beginning of the sequence, the CH_4 emission extended over about 10 arcsec. The slope of the spectrum shows spectacular variations of the CH_4 multiplets. In a preliminary report of these observations (Encrenaz et al., 1994), we obtained a first-order estimate of the rotational temperature, assuming that the lines are not saturated (i.e. the observed intensities are proportional to the strengths of the multiplets). However, this assumption is probably crude, and a complete radiative transfer modelling will be required. In the first image, the peak of intensity, at the centre of the emission, corresponds to a rotational temperature of about 700 K. On the edge (leading side), a very different spectrum is observed, with a much weaker intensity, which may indicate different temperature profiles in the centre and on the wedge (Fig. 1).

The observed emission, which has never been seen on Jupiter before, is probably the result of a strong and rapid increase of the temperature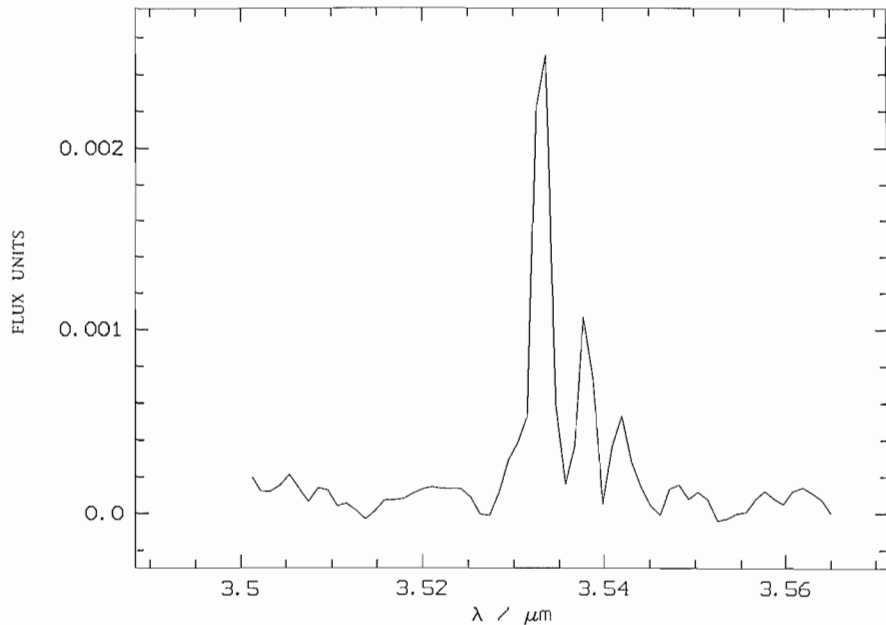 in the Jovian stratosphere, possibly coupled with an upward ejection of methane at these levels. A modelling of the spectrum of the central region can be fit with a nominal methane abundance, if a hot temperature profile (typically with temperatures of the order of 500 K) is used at pressures lower than 10 microbars. Such profiles should be hotter than the profiles measured in the auroral regions, as CH_4 has never been observed in the 3 μm ν_3 band in the Jovian aurorae.

Emissions of H_3^+ at 3.5 μm

A few years ago, stratospheric emissions of H_3^+ were first detected at 2 μm, and later at 3.5 μm, in the polar regions of Jupiter (Drossart et al., 1992). During our observing run, emission spectra of H_3^+ were recorded on many impact sites (Fig. 2). In several cases, a multiplet was observed over a weaker continuum; this multiplet will allow a measurement of both the stratospheric temperature and the H_3^+ column density, following the method used by Drossart et al. (1989, 1993). As a general rule, the observed H_3^+ emissions were more intense above more evolved impact sites, as compared to the fresh impact sites. As an example, H_3^+ was not detected on impact site H less than an hour after impact, when the methane emission disappeared. This result seems to suggest that there is a time delay of at least several hours between the impact time and the formation of H_3^+.

After July 22, 1994, H_3^+ emissions were discovered in the northern hemisphere. As discussed by Schulz et al. (this issue), they were clearly associated to regions located at $l = +44°$, and at the same longitude as the impact sites. Spectra of the northern "image sites" exhibited a strong H_3^+-line emission, but no continuum. In the equatorial region, a weak H_3^+ emission was detected, associated to two other unidentified lines; their analysis is in progress.

The 2.12 μm Spectra

Impact sites and their images in the northern hemisphere were also easily detectable at 2.12 μm. Shortly after the impacts, spectra recorded in the 2.107–2.135 μm range with a resolving power of 3000 show a drastic increase of the signal and a change in slope, with a maximum peaking towards shorter wavelengths. The simplest explanation is that there is a very strong scattering over a newly-formed stratospheric haze. This component sometimes hides the H_2 quadrupole line. From the slope of the spectrum, we hope to be able to retrieve information about the particle size; from the intensity of the quadrupole emission an estimate of the stratospheric temperature will be obtained.

In conclusion, the present observations should provide unique and precious information about the behaviour of the Jovian stratosphere, its temperature and chemical composition, just after the impacts, as well as its evolution during the following hours and days.

References

Encrenaz Th. et al., 1994, IAUC No. 6034 July 22, 1994).
Drossart P. et al., 1989, Nature, 340, 539.
DrossartP. et al., 1992, Icarus, 97, 10.
Drossart P. et al., 1993, Astrophys.J., 402, L25.
Schulz et al., The Messenger, this issue.

CCD Imaging of Jupiter During the Comet Shoemaker-Levy 9 Impact Using the Danish 1.54-m Telescope at ESO

N. THOMAS[1], L. JORDA[2], and B. SICARDY[2]

[1] Max-Planck-Institut für Aeronomie, Katlenburg-Lindau, Germany; [2] Observatoire de Paris, France

1. Introduction

After the discovery of the disrupted nucleus of comet Shoemaker-Levy 9, it was quickly established that the sub-nuclei would strike Jupiter in mid-July 1994. Based on hydrodynamics models [1], it was estimated that although the impact sites could not be seen directly from the Earth, the flashes from the impacts might be observed reflected from the surface of the Galilean satellites or from the thin Jovian ring. As the time of the impacts neared and more precise positions became available, it became clear that the fireball, which might reach a total luminosity of $3 \ 10^{25}$ erg s^{-1}, might even be visible above the limb of the planet. The programme at the Danish 1.54-m telescope was designed to search for evidence of the impacts.

A special HiSis 22 camera, designed by a small French company managed by amateur astronomers, was mounted at the Cassegrain focus of the telescope. The detector was an anti-blooming Kodak KAF-0400L CCD with 768×512 pixels. The pixel size of 9 microns corresponded to 0.14 arcsec at the focus of the Danish telescope. One-third of each pixel was insensitive because of the anti-blooming gate structure. The peak quantum efficiency reached about 35% around 750 nm. The read-out was fast: about 4 s to read the CCD frame when binned 2×2 with a read-out noise of 12 e$^-$ at -10 C. A rapid read-out was also available for a specified window on the CCD giving near-continuous imaging. This mode was used to observe flashes at the limb of Jupiter. The camera was cooled by Peltier effect and was very simply connected to a PC via the parallel port.

When flashes were not expected, it was planned either to observe Jupiter's disk (to search for post-impact phenomena) or to observe the Io plasma torus (to search for changes produced by cometary dust entering Jupiter's magnetosphere). The latter programme proved impossible probably because the gain of the CCD was not set high enough. We also failed to obtain any useful data on Jupiter's ring. However, the observations of Jupiter's disk are of high quality and are providing good information on the de-velopment of the appearance of impact sites.

2. Available Data and Current Reduction Status

The run began on the night of July 17 (the night after the first impact). Despite poor weather conditions in the middle of the run, good data were obtained on several nights. The anti-blooming CCD system proved to be an excellent tool for the study of flashes from the impacts. A continuous data set was obtained near the time of the F impact while an attempt was made to observe the L impact in daylight (16:30 local). The F impact was not detected which appears to be consistent with other reports (e.g. from the observers on the 3.6-m using TIMMI) that this impact was unusually weak. Although some observations near the time of impact L were obtained, persistent heavy clouds eventually forced us to close a few minutes before the predicted impact time.

The main data set therefore comprises a number of high-quality images of Jupiter's disk in four wavelengths (894 nm, 829 nm, 727 nm and 751 nm). The images obtained are summarized in Table 1.

At the time of writing, data from the night of July 17–18 are reduced and calibrated. The absolute calibration of the instrument was performed by comparing the brightness of Jupiter's disk with standard star frames obtained immediately afterwards at a time when the atmosphere was clear and stable. This observation of Jupiter's disk was then used as a standard and all images were normalized to this. At present, we estimate the flux calibration to be good to around $\pm$ 15%. The resolution was seeing limited and quite variable particularly on the first three nights.

3. Preliminary Results

3.1 General appearance of impact sites

The absorption of sunlight by methane in Jupiter's atmosphere is strong at 8900 Å giving rise to a Jovian geometric albedo of only about 5% (see e.g. Tomasko (1976) [2]) compared with a value of 40% in the continuum. The impact sites proved to be clearly visible as bright spots against the dark background of Jupiter at 8937 Å. This contrasted sharply with the dark appearance of the impact sites relative to Jupiter's continuum. In Table 2, we catalogue the maximum observed deviation of the brightness of site H (three hours after the impact) from Jupiter's normal brightness. It should be noted that these deviations form lower limits because of the effects of "seeing". Although the 7270 Å filter is also centred on a methane absorption, this absorption is not as deep as at 8990 Å. We also give an estimate of the reflectivity (I/F where π F is the solar flux) of the impact site at the same phase angle before the impact occurred. The error on this value is estimated to be about 20%.

3.2 The morphology of impact sites D and H

The shapes of the impact sites were clearly asymmetric. The site of impact H is a good example of this (Fig. 1). Impact H occurred at 19:26 UT on July 18. Im-

TABLE 1. *The data set obtained with the Danish 1.54-m telescope*

Date	UT Coverage	Conditions	Image obtained
17–18/7	23:46–03:53	in patchy cloud	163
18–19/7	23:01–02:10	in occasional heavy cloud	56
19–20/7	22:10–02:16	in very poor conditions	21
20–21/7		N O D A T A	
21–22/7		N O D A T A	
22–23/7	21:23–22:58	in daylight	96
	02:46–03:37	good data	54
23–24/7	23:067–03:35	quality data 0.7" seeing	249

The Effect of Impact H

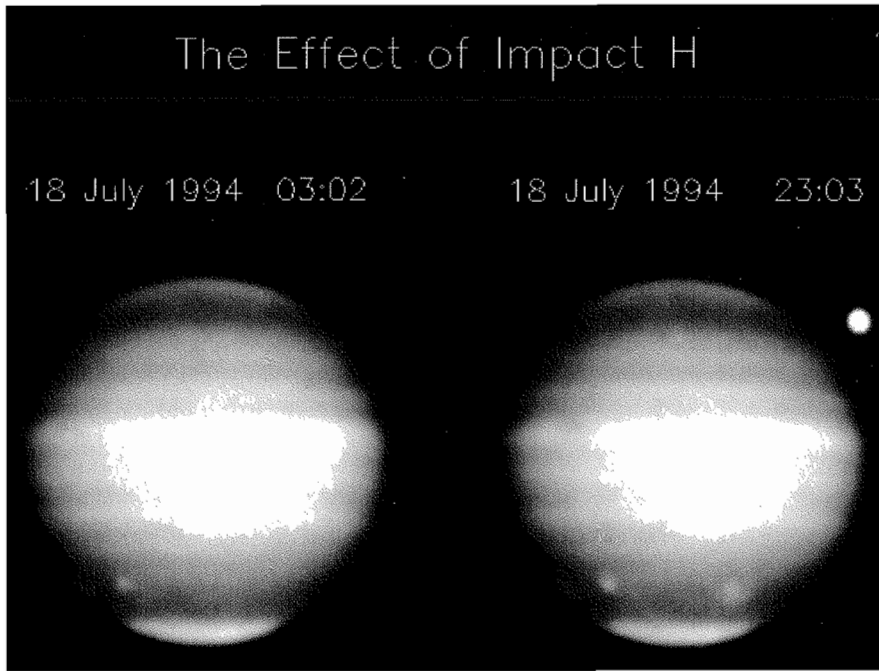18 July 1994 03:02   18 July 1994 23:03

Figure 1: *Impact H occurred at 19:26 UT on July 18, 1994 during daylight at La Silla. An image taken the previous night shows the sites of E and A. The large white spot is actually the Great Red Spot. North is up, celestial east (the dawn terminator) is to the left. Twenty hours later, after 2 Jovian rotations, the effect of impact H can be seen (lower right). It appears to be asymmetric with a diffuse arc-shaped structure to the south-west. The bright spot in the upper right corner is Ganymede.*

TABLE 2. *The maximum change in brightness near site H three hours after impact*

Filter Å	Bandwidth	Description	Reflectivity of site before impact	Change in brightness (%)
8937	43	methane	0.035	53
7271	19	methane	0.217	−11
8290	46	continuum	0.550	−12
7508	47	continuum	0.417	−20

ages of the impact site were first obtained at 23:00 UT. The images through the 8937 Å filter showed that the effects of the impact already covered roughly 10^8 km^2. The highest intensity was observed in the north-east with a shallow gradient to the south-west. The appearance to the south-west gives the impression of an arc turning through 90° about 4200 km (9 pixels) from the brightest point.

The appearance in the other filters used is less clear. In the 7271 Å filter the contrast between the impact site and the surroundings is quite poor and no structure of the site is immediately apparent. At both 7508 Å and 8290 Å, the site again gives the impression of being extended to the south and west.

The increase in intensity produced by impact D was not so large. Subtracting the average intensity of Jupiter's disk in the methane band at that latitude from data obtained around July 18, 00:00 UT

(12 hours after the impact) shows site D to have a similar morphology to that of the impact site H.

If the morphologies of the intensity increases seen in the 8937 Å filter were caused by the transmission of energy through the atmosphere, the velocity of the disturbance would have to have been around 330 (±60) m s^{-1}. There are two alternative explanations, however. Firstly, the impactors entered the atmosphere at an angle of around 45°

while the fireball produced was probably directed vertically upwards. The entry of the impactor would therefore have affected the atmosphere at higher latitudes before it was destroyed. However, this allows an estimate of the depth at which the object exploded by dividing by the tangent of the entry angle giving a depth of 0.06 R$_J$. This is far deeper than predicted by the hydrodynamics models [1]. A second alternative is that the objects broke up before impact with debris entering over a much greater surface area. The impactors did appear to be elongated in images obtained at the beginning of July but, of course, they were not resolved. The difficulty here is to explain why impact sites D and H look so alike with the brightest point in the north-eastern corner when one might expect the debris to be more randomly distributed over the surface.

3.3 The persistence of impact sites A and E

The data from July 17 and 18 can be used to compare the brightness of impact site E after 2 Jovian rotations. The results can be seen in Table 3 and show that impact site E appeared to remain constant or possibly increase slightly in brightness at 8937 Å with time during this period. An increase in brightness may indicate cooling and subsequent condensation of gases in the upper atmosphere.

The persistence of the impact sites over several rotations was a major surprise. Figure 2 shows an image taken on the last night of our observations. This night provided excellent seeing (less than 0.7 arcsec) as can be seen from Figure 2. Many impact sites could be seen during the night with complex structures evolving from multiple impacts on the same region. In the centre of Figure 2, however, there is a small spot which is the remnant of impact A, more than 7 days and 17 Jovian rotations after the initial event.

4. Future Work and Conclusions

The main priority at present is to complete the reduction of all images and make an assessment of the morphology of each impact site. The observed

TABLE 3. *The intensity of impact site E through the 8937 Å filter*

Date	Time (UT)	Peak increase in intensity relative to pre-impact (%)	Estimated increase in intensity of 10^8 km^2 area (%)
18 July	03:03	54	13
18 July	23:02	64	16

43

Figure 2: *The disk of Jupiter on July 23, 1994, 23:17 UT. Impact site A was almost on the sub-solar meridian and can still be seen more than 7 days after the initial impact.*

changes in the brightness of the impact sites are also of considerable interest. The observations through different filters will allow an estimate of the scattering properties of the aerosols produced by the impacts. Models currently being used by us to determine the effects of aerosols on Martian surface photometry will be useful in this study.

References

1. Zahnle, K. and Mac-Low, M.-M. (1994) *Icarus* **108**, 1.
2. Tomasko, M.G. (1976) in *Jupiter.* Ed. Gehrels. T., Univ. of Arizona Press, Tucson.

The Distribution of Near-IR Emissions in the Jovian Stratosphere Caused by the SL-9 Impact

R. SCHULZ[1], TH. ENCRENAZ[2], J.A. STÜWE[1] and G. WIEDEMANN[3]

[1] *Max-Planck-Institut für Aeronomie, Katlenburg-Lindau, Germany;* [2] *DESPA, Observatoire de Paris, Meudon, France;* [3] *ESO-Garching*

Between July 16 and 31, Jupiter was monitored spectroscopically in the near-IR with the IRSPEC spectrometer at the 3.5-m New Technology Telescope (see Encrenaz et al., this issue). During the week of impacts, the 4."4 slit was aligned along the parallel of the impact sites (lat.: −44°) allowing a spatial analysis in this direction. Starting on July 23, we also observed the counterpart of the impact region in the northern hemisphere (lat.: +44°) and proceeded with a mapping of the entire planet. Data were recorded in several spectral regions between $2\,\mu$m and $5\,\mu$m with preference to the regions around the the H_3^+ multiplet at $3.5\,\mu$m and the H_2 S(1) quadrupole line at $2.12\,\mu$m attributed to the Jovian stratosphere.

1. Observations During the Impact Week (July 16–22, 1994)

On July 16, 23:13 UT, we started observing the phenomena in the Jovian stratosphere resulting from the impacts. The impact regions of fragments A to H were monitored in the ranges $2.107\,\mu$m–$2.135\,\mu$m and $3.501\,\mu$m–$3.566\,\mu$m. Due to bad weather we had to interrupt our observations and could resume only on July 22 after the final impact had taken place. Our last useful observation during the week of impact was taken on July 18, 20:24 UT. However, we were able to obtain spectra at the impact times of fragments B, F, and H. The impact of B was observed at $2.12\,\mu$m and H was watched in the $3.5\ \mu$m region. For im-

pact F we recorded data in three spectral regions ($3.3\,\mu$m, $3.5\,\mu$m, $2.1\,\mu$m) until three hours after impact. No H_3^+ was detected in the $3.5\,\mu$m observations of impact regions H and F within about an hour after the event, whereas it was clearly present in more evolved impact regions. For more details on impact H see Encrenaz et al., this issue. Figure 1 shows a spatially resolved spectrum obtained at $2.1\,\mu$m about 2 hours after impact F. Since fragment F almost fell on impact site E, both sites lie side by side very close together and can only be distinguished by their distinctly different spectra in the $2.1\,\mu$m region. As demonstrated in Figure 2 the spectrum of F is characterized by a strong featureless continuum, whereas the already evolved site E
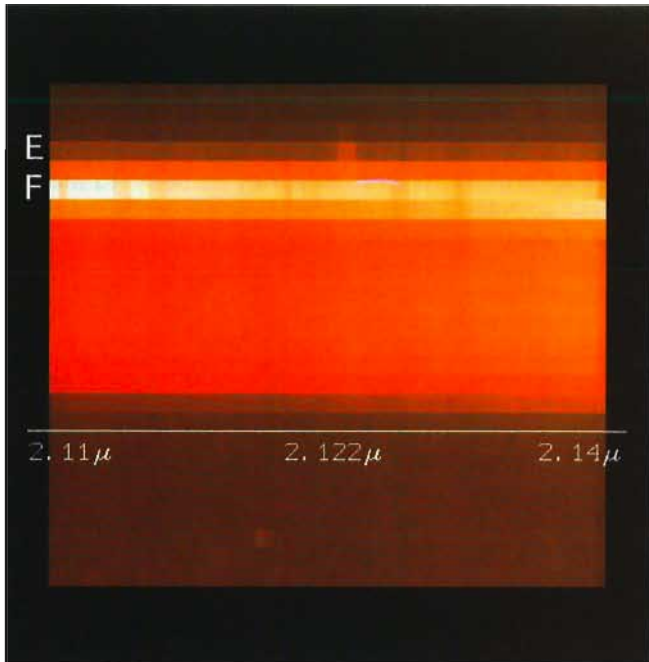
44

Figure 1: *A spatially resolved spectrum showing impact sites E and F in the 2.1 μm range about 2 hours after impact F (July 18, 2:34 UT).*

Figure 3: *Emissions in the 3.5 μm range at the impact sites (lat. = −44°) and their northern counterparts (lat. = +44°). The intensity of the emissions is enhanced at the longitudes of impact sites of fragments Q_1, Q_2, N, R, S, D, G, B and V, T, E, F. See text for details.*

showed little continuum, but a strong H_2 line.

2. Emissions in the Northern Hemisphere

After July 22, emissions clearly associated to the impacts were detected in the 2.1 μm and 3.5 μm regions also in the northern hemisphere (lat.: +44°). Figure 3 shows one example for the emissions detected in the northern hemisphere (upper half) in comparison to those present at −44° latitude (lower half). Both latitudes on the Jovian disk shown in Figure 3 are spatially resolved in longitude (y-axis). The H_3^+ emission line at 3.533 μm in the northern hemisphere is clearly enhanced at the longitudes of the impact sites visible in the southern half of Jupiter. The main difference between the spectra of the impact regions and their northern counterparts is the lack of continuum in the latter. However, the comparison of the longitudal distribution of the 3.533 μm H_3^+ emission at the latitude of the impacts and its northern counterpart clearly indicates a connection between the emissions at +44° and the impact sites. They could result from the transfer of charged particles along the Jovian magnetic field lines. For a more detailed study the entire planet was mapped in the 2.1 μm and 3.5 μm regions simply by scanning the planet along its rotational axis from pole to pole. The evaluation of the data in the 2.1 μm region and the construction of the maps is still in progess. However, the preliminary analysis showed that the H_3^+ emission was, as expected, strongest in the auroral regions where its was uniformly distributed. It was also strong at the impact sites and their northern counterparts. Apart from these regions it was extremely weak, although the strongest H_3^+ line at 3.533 μm could be detected at all latitudes. In the equatorial region the spectra around 3.5 μm exhibit two additional lines, which are still to be identified.

The mapping of the planet continued until July 31, 1994, when the impact sites and their northern counterparts were still observable. Thus, the maps of the Jovian disk provide information on the spatial and temporal evolution not only of the impact sites and their counterparts in the northern hemisphere, but on the entire planet in two different spectral regions.

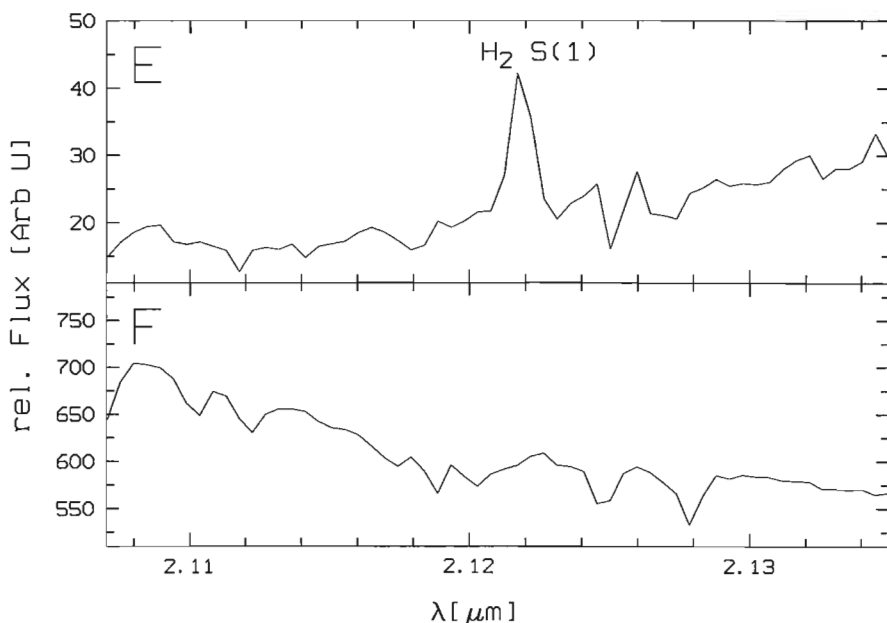### References

Encrenaz et al., *The Messenger*, this issue.

Figure 2: *One-dimensional scans through the spectrum of impact regions E and F shown in Figure 1.*
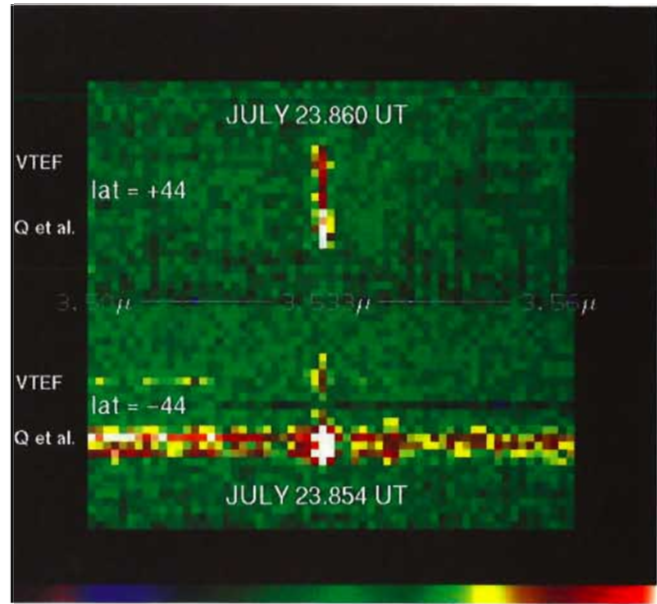
Jovian Quakes

B. MOSSER, Institut d'Astrophysique de Paris, France

1. Introduction

Two coordinated programmes have been carried out jointly with the TIMMI camera at the ESO 3.6-metre telescope during and after the impact of comet SL-9 on Jupiter. They were concerned on the one side with the chemical and meteorological consequences of the impact (see the article in this *Messenger* issue), and on the other side with the search for possible seismic consequences[1].

Less than two months after the observations, it is still impossible to say whether this first attempt to observe seismic effects with an IR camera has been successful. However, we may expect that the energy release by some of the biggest impacts (impact H in our case) has been strong enough to excite seismic waves.

The TIMMI camera (Käufl et al. 1992, 1994), developed by the Service d'Astrophysique (CEA), allowed us to monitor the atmospheric temperature over the full planetary disk, with 64×64 pixels and a resolution of 0.6"/pixel. According to the expected temperature resolution (10 mK with 100 sec exposure time), the adiabatic thermal waves created by a single impact and crossing the entire planet in about 2 hours (similar to the waves obtained when throwing a stone into a pond) can be detected under the condition that the energy of the impact exceeds 10^{20} J. Detectable pressure modes, corresponding to resonant low frequency waves, require an energy impact of about $2 \cdot 10^{21}$ J (Lognonné et al. 1994). For a review on Jovian seismology, see Mosser (1994).

During the Impacts

The optimal time partition suitable for both programmes during the impact period was decided as follows. The first two hours following each impact were dedicated to the search for the waves excited by the impact; this requires a rapid acquisition rate, without any change of filters, contrary to what is needed during the following hours which were dedicated to the atmospheric programme.

Four impacts (A, B, F and H) have been observed. Only accurate data processing will eventually reveal if TIMMI actually detected impact B. For each impact we have recorded a quasi-continuous series of images, at the rate of about 1 image every 3 seconds. About 10,000 images of the full disk of Jupiter were recorded for the seismic programme. These images were not nodded, in order to obtain the high acquisition frequency required for the observation of the high frequency primary waves excited by the impact. This acquisition procedure has allowed us to obtain a first spectacular result: the light curve of impact H, showing either the entry of the bolide into the very high atmosphere a few minutes before the emergence of the impacted region, or its explosion.

Even if seismological considerations would have favoured the use of a 7.8 μm filter (i.e., by isolating the stratospheric methane emission lines), the use of a broad band filter (from 9 to 10.4 μm), which isolates the Jovian tropospheric regions, was preferred. First, the absorption due to telluric water and methane is important in the methane band, and secondly, the thermal emission of Jupiter and the sensitivity of the array are more favourable at 10 μm.

The data reduction consists of the following steps. First, each image will be corrected using the flat fields and the point-spread function, and the position of the planet will be re-centred. Then, new geographical coordinates, with the impact point as origin, will be calculated, in order to obtain seismograms (seismic signal versus time at a given epicentric distance). The signal-to-noise ratio will be increased by stacking all regions at the same angular distance with respect to the impact. Finally, the hodograms (arrival time versus epicentric distance) will be calculated, from which the interior sound speed profile can be inferred.

After the Impacts

Half of the six "nights" following the impacts period have been devoted to the search of pressure modes (resonant waves with periods in excess of 5.5 minutes) trapped in the Jovian cavity. The same broad-band filter was used as during the period of the impacts, but rapid acquisition was now not necessary; this permitted to record nodded images (about 1 per minute). IR thermal observations, starting not later than 2 PM local time, have permitted us to obtain during the 6 half-"nights" a total of more than 22 hours of observations.

In order to perform a Fourier analysis of these data, they will be mixed with the ones obtained in similar conditions at the 2.5-m Nordic Optical Telescope (NOT) at La Palma with the CAMIRAS camera developed by the Service d'Astrophysique (Saclay), as well as with those from the CFHT with the C10μm camera developed at the Observatoire de Lyon. Data during no less than 40 hours of observations were collected at these three sites. The good weather, a favourable southern latitude and early opening of the dome explain why half of the data were obtained at La Silla.

The combination of the three different data sets is possible because they have been collected under very similar conditions, and is in fact necessary in order to decrease the "window effect" (i.e., the fact that false periods may be found because the observations at each observatory only cover a fraction of 24 hours and are done at daily intervals). Overlaps between the data collected at the NOT and at ESO will make this operation easier. The data reduction will be similar to the one commonly used in helioseismology: decomposition of the signal in spherical harmonics, each harmonics contributing to a given Fourier spectrum.

References

Lognonné Ph., Mosser B., Dahlen F.: 1994, "Excitation of Jovian normal modes and seismic waves by the Shoemaker-Levy/9 cometary impact", *Icarus*, in press.

Mosser B.: 1994, "Jovian seismology", Proceedings of IAU colloquium No.147, St.-Malo, France (G. Chabrier and E. Schatzman, Eds.), 14-18 June 1993, 481–511.

Käufl H.U. et al., 1992, *The Messenger* **70**, p. 67.

Käufl H.U. et al., 1994, *Infrared Phys. Technol.*, **35**, p. 203.

---

[1] The following colleagues have also contributed to this programme: Tim Livengood (GSFC), Hans-Ulrich Käufl (ESO), Marc Sauvage, Pierre-Olivier Lagage (SAp, CEA), Philippe Lognonné (IPGP), Daniel Gautier, Pierre Drossart (DESPA, Observatoire de Meudon), Françoise Billebaud (ESTEC), Mark Marley (NMSU,) Juan-Antonio Belmonte, T. Roca-Cortes (IAC) and François Sibille (Observatoire de Lyon).

The SL-9/ESO Web Encounter

F. MURTAGH and M. FENDT, ESO-Garching

The ESO Information System on the World-Wide Web (address: http://www.hq.eso.org/eso-homepage.html) was very much in the firing line during the Jupiter/Shoemaker-Levy 9 event. It was Monday morning, July 18, after the first impacts, when the WWW server collapsed with 250 simultaneous users, compared to a more usual figure of 10 before that. More simultaneous users were permitted, even if this meant that the system slowed to a halt. So it was to remain for many days.

The graph shows the impact caused locally, from July 16. "File accesses" includes the ornamental files – icons and so on. These are generally small, so they can be discounted in the number of bytes transferred. By Tuesday July 19, we were touching on a transfer of 0.7 GB. On Wednesday there was a slackening off. The intense media interest in the Q impacts led to a new high on Thursday.

About 5 to 6 % of the intense traffic was local in origin. The largest national affiliations of users of the ESO Web at that time (as derived from the email addresses of users) were (1) Germany – 80,000; (2) USA educational, commercial and governmental – 73,500; (3) ESO Garching and La Silla – 17,000; and (4) France – 12,000. Distribution of data by anonymous FTP also took place on a heroic scale. In addition, there were animations, and material was made available in many different forms, to cater for the unquenchable thirst of the television crews, the in-

ESO WWW Server during SL-9 event: Daily Accesses

1-31 July 1994
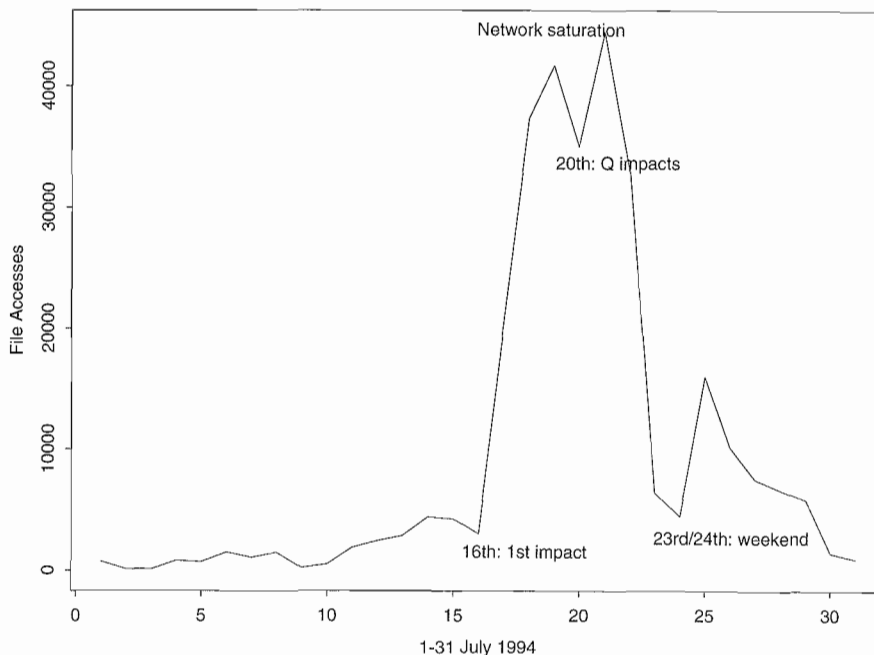
terested public, and astronomers for visual information.

Other sites experienced similar impacts from SL-9. The Shoemaker-Levy homepage at JPL recently (early September) reported that their access count since mid-July had passed the 2 million mark. Commercial information

providers also saturated when faced with the new requirements to deliver images and text, colourfully and fast. By July 27, on CompuServe (ESO's press releases appear in the Astronomy Forum), 37 observatories had material available, with 25.3 GB of data being downloaded during the "comet week".

The Comet, Jupiter, and Everything: SL-9 and the Media – a Strictly Personal Impression

R. ALBRECHT, ST-ECF, Garching

It is not often that Richard West shows up in my office. "Don't plan on getting sick next week", he said. What had happened? The number of registrations for the media event at the occasion of the impact of fragment A had exceeded 100.

With just a few days to go, gigantic trucks had started to appear behind the ESO building, deploying huge dishes and pointing them at the sky. Bundles of cables were running down the circuitous hallways of the ESO building, camera positions were constructed in the auditorium and in the remote control room.

We were starting to get nervous. With the observers on La Silla we were just a few astronomers facing what in the end turned out to be about 120 media representatives. And

remember, at that time we were not at all sure that we were going to see anything spectacular. Dim memories of the Comet Kohoutek media disaster in 1974 came to our minds.

With the help of many of our colleagues, the ESO infrastructure was moulded into a support system for the event. The Council Room was turned into a press centre. The speaker system in the auditorium was connected to the telephone for remote call-in. A huge crane lifted a telescope onto the roof of the ESO building. Gotta have a telescope if you are an observatory, right? The idea was to connect a TV camera to the telescope and show the image in the auditorium.

And then they came. The serious representatives of government TV and the agile oper-

ators from the private stations; respected science writers and people from tabloid newspapers. Lights, camera, action! What will we see? We told you, we don't know. What will happen to Jupiter? Nothing. What will happen to the Earth? Nothing. What will happen to the comet? Crash! What would happen to the Earth if it were hit by the comet. Crash!

"Would you be available for a comment during a 30-second newsbreak following the impact?" one of the private operators was asking. "Sure", I said. Big mistake. They dragged me into the remote control room; they had established a phone link to Sutherland Observatory; the newsflash started exactly at the theoretical time of the impact; the reporter on the phone says to David Laney down in Suther-

Figure 1: *Richard West juggling languages while tracking down the observers on La Silla. The path of the comet is indicated on the blackboard.*

land: "Dr. Laney, thirty seconds ago the first fragment impacted, what do you see?" "Nothing", says David. A camera turns around and somebody sticks a microphone into my face. "We were just told that there is nothing to see; what do you have to say?". I really can't remember just what I said in the 20 seconds which were mine to say it in.

But within minutes we were vindicated. An e-mail message popped up, Calar Alto reported a huge fireball on the limb of Jupiter. And although it was still daylight in Chile, the impact was recorded just a few minutes later on La Silla. We asked for the image to be sent through the computer network. On the screen in the auditorium the image started to build in chunks from the top down. The lower left quadrant of a fuzzy disk took shape. When the display routine got to the 7 o'clock position, a large explosion became visible. Applause in the auditorium. Relief among the ESO people. But there was a moment of tension. "Wait", somebody said, "this might be a Jovian satellite". It was not. But it did take several minutes to clear things up.

The night wore on, but with the excitement thus kindled and impact B expected to be well visible from Chile, most people decided to stay. Food appeared in the ESO cafeteria, and it became apparent that some of the TV support crews must have had access to adequate amounts of good cheer.

Impact B was a surprise of a different kind – it was just about invisible. But reports kept coming in about A, so everybody was happy during the Sunday morning press briefing, especially since the photolab people had cranked out hundreds of hard copies of the images. Impacts C and D cooperated and produced nice fireworks. I called it quits at midnight on Sunday, Richard West stayed on: it was just getting night in Chile, and the bulletin for the Monday morning press briefing had to be produced.

Well, we thought, this worked out all right. It gave a nice show, we successfully projected the image of astronomy as a modern natu-
ral science, we showed them the world wide cooperation, the coordination between ground and space, and on and on. Now let's go back to work. Right? Wrong.

One of the few things we had not arranged was for Germany to be eliminated from the Soccer World Cup. In other words, some of the media were looking for something spectacular to concentrate on. So with fireballs having been seen, and the largest fragments yet to come, everybody decided to get a piece of the action.

For a vivid description of what happened, talk to Mrs. Völk, Richard West's secretary, who ably managed to channel the onslaught. It was only my knowledge of the internal passage ways of the ESO building which allowed
me to get from my office to a bathroom without being swamped.

Mrs. Völk will also be able to tell you some of the questions which she got from the public. One of the largest circulation daily papers had published her telephone number; she got all the questions which you can possibly imagine and a lot more which you cannot.

The wording "organic molecules" appeared in some of the messages from the observatories. Organic, as in organism, as in life. Life on Jupiter! Or on the comet? The comet inseminating Jupiter? Microscopic dinosaurs living on clouds of liquid hydrogen being mass-extinguished by the comet. Great stuff!

Thus inspired and further motivated by the fact that the largest impact, fragment Q, was going to happen during evening prime time, a "live show" was demanded. Three hours of continuous live coverage! What had started as an interesting experience on Saturday had turned into tedious work by Thursday. Also, the lack of sleep was beginning to catch up with us. The questions were becoming repetitive, and one of my main problems was to keep my answers from sounding that way.

During impact week we had no chance of seeing the results of our efforts in the media. When we finally did, weeks later, we found a considerable number of quite good accounts, we were surprised at some of the reports, amused by others, and angry about a few. Of course we were called astrologers at times; some of the condensed versions of some of the interviews had taken on a slant which was totally surprising to the interviewee.

Altogether it worked out quite well. ESO as a scientific organization came out quite positively; it is also nice to think that we might have kindled the interest for science in some of the kids who were watching.

I got what is probably the most relevant question from a young lady working for a Munich private radio station. "This is all very exciting", she said as she watched pandemonium unfold itself in the auditorium, "but is it interesting?"

Figure 2: *One of the daily press briefings. Richard Hook (centre, in front of the terminal) keeping watch over the computer network.*

High-Resolution Imaging of the Active Galaxy PKS 0521–365 and its Optical Jet

R. FALOMO, Osservatorio Astronomico di Padova, Italy

1. Introduction

The galaxy hosting the radio source PKS 0521–365 is among the most remarkable extragalactic objects in the southern hemisphere. The source is at $z = 0.0554$ (Danziger et al. 1979) and exhibits a variety of nuclear and extranuclear phenomena. For these reasons 0521-365 was classified as N galaxy, Seyfert galaxy and BL Lac object.

A number of spectroscopic and imaging studies have been carried out (Danziger et al. 1979, 1985; Cayatte and Sol 1987; Boisson et al. 1989) showing the complex phenomenology of this object. The bright nucleus exhibits radio and optical flux variability together with strong polarization. Conspicuous variations were also found in the optical spectrum (Ulrich 1981; Scarpa et al. 1994) with large changes of equivalent widths of the broad lines. The broad-band energy distribution (see Pian et al. 1994) is dominated by a non-thermal component with a hard X-ray tail. This likely extends to higher energies as suggested by the recent detection of the source in the γ-rays (up to 100 MeV) by Fichtel et al. 1994.

Beside the nuclear activity the object shows also an extended emission region of gas of arc-like shape located up to 21 kpc from the nucleus (Boisson et al. 1989). The most remarkable feature is, however, the presence of a prominent optical jet (Danziger et al. 1979; Keel 1986; Macchetto et al. 1991) which extends for about 6″ to the NW from the nucleus.

The optical radiation from the jet is polarized indicating a non-thermal nature of the jet emission (Sparks et al. 1990). Radio mapping of the jet at 2 cm with VLA (Keel 1986) indicates the presence of a knotty structure similar to the jet in M87 with the brightest knot, at 1.7″ from the nucleus and elongated transverse to the jet direction.

High-resolution imaging of the galaxy surrounding 0521–365 and of its close environment is clearly an important tool to investigate the relationship between the activity and the host galaxy. In this paper we present the results obtained from high quality images for this source, obtained during a programme aimed at studying the properties of the environment of a sample of BL Lac objects.

2. Observations and Data Analysis

The observations were obtained on 5–6 January 1994 using the ESO NTT operated via remote control from Garching. Conditions were photometric and seeing was very good (FWHM < 0.7 arcsec) which favoured the use of SUSI to image the close environment of some objects.

The first night we obtained two images (2 and 15 minutes exposure) in the R filter, and a CCD (TK 1024) with 24 μm pixel size corresponding to 0.13 arcsec on the sky and seeing of 0.7″. One additional 15-minute exposure was secured the second night with 0.5″ seeing. A small ellipticity ($\lesssim 0.04$) was present for stellar objects in all images. The relevant portion of the 0.5″ seeing SUSI image is

Figure 1: *The central portion (field ∼1′ × 1′) of the NTT+SUSI image of PKS 0521–365 (R filter; 15-min exp.). North is at the top and east is to the left.*
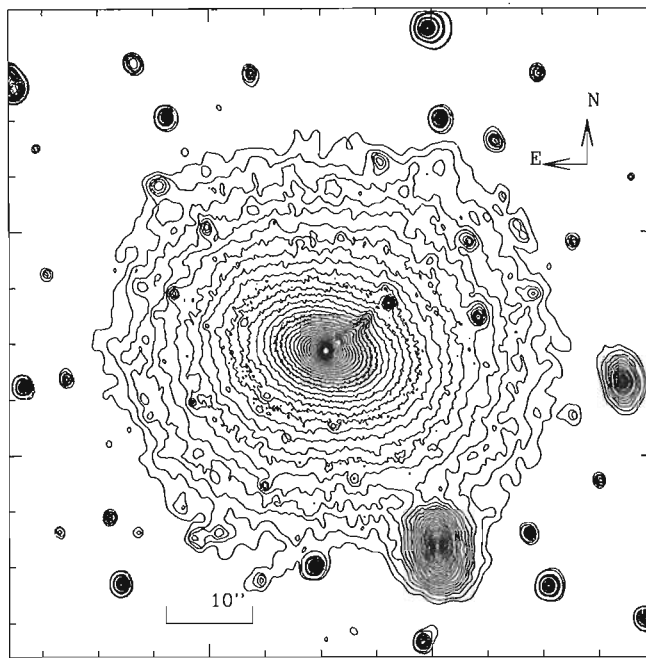

Figure 2: *A contour plot of the R-band image of the field centred on PKS 0521–365. The lowest isophote is $m_R = 25.5$ mag/arcsec^{-2} and spacing between isophotes is 0.25 mag.*
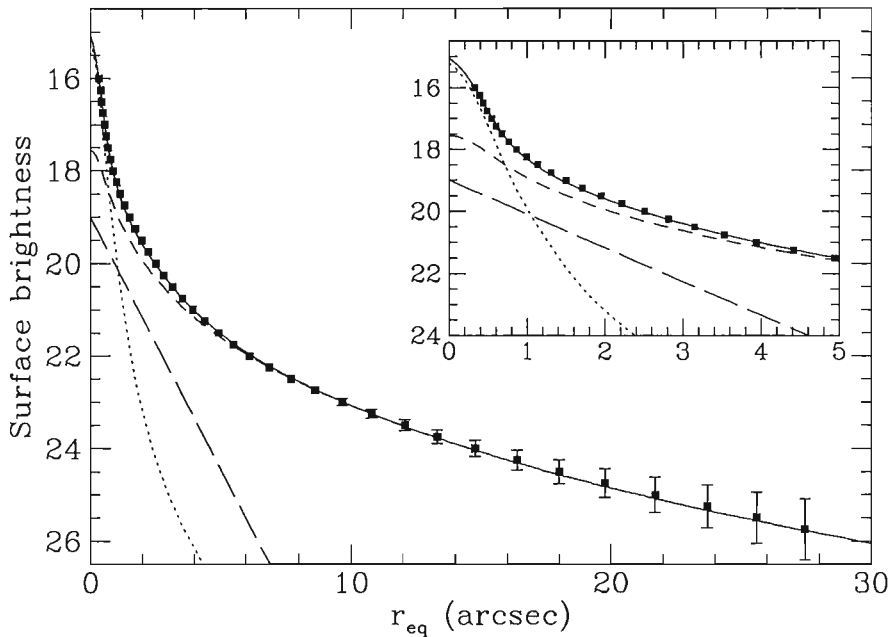
Figure 3: *The surface-brightness profile of PKS 0521–365 in the R-band filter (filled squares). The solid line is the sum of a PSF (dotted line) plus an elliptical $r^{1/4}$ law (short-dashed line) with r_e = 6.2 arcsec and an exponential disk with r_d = 1 arcsec (long-dashed line). The inset shows the inner region of the galaxy.*

reproduced in Figure 1 showing the host galaxy as well as the optical jet.

After standard reduction of the images (including cleaning of cosmic rays) we performed a surface photometry analysis using the numerical mapping package AIAP (Fasano 1994, in preparation). We computed isophotes down to μ_R = 25.75 mag/arcsec^{-2} (see Fig. 2) and then fitted them by an ellipse with free parameters. All the regions affected by fainter objects superposed to the galaxy were excluded

by the fit using an interactive masking procedure. As a result of the analysis we obtain for each ellipse representing the isophote (with chosen spacing of 0.25 mag) the coordinates of the centre, the major axis, the position angle and the ellipticity. Moreover, the fourth cosine Fourier coefficient describing the deviations of the isophote from the pure ellipse is also provided. The analysis was performed for all three images giving consistent results but with the highest resolution

image showing some more details. In the following we refer to the higher resolution image unless otherwise stated.

The surface photometry analysis may be used to study the galaxy morphology through the photometric and structural profiles (surface brightness, ellipticity, Fourier coefficients, . . .). To study the brightness profile, we consider the surface brightness μ_R as a function of the equivalent radius r_{eq} ($r_{eq} = \sqrt{ab}$ where a and b are the semi-axes of the ellipse). The radial profile was modelled by a de Vaucouleurs ($r^{1/4}$) law, convolved with the point spread function (PSF), plus the contribution of the point source in the nucleus. In order to derive a reliable PSF that properly accounts for the core and wing components, we used unsaturated stars in the same frame as the target for modelling the core, and slightly saturated stars in other frames to derive the faint wing component.

In addition to the profile analysis, the mapping can be used to construct a model of the galaxy plus nuclear source to be subtracted from the original image in order to enhance the fine structures or the objects masked in the fitting procedure.

3. Results

The galaxy extends out to 30″ (at μ_R = 25 mag/arcsec^2) from the centre of the object and appears to be centred on the nucleus to within 0.1 arcsec. The isophotes beyond the region influenced by the central point source exhibit an ellipticity e = 0.3 and position angle PA = 75°. In the external regions ($r \gtrsim 10″$)
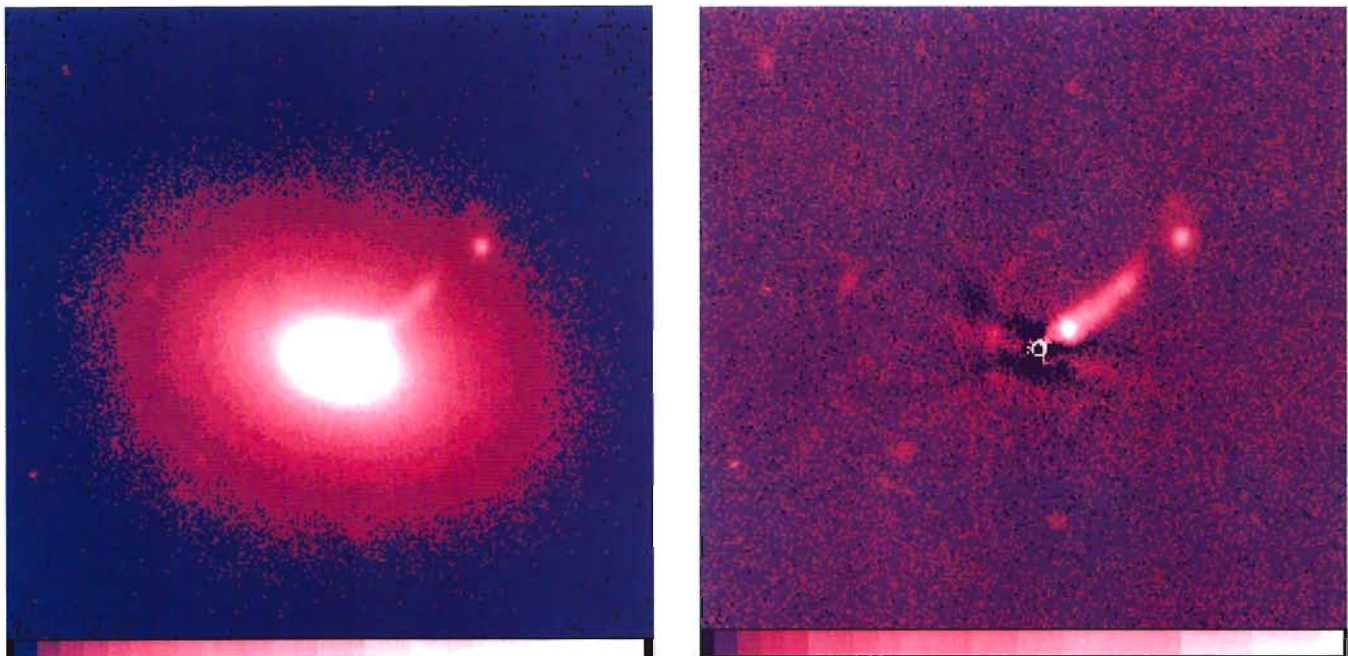

Figure 4: *The optical jet of PKS 0521–365 as imaged by NTT + SUSI in the R filter with 0.5 arcsec seeing before (left) and after (right) the subtraction of a model of the host galaxy plus nucleus. Note the knotty structure of the jet and its curvature. The field shown is 30″ × 30″.*
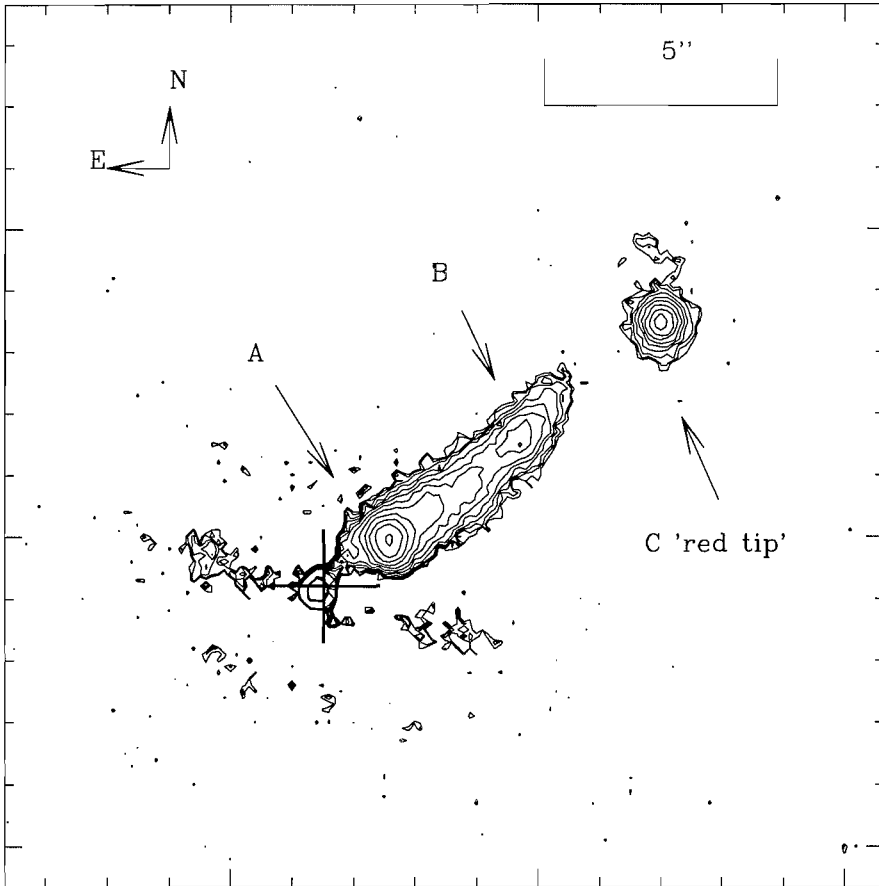
Figure 5: *Contour plot of the jet of PKS 0521–365 in the R band. The big cross represents the centre of the galaxy as derived from the surface-photometry analysis. Objects A and B are the primary and secondary knot in the jet. The nature of object C is unclear (see text).*

To study the optical jet, we have subtracted a model of the galaxy plus the nuclear source to the original image. This is an effective way of enhancing fine structures and it has been discussed in a recent issue of *The Messenger* (Reduzzi *et al.* 1994).

In Figure 4 both the original and the model-subtracted image of the $30'' \times 30''$ arcsec^2 around the nucleus are shown. The jet is clearly apparent together with the bright knot at $1.65''$ and the object (known as the 'red tip') at $9''$ from the nucleus in the direction of the jet.

In Figure 5 we report a contour plot of the jet with the main structures labelled. Figure 6 shows the intensity profile along the jet obtained averaging a strip of $1.3''$ across the jet. The jet is clearly bent with upward concavity. The curvature radius of the jet is $\sim 80''$. The whole jet (excluding the knot C) has an integrated magnitude $m_R(jet) = 19.3$. The bright knot (A) which is $1.65''$ (PA = $302°$) from the nucleus (big cross) is resolved and elongated along the direction approximately perpendicular to the jet. Its magnitude is $m_R(A) = 19.9$. There is a secondary knot (B) at $5.0''$ from the nucleus (PA = $308°$) with a magnitude of ~ 21.5. Finally the 'red tip' (C) at $9.0''$ and $m_R(C) = 21.4$ is also resolved indicating that it is not a galactic star.

4. Discussion

The analysis of the high-resolution images of PKS 0521–365 have allowed to study the optical properties of the host galaxy and of the optical jet. We found

a slightly decreasing ellipticity is found. The brightness profile (see Fig. 3) is generally well described by the $r^{1/4}$ de Vaucouleurs law with $r_e = 6.2''$ plus a point source over the whole range, but around $r \sim 1.5''$ there is an excess of emission with respect to the model. To account for this excess we add an exponential component which may represent the contribution of a faint disk to the inner part of the galaxy. The fit is substantially improved with a significant decreasing of the χ^2. The presence of a disk component is also suggested by a positive Fourier coefficient in the region between 1 and 4 arcsec. The best decomposition of the profile is thus obtained with a small exponential disk of characteristic radius $r_d = 1''$ and integrated magnitude 17.0. The magnitude of the galaxy derived by the model, including the bulge and the small disk, and integrated down to $\mu_R = 25.5$ mag/arcsec^{-2} is $m_R = 14.65$, while the point source in the nucleus has a magnitude $m_R = 16.0$.

Assuming H$_o$ = 50 km s^{-1} Mpc^{-1} and q$_o$ = 0, the galactic extinction A$_R$ = 0.15 and K-correction of 0.07, we found the absolute magnitude of the galaxy is M$_R$ = -23.2, that corresponds to M$_V$ = $-2?.4$ (if V − R = 0.8), which is typical for galax-

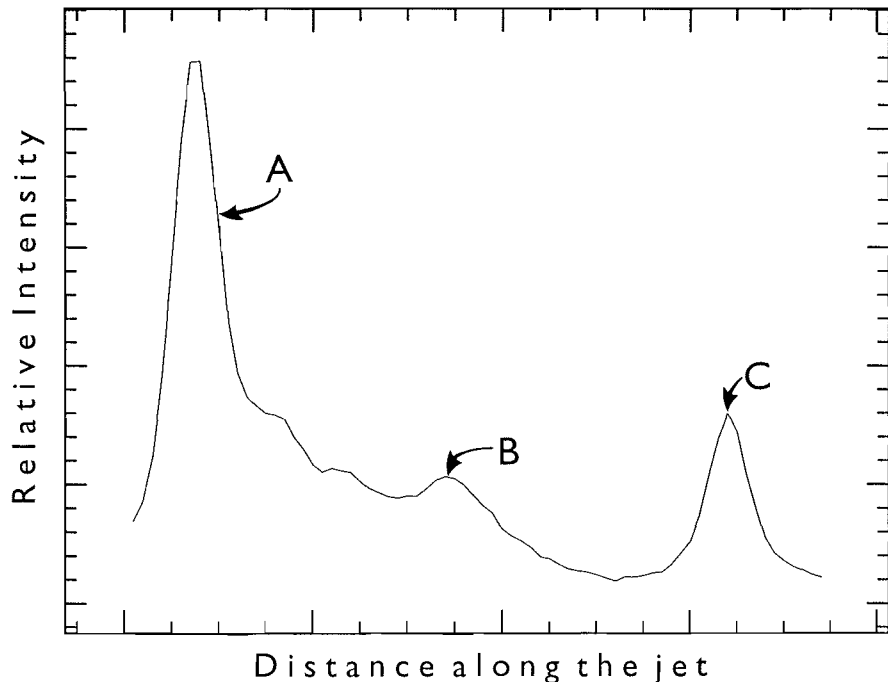ies hosting BL Lac objects. The effective radius is $r_e = 9.2$ kpc.

Figure 6: *Relative intensity along the jet obtained averaging the signal over a strip 1.3'' wide. Each large tick in the abscissa corresponds to 2.6 arcsec.*

the host galaxy to be a giant elliptical in agreement with previous studies but with probably a faint stellar disk. A similar feature was also found in the galaxy hosting the BL Lac PKS 0548-32 and may be not uncommon in early-type galaxies (see e.g. Scorza 1992). Its relation with the active nucleus (e.g. by accretion events) needs, however, a complete study for a larger sample of objects.

The optical jet is markedly knotty and resembles that of M 87 although it is more than a factor of 2 intrinsically brighter in the R band (cf. Biretta *et al.* 1991). Also the projected length of the jet (10 kpc) is much larger than that ($\sim$ 2 kpc) observed in M 87. The presence of the secondary peak (B) was suggested by the FOC image obtained with HST before the introduction of COSTAR and is well detected here. The decreasing optical intensity along the jet follows a behaviour very similar to that observed at 2 cm by Keel (1986).

Although the feature (C) is resolved, it remains unclear whether it is associated with the jet in some way or whether it is just a projected object. The lack of radio emission and of optical polarization favours the hypothesis that it is a projected faint galaxy. The centre of the 'red tip' is however very closely aligned with the bright knot and the centre of the galaxy.

Acknowledgement

References

Biretta, J.A., Stern, C.P., and Harris, D.E. 1991, *AJ*, **101**, 1632.
Boisson, C., Cayatte, V., Sol, H. 1989, *A&A*, **211**, 275.
Cayatte, V., and Sol, H. 1987, *A&A*, **171**, 25.
Danziger, I.J., Fosbury, R.A.E., Goss, W.M., and Ekers, R. D. 1979, *MNRAS*, **188**, 415.
Danziger, I.J., Shaver, P.A., Moorwood, A.F. M., Fosbury, R.A.E., Goss, W.M., and Ekers, R.D. 1985, *The Messenger*, **39**, 20.
Fichtel, C. E., et al. 1994, *ApJS*, in press.
Keel, W. C. 1986, *ApJ*, **302**, 296.
Macchetto, F., et al. 1991, *ApJ*, **369**, L55.
Pian, E., Falomo, R., Ghisellini, G., Maraschi, L., Sambruna, R.M., Scarpa, R. & Treves, A. 1994, *Ap.J*, submitted.
Reduzzi, L. *et al.*, 1994, *The Messenger*, **75**, 28.
Scarpa, R., Falomo, R., & Pian, E. 1994, *PASP*, submitted.
Scorza, C., 1992, ESO/EIPC Workshop, *Structure, Dynamics and Chemical Evolution of Elliptical Galaxies*, p. 115, Ed. I.J. Danziger *et al.*
Sparks, W. B., Miley, G. K., and Macchetto, F. 1990, *ApJ*, **361**, L41.
Ulrich, M. H. 1981, *A&A*, **103**, L1.

Molecular Hydrogen Observations Towards Herbig-Haro Objects

R. GREDEL, ESO-La Silla

1. Introduction

The small optical line emission nebulae known as Herbig-Haro (HH) objects have received considerable attention in recent years. This is because HH objects are associated with young stellar objects, and their study may give insight into the processes that occur during star formation. It is believed that during the formation of a low-mass star a collimated jet of material is produced that emerges with supersonic speeds. The formation of jets may help to remove angular momentum from the forming stars. In the interaction regions of the jets with the ambient interstellar medium, bow shocks are created where the bulk energy of the outflowing material is converted into thermal energy. Temperatures in the shocks are raised to 2000–3000 K.

In recent years, it became evident that HH objects are also prominent emitters of molecular hydrogen lines in the near-infrared. To our delight, the near-infrared emission offers new possibilities to study the processes that occur in the shocked gas. The ground state of H_2 has a multitude of vibration-rotation levels with excitation energies ranging from less than 1000 K to several 10,000 K. The lowest levels, with vibrational quantum number $v \leq 3$, can be collisionally excited in the shock-heated gas. This case is referred to as thermal excitation. Levels above $v > 3$ are too high in energy and are not excited.

Two alternative, non-thermal, excitation mechanisms have also been discussed in connection with HH flows. In many cases the shocks are fast enough to produce ultraviolet and X-ray photons. The radiation might fluorescently excite the electronic states of H_2, or lead to excitation of the electronic states via impact by the secondary electrons produced by the X-rays. The decay of the electronic states competes with the collisions to populate the vibrational levels in the ground state, and, in particular, it populates levels in $v > 3$. If the shock speeds become too high, the shocks are dissociative and H_2 is destroyed. Nevertheless, H_2 emission can still occur, because H_2 eventually re-forms in the post-shock region where the gas is cooling. Part of the energy that is released when two H atoms combine to form H_2 is converted into excitations of the vibrational levels, which also include $v > 3$.

It has been suggested that each of the non-thermal excitation scenarios described here is strong enough to lead to observable effects. Schwartz *et al.* (1987) have performed calculations for the specific case of HH 43. The authors considered excitations by ultraviolet Lyα photons and predicted the resulting near-infrared emission spectrum. They also obtained a low-resolution CVF spectrum which appeared to contain emission lines from $v > 3$. Wolfire & Königl (1991) discussed low-resolution CVF spectra obtained by Harvey *et al.* (1986) towards HH 1, and suggested that the H_2 emission is primarily excited by UV continuum fluorescence and by collisions in an UV and X-ray heated gas, rather than by collisions in a shock. And finally, Carr (1993) proposed that the weak emission towards HH 11 is caused by reforming molecules behind a fast dissociative shock. However, recent medium-resolution H_2 spectra of HH objects, obtained with IRSPEC, have cast new light on these interpretations.

2. IRSPEC Observations

IRSPEC, the ESO near-infrared spectrograph on the ESO 3.5-m New Technology Telescope (NTT), is an ideal instrument to obtain accurate spectroscopy in the 1–5 μm range. IRSPEC provides long-slit capabilities and a spectral res-
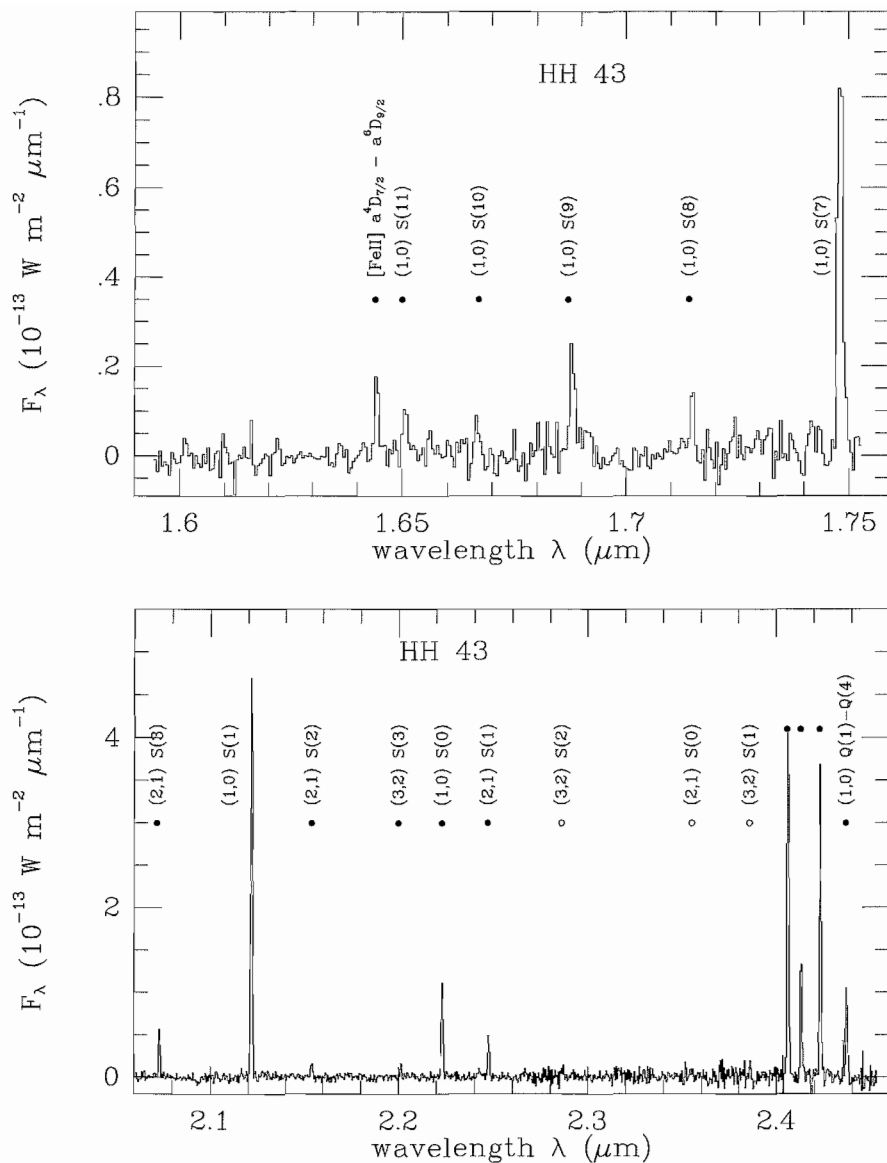
Figures 1a, b: *H- and K-band spectra of HH 43. Monochromatic fluxes F_λ in units of 10^{-13} W m^{-2} μm^{-1} are plotted vs. wavelength λ (in μm).*

olution of R = $\lambda/\Delta\lambda$ of a few 1000. The observations are reduced in a straightforward manner, using the IRSPEC context in MIDAS, which is now becoming available on-line. A graphical user interface is presently being installed at the NTT. It was developed on La Silla, with the aim to aid on-line data reduction within MIDAS, and will be described in a forthcoming article.

The high quality of near-infrared spectra that are obtained with IRSPEC is demonstrated in Figures 1a and 1b, which contain the H- and K-band emission towards HH 43. The spectra were constructed from about 20 individual grating settings, with 5–10 minutes of integration time each, equally shared between the object and the sky. It turns out that all the detected H_2 emission lines arise from vibrational levels $v \leq 3$, a strong indication that only collisional excitations occur. Upper limits for the fluxes

of lines from $v > 3$ are $F \leq 5 \times 10^{-18}$ W m^{-2}. This is in contrast with the calculations of Schwartz et al. (1987) who predicted line fluxes around $F \approx 10^{-16}$ W m^{-2} for a number of lines arising from $v > 3$, such as the (6,4) Q(5) line near 1.643 μm. The authors presented a CVF spectrum towards HH 43 as well, which contained a feature near the latter line, with a flux of $F \approx 10^{-16}$ W m^{-2}. From the recent IRSPEC spectrum, shown in Figure 1b, this feature is unambiguously assigned to arise from the $a^4 D_{7/2} - a^6 F_{9/2}$ transition of [Fe II], at a wavelength near 1.644 μm.

The measured line intensities can be used to infer the population distribution among the various vibrational levels. It is conveniently examined in excitation diagrams such as those shown in Figures 2 and 3. In such diagrams, the data points can be fitted by a linear regression if, and only if, the population distribution is

relaxed to a uniform excitation temperature. This is indeed the case for HH 43, with a corresponding excitation temperature of 2200 K, represented by the full line. The dashed line is a fit to the four lowest data points and corresponds to 1900 K. H- and K-band spectra were also obtained towards a number of other HH objects. Emphasis was put to accurately measure the 1.60–1.65 μm wavelength interval, because this region is expected to show detectable emission from a number of high-excitation lines, if H_2 is non-thermally excited. None of the obtained spectra shows such lines, with upper flux limits similar to values given above. Instead, all emission arises from $v \leq 3$; the inferred population distribution is thermal in all cases and can be described by single excitation temperatures. This is demonstrated in Figure 3, where values of 2600 K, 2400 K, 2100 K, and 2100 K, respectively, were inferred for HH 54E, K, HH 56, HH 99A, and HH 106.

3. Discussion

What is the nature of the shocks that lead to the observed near-infrared emission? Since the first observation of molecular hydrogen emission in dense molecular clouds, there is considerable controversy about this question. There are two classes of shocks, which require largely different physical conditions to form. C-type (Continuous) shocks were favoured until recently, because they form under conditions that were thought typical for dense molecular clouds – low fractional ionization $x_e \approx 10^{-8}$–10^{-7}, and relatively strong magnetic fields. The fractional ionization x_e is the ratio of the electron density and the neutral gas density. J-type (Jump) shocks, on the other hand, require $x_e \geq 10^{-5}$, and can only form if the magnetic field is weak.

Near-infrared observations, together with theoretical calculations, can be used to distinguish between the two types. First, the inferred H_2 excitation temperatures are all very similar, and a single temperature is enough to fit the data for a given object. This finding points to an excitation mechanism which is insensitive to the physical conditions that prevail in the shocked regions. Such is expected for J-shocks. C-shocks, on the other hand, produce an H_2 excitation that is strongly dependent on the pre-shock density, the magnetic field strength, and other physical parameters. The observed column densities of shocked H_2 are also well modelled by slow J-shocks. C-shocks with velocities above 20 km s^{-1} produce H_2 column densities that are 2–4 orders of magnitude higher. Lower columns are produced in slower C-shocks, but then the shocks cannot raise the temperature above 1000 K,
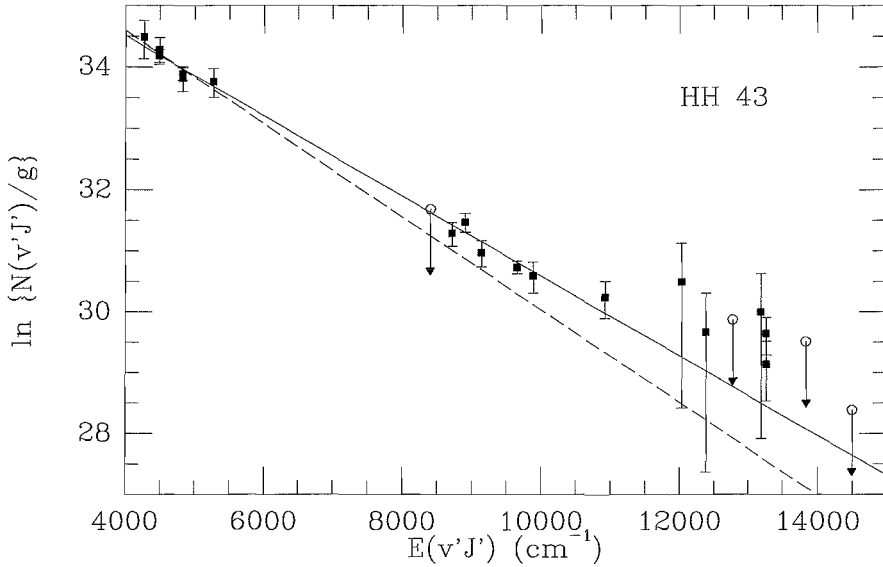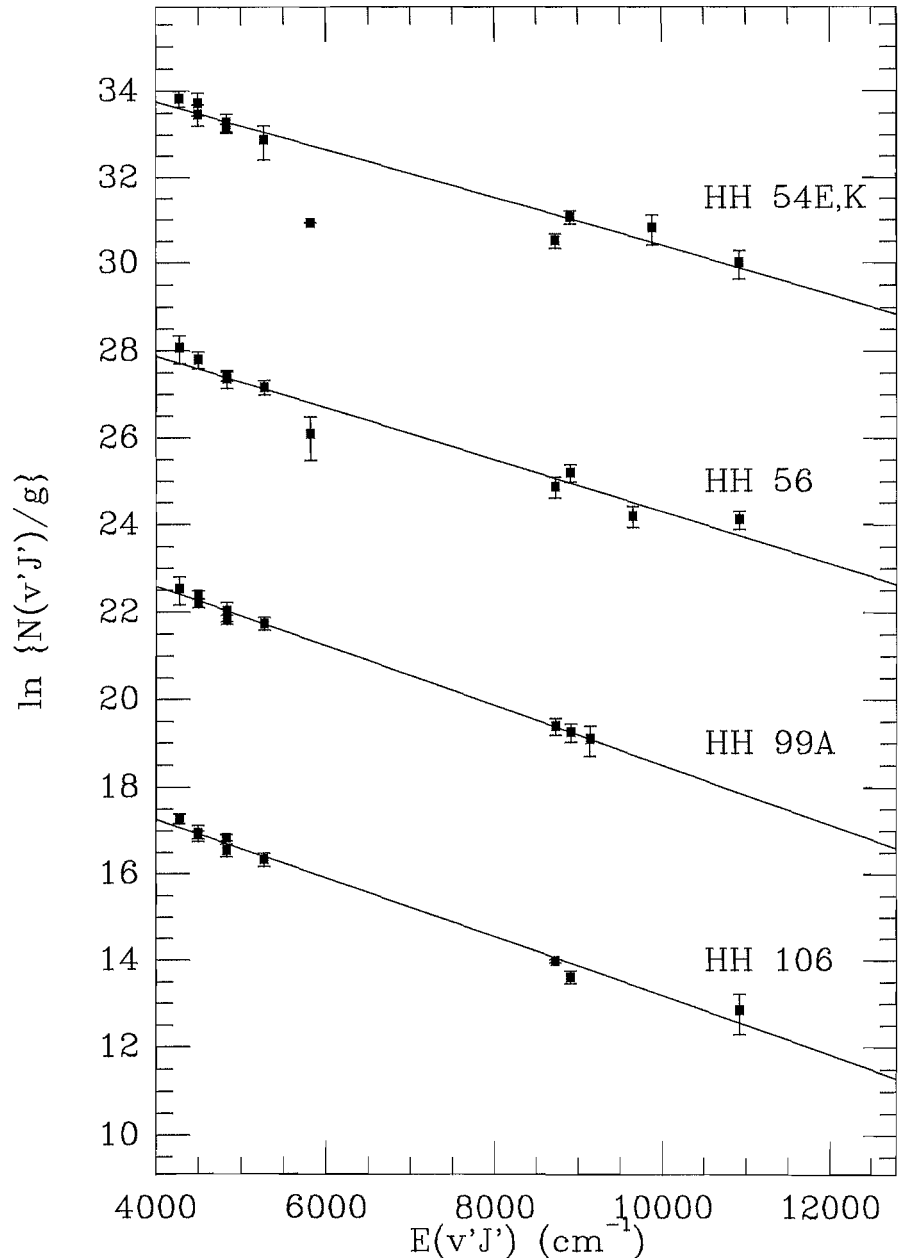
Figure 2: H_2 excitation diagram for HH 43. The full line characterizes a thermal distribution of 2200 K. The dashed line is a fit to the population density in the four lowest levels and corresponds to a temperature of 1900 K.

It has been demonstrated that low-resolution CVF spectra are not adequate to properly interpret the near-infrared spectra of HH objects, but that indeed a resolution such as the one provided by IRSPEC is required. The need is evident to perform similar studies towards other HH objects for which non-thermal excitation has been claimed, and in particular towards those where such claims are based on low-resolution spectra. Such work is in progress.

References

Carr, J.S. 1993, *ApJ* **406**, 553.
Schwartz, R.D., Cohen, M., Williams, P.M. 1987, *ApJ* **322**, 403.
Wolfire, M.G., Königl, A. 1991, *ApJ* **383**, 205.

which is in contrast with the observations. In addition, C-shocks do not produce emission from ionized species such as [Fe II], which is present in all objects observed here. The observed [Fe II] intensities, typically a few 10^{-5} erg s^{-1} cm^{-2} sr^{-1}, agree well with the predictions of J-shock models. Last but not least, the [Fe II] observations afford the possibility to determine electron densities in the shocked region. The electron densities can then be compared with lower limits in the neutral gas density, which can be estimated from diagrams such as those shown in Figures 2 and 3. The resulting fractional ionization is high enough to mediate J-shocks.

4. Conclusions

The main result of this study is that the H_2 emission in the observed HH-objects is thermally excited by shocks. The shocks are most probably J-type, which then indicates weak magnetic fields and high fractional ionization, $x_e \geq 10^{-5}$, in the surrounding molecular clouds. Such high values of x_e may indicate that the molecular clouds have a highly clumpy, or fractal, structure. This would allow the ultraviolet photons from nearby stars to permeate deeply into the molecular material, ionize the surfaces of the clumps, and thus provide the required fractional ionization levels.

Figure 3: H_2 excitation diagrams for HH 54E, K, HH 56, HH 99A, and HH 106, with corresponding thermal population distributions of 2600 K, 2400 K, 2100 K, and 2100 K, respectively, indicated by the full lines.

Towards a Deep IR ESO Sample

P. SARACCO[1,2], A. IOVINO[2], G. CHINCARINI[1,2], B. GARILLI[3] and D. MACCAGNI[3]

[1]Università degli Studi di Milano, Italy; [2]Osservatorio Astronomico di Brera, Italy;
[3]Istituto di Fisica Cosmica e Tecnologie Relative, CNR, Milano, Italy

As soon as the near-IR arrays became available, various observatories started to experiment with infrared cameras in order to achieve high-accuracy two-dimensional images in the near-infrared. The work of ESO in this field has been briefly illustrated by Morwood et al. 1992.

Cowie (1991) showed that the counts of galaxies in the K′ magnitudes were in disagreement with the counts obtained in the blue band in the sense that, in this colour, we would not measure the large excess of faint galaxies observed at shorter wavelengths. The observed difference in the counts is obviously deeply connected also with the understanding of galaxy evolution since (a) in the blue we are detecting objects which we obviously do not see in the near-IR and (b) we should be able to understand which kind of objects are causing such a difference and at which redshifts they are, i.e. intrinsically faint and at low-medium redshift or intrinsically bright and far away. Merging among field galaxies could explain in part the observed dichotomy (Broadhurst et al., 1992). However, more observations of deeper samples are extremely important to understand what is going on. Indeed, it is fundamental, also in relation to the new class of very large telescopes, to be able to have catalogues of faint and distant objects in order to study the detailed properties of galaxies at large redshifts.

In this paper we will briefly describe the accuracy achieved in data reduction of the fields we observed in the IR using IRAC2 (NICMOS III array) at the 2.2-m telescope of ESO. The project aims at galaxy counts in the K′ band and to the preparation of a faint-object catalogue for detailed studies. The full analysis, the details of the reduction procedure and the science results will be the subject of a later publication.

The sample had been selected according to the following criteria: (a) it had to cover a large area, (b) it had to go deep enough to be significant for counts of galaxies statistics and form, in any case, a catalogue on which to base the spectroscopic observations of faint non-cluster galaxies, and (c) its field had to be selected at high galactic latitude to minimize the extinction. In addition, and due in part to the limitations in the setting of the telescope and to the suggestions by Morwood, all fields had to include a medium-brightness star, about 14th magnitude, in order to optimize the stacking of the different IR frames. Having in mind this recipe, we searched the sky around the southern galactic pole for UK-ESO blank fields of $\sim 2 \times 2$ arcmin (which is about the size of the CCD on the focal plane of the 2.2-m telescope) with either one or two stars with magnitude in the range 13–15. At the moment of the observations we preferred to select fields with two stacking stars. This would give a very accurate reference for stacking of observations obtained in different observing years. The strategy we adopted, due also to some unknowns about the final performance of the array and the reduction procedure, was to select 3 fields on which to go deeper, down to K′ $\approx$ 20.0, and 8 fields for which we planned a shallower limiting magnitude with the purpose of having a good statistics at somewhat brighter magnitudes. This is the only sample of faint galaxies selected in the K′ band done at ESO and consists of 11 fields of 2.8 arcmin². This sample and its analysis will give us also accurate information on the limiting magnitude we can reach, by increasing the number of observations, within a reasonable amount of telescope time.

Linearity

Images were obtained at the telescope using all the integration times which were feasible without saturating the chip, in the K and K′ band. In practice, the integration time varied between 0.882 and 4.155 sec. We tested then the CCD as a whole and its four 128 × 128 quadrants. The result is that each quadrant, and the CCD as a whole, has a linear response[1] with

---

[1]The linearity of the detector can be defined according to the relation:
$$L = \sqrt{l/n}\Sigma[l - N_i^{real}/N_i^{ideal}]^2$$
where n is the number of measurements obtained in that range and N_i^{real} and N_i^{ideal} are the expected and measured counts.
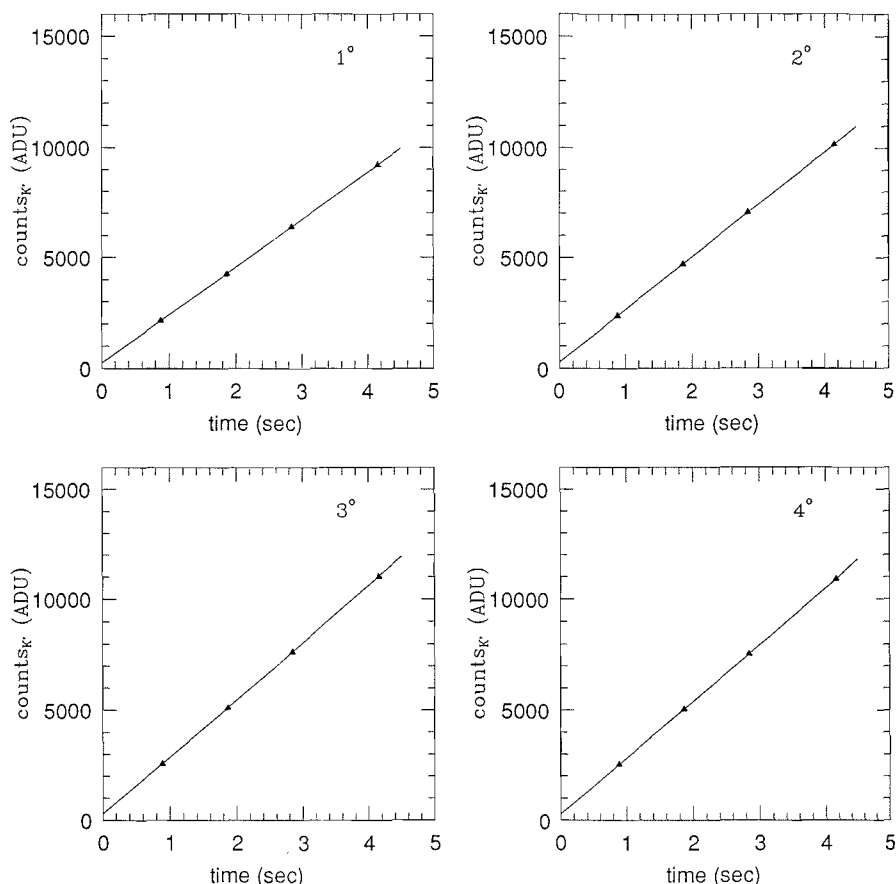

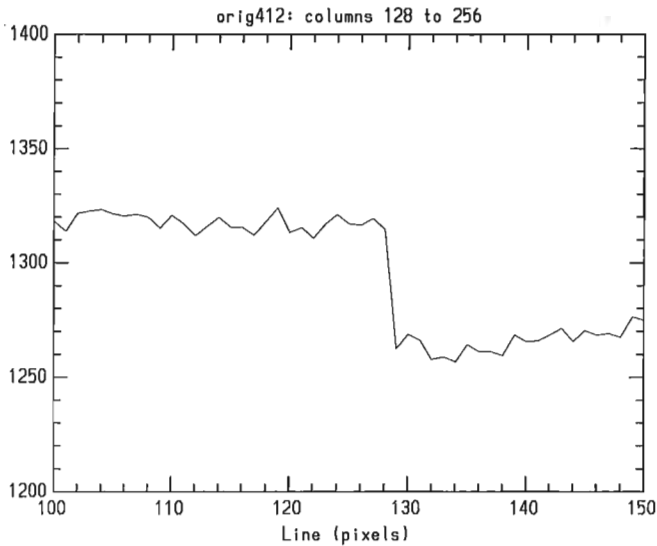Figure 1: Linearity test on the 4 quadrants of the NICMOS III array.

Figure 2: *Sensitivity difference between the two halves of the array.*

Figure 3: *Magnitude of one of the "stacking stars" measured in 25 different frames.*

a deviation from linearity smaller than $5 \cdot 10^{-3}$. The slope differs, however, from quadrant to quadrant, Figure 1, with the main difference being beetween the upper and lower half, Figure 2. This effect, which is present also on smaller scales and amounts to about 1 %, is corrected by dividing the images by the FF.

Flat Field (FF)

A variety of tests have been done in order to optimize the S/N of the reduced images, both using dome and sky flats. The optimum procedure resulted in constructing the flat-field image for each frame from the median of the adjacent sky images. The selection criterion, among the different methods, has been based on the minimization of the error estimated on the standard stars which have been observed on each quadrant of the CCD array. The rational of using a small group of adjacent sky frames (~ 9) is that (a) by using the whole set (≥ 27 frames per field of two minutes each) we would be sensitive to long-period sky variations, and that must be avoided and (b) by using a small number of adjacent frames we smooth out the small-period sky variations which may affect each single frame in a rather random way. To each target frame is then assigned its own flat field.

For these stars we also measured their profile. The aperture used to determine the magnitude is that for which the magnitude derived is the same, within the error, as the magnitude measured using the next larger aperture.

The Zero Point

After applying the FF correction described above, for the images of the standard stars (each star was imaged in each frame on the 4 quadrants) we
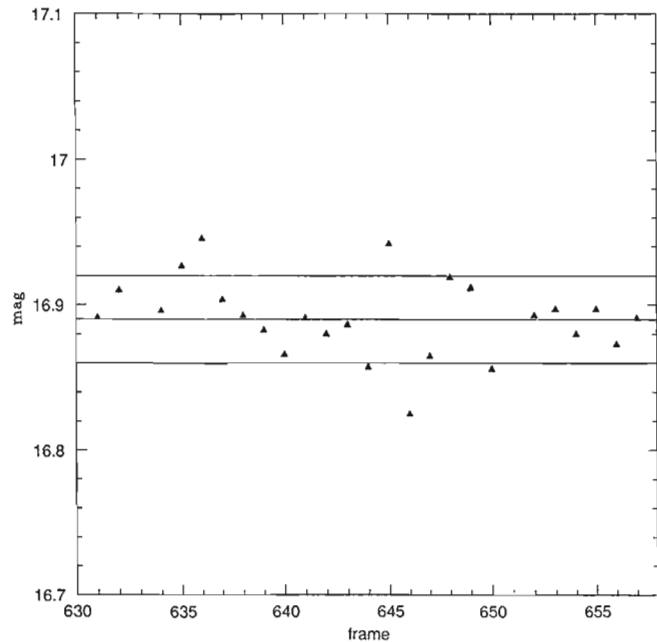
measure as typical values: σ(1st night) = 0.04 mag, σ(2nd night) = 0.033 and σ(3rd night) = 0.035.

The K′ zero point of our photometry was derived using the relation

K′ − K = 0.20 (H–K)

and the K′ zero point error for the standard stars on each single night was: σ_0(1st night) = 0.04, σ_0(2nd night) = 0.02
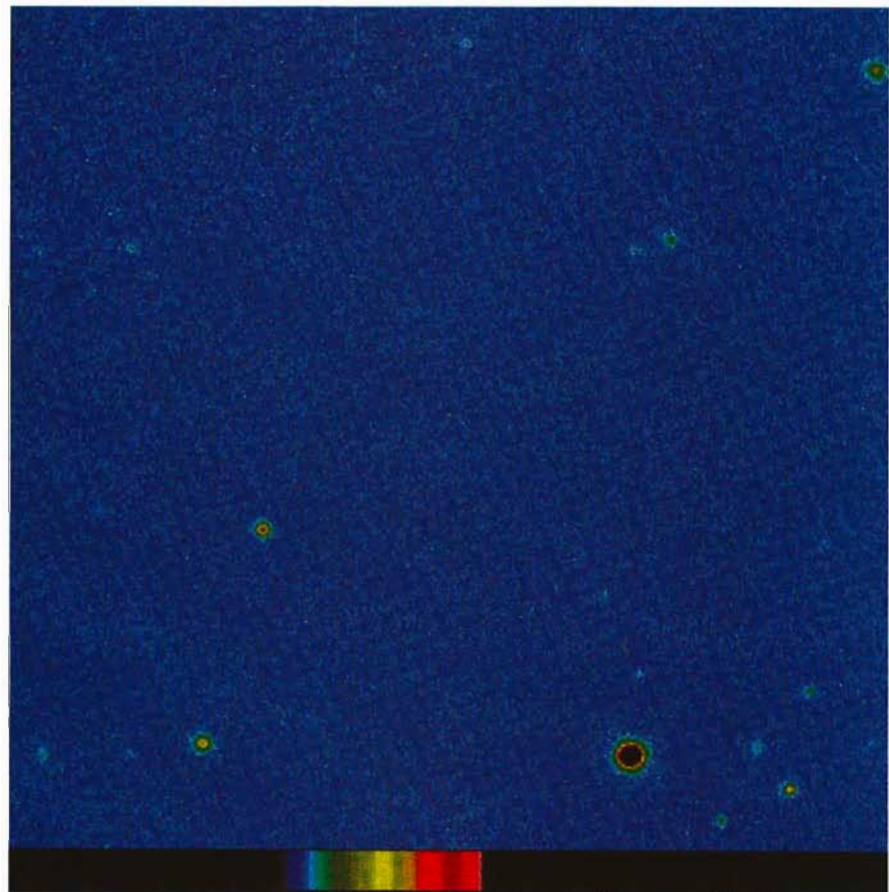

Figure 4: *Image of one of the deep fields. Integration time is 162 minutes. The faintest objects visible are of $m \sim 20$ in K′.*

and σ_0(3rd night) = 0.03. As a check of the quality of our photometry we measured the magnitudes of the stacking stars we had on the target frames, the run of magnitude versus frame number is illustrated in Figure 3 and shows perfect agreement with the estimates given above.

Note that the Poisson photon noise due to the sky (gain factor = 5.2) is estimated to be of 0.01 mag so that the accuracy attained is close to the theoretical limit expected and shows that with IRAC2 it is possble to achieve high-accuracy photometry. A target frame, deep exposure, has been reproduced in Figure 4.

Acknowledgements

References

Broadhurst, T.J., Ellis, R.S. and Glazebrook, K., 1992, Nature, **355**, 55.
Cowie, L.L., Songaila, A. and Hu, E.M., 1991, Nature **354**, 55.
Moorwood, A., Finger, G., Biereichel, P., Delabre, B., Van Dijsseldonk, A., Huster, G., Lizon, J.-L., Meyer, M., Gemperlein, H. and Moneti, A., The Messenger, No. **69**, p. 61.

The 4th ESO/OHP Summer School:

TWO WEEKS IN PROVENCE; STARS, COMETS, GOOD FOOD AND WARM HOSPITALITY

M. VÉRON, Observatoire de Haute-Provence, France, and
E.J. WAMPLER, ESO-Garching

1. Introduction

The fourth biennial ESO/OHP Summer School was held at the Observatoire de Haute-Provence from July 18 to July 29. This Summer School gives 18 selected astronomy graduate students practical experience in observing techniques, data reduction and the software systems that are in use in the ESO member states. Afternoon lectures by experts on the various tools used by modern observers introduced the students to the sweep of techniques used in ground-based astronomy. And the enthusiasm of the summer school students moved even their stodgy teachers. Relaxation during breaks came from the swimming pool, pastis and after dinner pétanque (boules) competitions. As usual, the student attendees were highly convivial and this led to warm relationships developing among the students and between the students and the School staff.

The Observatoire de Haute-Provence, located in a particularly lovely region of southern France, is one of the very few places in Europe where the summer climate and modern astronomical facilities combine to insure the success of a summer school devoted to teaching observing techniques to astronomy graduate students. The OHP summer school thus helps to fill a gap in the formal education of promising young European observers.

2. Practical Work

The curriculum of the 1994 Summer School followed the general pattern that proved to be useful in the three earlier ESO/OHP Summer Schools (cf. *The Messenger* No. 53, p. 11, No. 61, p. 8 and No. 69, p. 17). The 18 students were divided into groups of three, and six tutors (Denis Gillet, Sergio Ilovaisky, and Philippe Prugniel from OHP, Agnes Lèbre from Montpellier, Pascale Jablonka from

Figure 1: *At the break during Ray Wilson's talk, the group posed for an official photograph. From the left: first row: R. Wilson, M. Véron, A. Fishburn, b. Milvang-Jensen, M. Chadid, S. Ruphy, V. Doublier, P. Jablonka, A. Gemmo. First step: S. Leon, S. Och, M. Serote-Roos. Second Step: V. Hill, I. Rentzsch-Holm, N. Troelsgaard-Jensen, T. Preibisch, L. Vanzi, L. Lucy. Back group: F. Courbin, J. Wampler, M. Gray, M. Federspiel, G. Rauw, P. Véron, M. Nauta and R. Noordhoek.*

Figure 2: *Cool water was a welcome treat at break time during the afternoon talks.*

Meudon and Alessandra Gemmo from Garching) each assisted one student group with a short, pre-planned observing programme.

D. Gillet led V. Doublier, N. Troelsgaard-Jensen and L. Vanzi in a study of the β Cephei star BW Vul to attempt to distinguish between Stark broadening introduced by the passage of the compression wave and shock emission during the line-doubling phase. They used the AURELIE spectrograph to measure variations in the Hβ line. Their imaging project was to see if the small migrating bump reported on the light curve of XX Cygni is real or if it is an artifact of the interpretation of previous observations.

A. Gemmo helped F. Courbin, M. Nauta and I. Rentzsch-Holm observe poorly-known Cataclysmic Variable stars (CV stars). The spectroscopic part of the programme was aimed at obtaining low-resolution spectra with the 1.93-metre telescope of those CV stars with good coordinates but with little or no spectral information. The photometry programme with the 1.2-metre telescope was directed to finding the physical parameters, in particular the period, of the programme CV stars.

S. Ilovaisky led M. Federspiel, G. Rauw and S. Ruphy in a search for an optical counterpart for ROSAT X-ray sources. They used the 1.2-metre telescope to obtain images of the X-ray fields to try and identify candidate objects. Low-resolution spectra were then taken of the candidates with CARELEC. The resulting data were searched for peculiar spectral features in an attempt to identify likely X-ray candidates.

P. Jablonka guided V. Hill, R. Noordhoek and T. Preibisch in an observational comparison of high-and-low metallicity globular clusters. Long-slit spectra with the 1.93-metre telescope were used to obtain the integrated metallicity of two globular clusters (M 13 and M 56). With the 1.2-metre telescope, images taken through the B and V filters were used to obtain colour-magnitude diagrams of the two clusters.

A. Lèbre worked with S. Leon, B. Milvang-Jensen and S. Och to investigate the stages of stellar evolution: RV Tauri stars and planetary nebulae. AURELIE was used to obtain spectra for studying the shock-induced profile changes in the Hα and the sodium doublet lines. The 1.2-metre telescope was used to image planetary nebulae with narrow-band filters that isolated the lines of Hα, and [S II] $\lambda\lambda6717,31$. Particular attention was paid to Sh 2-71 in order to sort out the peculiar morphology of this object.

P. Prugniel helped M. Gray, M. Serote-Roos and V. Shcherbakov with observations of Comet Shoemaker-Levy 9. Imaging observations were obtained at the 1.2-metre telescope and spectra with a resolution of about 1 Å were obtained using the 1.93-metre telescope. Because the impacts turned out to be so spectacular, the findings of this group were watched with interest by the other groups.

As a special bonus for the 1994 School, the students were able to use the guiding telescope attached to the 90/60-cm Schmidt telescope to visually observe the impact spots made on the planet Jupiter by comet Shoemaker-Levy 9. Certainly such an unusual event occurring at the time of the summer school will make the school particularly memorable to all of the participants.

Readers of this article will note that the observing programmes for the students could produce interesting scientific results. Of course, the main aim of the Summer School was to teach the students how to observe using modern equipment, but the potential of obtaining publishable results motivated the students to work extra hard on their programmes. In fact, despite a few early evening clouds during the Summer School, all the students were able to successfully finish their projects.

3. Afternoon Talks

Following the tradition of previous Summer Schools, eight afternoons were devoted to talks by experienced astronomers about various aspects of instrumentation and data reduction.

The first speaker was Ray Wilson, who talked about modern telescope design and the contributions to telescope design by Karl Schwarzschild. Following his discussion of the optical design of large telescopes, Ray described the current situation with respect to manufacture and test technology. He concluded with a plea for more attention to be paid to the maintenance of telescopes and their optics.

Roser Pello and Joseph Wampler described spectroscopy and the design of spectrographs. The first concentrated on low-resolution spectroscopy, while the second described high-resolution spectrographs and, in particular, echelle spectrographs. Techniques for the extraction of the spectra from two-dimensional CCD frames were also described.

Leon Lucy gave an introduction to the principles of image restoration; describing Maximum Likelihood and Maximum Entropy. Following this, he discussed procedures that yield high photometric accuracy and considerations that are important when the observing programme requirements are influenced by the ability of modern reduction techniques to remove instrument signatures from the data.

Sergio Ilovaisky described imaging and photometry using CCDs. Sergio pointed out the various artifacts that the detector may have. He particularly stressed the importance of flat fields for removing these artifacts. He emphasized the need for careful determination of the linearity of the CCD detector. And standard star observations are needed for accurate photometry. Overall, Sergio emphasized the need for a deep understanding of the possible sources of er-

ror in the photometry in order to obtain reliable results.

Michel Dennefeld continued the discussion of detectors with a clear presentation of the techniques for storage and transfer of charge in CCD detectors. He described the photoelectric effect and contrasted it with the photoconductive effect. He again emphasized the problem of flat-fielding CCD detectors and described the various ways that the detector produces interference fringes. He finished his talk with a description of the special problems of obtaining detectors for large telescopes..

Jason Spyromilio gave a lively description of the techniques and special problems that face the infrared astronomer. In addition to tricky detectors, the designer of infrared telescopes and instrumentation must face a situation in which any warm piece of equipment glows at nearly the same temperature as the astronomical source. He illustrated his talk with many interesting astronomical images, including a spectacular IR image of Jupiter showing some of the impact sites of comet Shoemaker-Levy 9 on the planet.

The last talk was a lecture by Roger Ferlet on dark matter in the Universe. He emphasized the importance of dark matter in setting the conditions of the early Universe and the evidence for dark matter in the rotation curves of galaxies. Roger then turned to the search for brown dwarfs and the discovery of micro-lensing by three different groups. He finished by noting that the micro-lensing programmes will, as a by-product, give us a huge sample of variable stars.
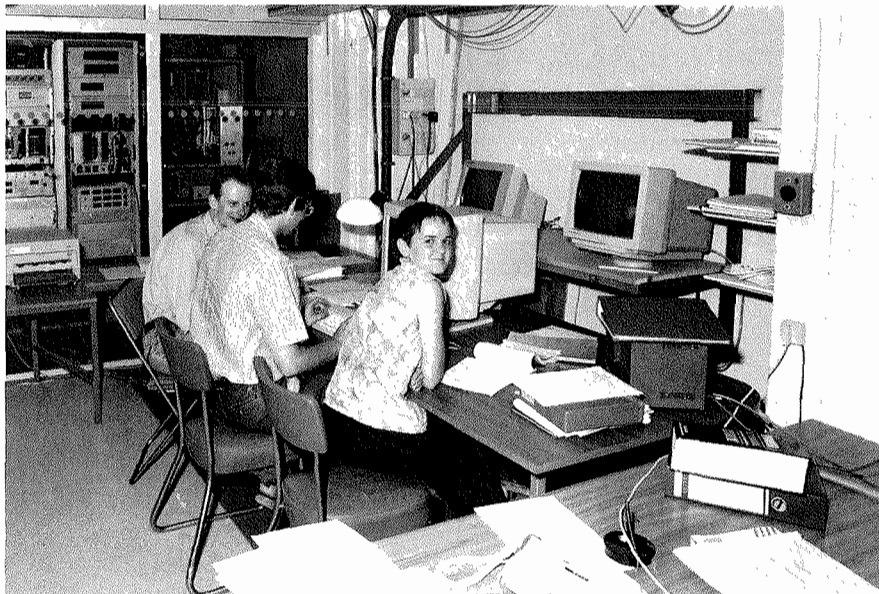
Overall, the afternoon talks gave a

Figure 3: *G. Rauw, M. Federspiel and S. Ruphy in the 1.93-metre telescope control room looking for X-ray stars.*

valuable theoretical underpinning to the night-time observing and the subsequent data reduction. The talks were enlivened by many not-to-be-forgotten experiences, from Jason's table pounding with a bamboo cane to Philippe's not-so-innocent tough questions. We are still not sure who won Jason's contest for the person who asked the most questions.

4. Memories

Among the memories that all of the participants will carry home with them are the social occasions that we had together. We particularly wish to thank Denis Gillet for taking us on a Sunday outing to the gorges at Oppedette and then on to the old village of Simiane. The gorges, the old towns and the scents of the Provençal countryside where the lavender harvests were underway, gave the visitors to Haute-Provence a real treat.

Also not to be forgotten was the Observatory swimming pool, the many late-night discussions, and the good fellowship at meal times, where Philippe told us certified true stories about famous astronomers, where Vanessa showed us her capacity for pastis, Bo his capacity for lettuce, and where Alessandra entertained us with her Italian jokes.

Programmes Approved for Period 54

ESO No.	Names of PIs (in alphabetical order)	Title of Submitted Programme	Telescope
D-0540	Abbott/Haswell/Patterson	Hunting the Orbital Period of H0551-819	1.5-m
D-0543	Abbott/Shafter	Time Series CCD Photometry of Old Novae	1.5-m Danish
D-0625	Aerts/Waelkens	Seismology of the β Cephei Star KK Velorum	1.4-m CAT
B-0026	Andreani/Cristiani/La Franca/Lissandrini/ Miller	The Cosmological Evolution of the Clustering of Quasars	3.6-m
E-0017	Antonello/Mantegazza/Poretti	First Overtone Cepheids in Magellanic Clouds	0.9-m Dutch
D-0425	Augusteijn/Abbott/Rutten/van der Klis/ van Paradijs	A Comparative Study of Disk and Halo Cataclysmic Variables	0.9-m Dutch
D-0426	Augusteijn/van der Klis/van Paradijs	Phase-Resolved Spectroscopy of Faint Cataclysmic Variables	1.5-m Danish
A-0951	Bedding/Fosbury/Minniti	Infrared Colour-Magnitude Diagrams for the Brightest Stars in NGC 5128 (= Cen A)	3.6-m
C-0878	Benvenuti/Porceddu	Can DIBs Be Originated from High-Latitude Molecular Clouds?	1.4-m CAT
A-0844	Bergvall/Oestlin/Roennback	An Hα Search for Galaxies at Intermediate Redshifts	2.2-m
D-0832	Bertoldi/Boulanger/Genzel/Sterzik	NIR Imaging of Young Stellar Clusters: Low-Mass Stars and Multiplicity	3.6-m
E-0976	Beuzit/Ferlet/Lagrange/Malbet/Vidal-Madjar	IR Observations of the β Pictoris Disk with Adaptive Optics and Coronograph	3.6-m
C-0557	Block/Grosbøl/Rupprecht/Witt	The Spatial Extent of Cold Dust in Spiral Galaxies	2.2-m
E-0914	Blommaert/Groenewegen/Habing/ Josselin/Omont/van der Veen	The Mass-Loss Rate of Supergiants and a Search for PAH	2.2-m
E-0914	Blommaert/Groenewegen/Habing/ Josselin/Omont/van der Veen	The Mass-Loss Rate of Supergiants and a Search for PAH	3.6-m
A-0133	Böhringer/Bower/Castander/Couch/Ellis	The Dynamical Structure of Galaxy Clusters at z = 0.5	3.6-m
F-0585	Böhnhardt/Rousselot/West	Investigation of Potential Target Comets of the ESA Rosetta Mission	2.2-m
C-0959	Boulanger/Combes/d'Hendecourt/Jourdain de Muizon/Schmitt/Trotta/Zagury	Very Cold Interstellar Matter in the Outer Parts of the Milky Way	NTT
D-0751	Bouvier/Beuzit/Corporon	High-Resolution Imaging of Close Pre-Main-Sequence Binaries	3.6-m
D-0032	Bragaglia/Lattanzi	Spectrophotometric Survey of Yellow Symbiotic Stars	1.5-m
D-0104	Brand/Wouterloot	Star Formation at the Edge of the Galaxy	2.2-m
C-0705	Brandl/Eckart/Genzel/Quirrenbach/Sams/ Tacconi-Garman/Zinnecker	Diffraction-Limited NIR Line and Continuum Imaging of R136 Using the Come-On+/Sharp II System	3.6-m
D-0911	Brandner/Zinnecker	Pre-Main-Sequence Binaries and Early Stellar Evolution	1.5-m Danish
D-0736	Bratschi/Blecha/Maeder	Simultaneous Photometric and Spectroscopic Observation of Variable Wolf-Rayet Stars	1.5-m
E-0658	Breitfellner/Fokin/Gillet/Mathias	Atmospheric Dynamics in the δ Scuti Star: ρ Puppis	1.4-m CAT
B-0086	Bremer/Fabian	Mapping Extended Lyα Emission Around Radio-Quiet Quasars at z > 3	NTT
E-0404	Brocato/Castellani/Ferraro/Testa	The Age of Old Magellanic Cloud Clusters	NTT
D-0698	Burwitz/Beuermann/Reinsch/Schwope/ Thomas	The Orbital Period Distribution of AM Herculis Binaries	0.9-m Dutch
E-0393	Cacciari/Bragaglia/Carretta/Fusi Pecci	Spectroscopic Study of Blue Horizontal Branch Stars in Globular Clusters	1.5-m
E-0337	Capaccioli/Piotto/Stiavelli/Veronesi/Zaggia	Structure of Galactic Globular Clusters	NTT
D-0819	Caraveo/Bignami/Goldoni/Mereghetti/ Mignani	Optical Studies of Isolated Neutron Stars Detected as X/Gamma Sources.	NTT
D-0589	Catala/Balona/Felenbok/Ghosh/Janot-Pacheco/Lagrange/Lawson	Line-Profile Variations of γ Doradus	1.4-m CAT
E-0128	Caulet/Landsman/Sweigart	The Extreme Horizontal Branch Star of M 79	3.6-m
E-0108	Cayrel de Strobel/Chmielewski/Friel	A Detailed Spectroscopic Study of the Old and Young Stellar Components of the Galactic Disk	1.4-m CAT
E-0954	Cayrel/Andersen/Barbuy/Beers/Nissen/ Nordstroem/Spite	Survey of Very Metal-Poor Stars in the Galaxy	1.5-m
B-0315	Cimatti/di Serego Alighieri/Fosbury	Is the [O III]5007 Line Partially Obscured in Powerful Radio Galaxies?	3.6-m
B-0036	Clements/Efstathiou/Lawrence/Maddox/ Mc Mahon/Rowan-Robinson/Saunders/ Sutherland	The Nature of Ultraluminous IRAS Galaxies: IR Imaging	2.2-m
B-0038	Clements/Efstathiou/Lawrence/Maddox/ Mc Mahon/Rowan-Robinson/Saunders/ Sutherland	The Role of Mergers in Ultraluminous IRAS Galaxies	2.2-m
A-0387	Collins/Guzzo/Nichol/Pisani	Multiobject Spectroscopy of Distant Clusters of Galaxies	3.6-m
D-0979	Corporon/Bouvier/Lagrange	A Search for Spectroscopic Binaries among Herbig Stars	1.4-m CAT
C-0580	Corradi/Frank/Mellema/Schwarz	Radiation-Gasdynamical Modelling of Planetary Nebulae	1.5-m
C-0580	Corradi/Frank/Mellema/Schwarz	Radiation-Gasdynamical Modelling of Planetary Nebulae	1.5-m Danish

ESO No.	Names of PIs (in alphabetical order)	Title of Submitted Programme	Telescope
E-0326	da Silva/de la Reza	Evolutionary Stage of the Very Li-Rich Giant Stars	1.4-m CAT
B-0774	Danese/Franceschini/Gallais/Granato/ Lagage	10-Micron Observations of Active Galactic Nuclei	3.6-m
D-0088	Danziger/Benetti/Cappellaro/DellaValle/ Lucy/Mazzali/Patat/Turatto	The Type Ia SN 1994D	3.6-m
D-0028	Danziger/Bouchet/Chugai/Della Valle/ Fransson/Gouiffes/Lucy/Mazzali	SN 1987A	2.2-m
D-0028	Danziger/Bouchet/Chugai/Della Valle/ Fransson/Gouiffes/Lucy/Mazzali	SN 1987A	3.6-m
D-0028	Danziger/Bouchet/Chugai/Della Valle/ Fransson/Gouiffes/Lucy/Mazzali	SN 1987A	NTT
D-0028	Danziger/Bouchet/Chugai/Della Valle/ Fransson/Gouiffes/Lucy/Mazzali	SN 1987A	1.5-m Danish
D-0033	Davis/Eislöffel/Lioure/Smith	First Complete J, H, K and L Spectra of Shocks in Outflows from Young Stars	NTT
D-0407	de Winter	Exploring and Modelling the Spectroscopic Variations of Bright Herbig Ae/Be Stars	1.4-m CAT
D-0356	de Winter	Detection of Circumstellar Material and Mass-Outflow Indicators of Young Stellar Objects of Intermediate Mass	0.9-m Dutch
D-0376	de Winter	Selecting Early-Type Pre-Main-Sequence Stars from Newly-Found Candidate Young Stars Associated with Strong IRAS Sources	0.5-m
D-0376	de Winter	Selecting Early-Type Pre-Main Sequence Stars from Newly-Found Candidate Young Stars Associated with Strong IRAS Sources	1.5-m
D-0325	Della Valle/Bartolini/Bianchini/Masetti/ Mirabel/Orio	Spectroscopic Observations of the Candidate Black-Hole Nova Vel 1993	NTT
A-0881	Della Valle/Giavalisco/Livio	A Search for Supernova Events in High-Redshift Galaxies	NTT
D-0607	Dennerl/Kürster	Identification of Highly Variable X-Ray Sources in the SMC	0.9-m Dutch
D-0889	Dieters/Groot/van Paradijs	Spectrophotometry of CP Pup: Weighing the White Dwarf	1.5-m
C-0063	Domgörgen/Dettmar	Physics of Diffuse Filaments in Late-Type Galaxies	1.5-m
E-0888	Dougados/Ghez/Lefevre/Lopez/Mekarnia/ Tessier	Mid-Infrared Imaging of Post-AGB Stars	3.6-m
A-0357	Dubath/Hesser/Queloz/Smecker-Hane/ Stetson	Search for Dark Matter in the Carina Dwarf Spheroidal Galaxy	NTT
E-0803	Duquennoy/Beuzit/Mariotti/Mayor/Perrier	Infrared Imaging of Very Low-Mass Companions to Nearby Stars	3.6-m
E-0511	Duquennoy/Mayor	Stellar Duplicity of Very Low Mass Stars	1.5-m Danish
A-0594	Durret/Gerbal/Lobo/Mazure/Slezak	Global and Structural Analysis of the Rich X-Ray Clusters of Galaxies ABCG 85 and ABCG 496. II. Photometry and Morphology	1.5-m Danish
A-0132	Ebeling/Böhringer/Oliveira/Voges	Optical Follow-Up of Poor ACO Supplementary Clusters Detected in the ROSAT All-Sky X-Ray Survey	1.5-m
E-0676	Edvardsson/Feltzing/Gustafsson/Lambert/ Morell/Tomkin	Europium and Carbon in the Galactic Disk	1.4-m CAT
B-0469	Falomo/Scarpa	Spectral Properties of Highly-Polarized Quasars	1.5-m
E-0396	Favata/Barbera/Giusi/Harnden/Sciortino	The Solar-Type X-Ray Source Population in NGC 2422	1.5-m
A-0593	Felenbok/Durret/Gerbal/Lobo/Mazure/Slezak	Global and Structural Analysis of the Rich X-Ray Clusters of Galaxies ABCG 85 and ABCG 496. I. Spectroscopy	3.6-m
D-0369	Fernandes/Brand/Lago	The Structure of Shocks in Herbig-Haro 46/47	NTT
E-0826	Ferrari/Bucciarelli/Lasker/Lattanzi/Le Poole/ Massone/Pizzuti/Postman/Siciliano	Photometric Calibrators for the Southern Sky Surveys	0.9-m Dutch
E-0409	Ferraro/Buonanno/Corsi/Fusi Pecci/Testa	Near-Infrared Imaging of Magellanic Cloud Clusters	2.2-m
E-0631	Festin/Andersen	Deep Near-IR Photometry for the IMF of the Open Cluster NGC 2516	2.2-m
E-0822	Foing/Char/Collier-Cameron/David/ Ehrenfreund/Houdebine/Jankov/Vilhu/ Walter	AB Doradus: A Key Target for Stellar Activity	0.5-m
E-0822	Foing/Char/Collier-Cameron/David/Ehrenfreund/Houdebine/ Jankov/Vilhu/Walter	AB Doradus: A Key Target for Stellar Activity	1.4-m CAT
A-0389	Fort/Bonnet/Kovner/Mellier	Detection and Measurement of Gravitational Shear Around Magnified Radio Sources	NTT
E-0413	Fusi Pecci/Bellazzini/Buonanno/ Corsi/Ferraro/Zinn	C-M Diagrams of the Globular Clusters in Fornax: a Step Towards the Understanding of the Galaxy Formation	NTT
E-0851	Gemmo	An Infrared Search for Companions to White Dwarfs	2.2-m
B-0747	Gerritsen/Barthel	Infrared Imaging of Quasar Host Galaxies	2.2-m
A-0130	Gieren/Barnes/Moffett	Independent Distances to Field and Cluster Cepheids in the Magellanic Clouds	0.9-m Dutch
B-0664	Goerdt/Fricke/Kollatschny	Star Formation in the Surroundings of AGN	1.5-m
A-0105	Goudfrooij/Binette/Hansen	Origin and Excitation of Gas in Cooling-Flow Galaxies	1.5-m
A-0106	Goudfrooij/de Jong/Hansen	Origin of Dust and Ionized Gas in Dominant Cluster Galaxies	1.5-m Danish
B-0866	Grandi/Fosbury/Hartman/Maraschi/Marconi/ Urry	Ground-Based Monitoring of Gamma-Ray Emitting Blazars: Optical Observations	0.9-m Dutch
D-0730	Grebel/Roberts	Ages, Abundances, and Evolutionary Histories of Binary Clusters in the Magellanic Clouds	NTT

ESO No.	Names of PIs (in alphabetical order)	Title of Submitted Programme	Telescope
C-0534	Gredel	The Nature of the Shocks in Herbig-Haro Objects	3.6-m
C-0729	Gredel/Reipurth	Physical Conditions in Herbig-Haro Bow-Shocks	2.2-m
C-0039	Greve/Johansson	Extinction Towards CO Clouds in the LMC	0.9-m Dutch
E-0021	Groenewegen/Blommaert/Omont	A Study of the Mass-Loosing ABG Stars in the LMC	2.2-m
F-0772	Hainaut/Albrecht/Barucci/Combes/ Coustenis/ Drossart/Dumas/Encrenaz/ Schober/Zellner	Diffraction-Limited Multi-Spectral Images of Vesta in the Near-IR	3.6-m
D-0042	Hanuschik	Shell Lines in Be Stars	1.4-m CAT
B-0740	Hasinger/Roth/Schwope/Trümper/Voges	Optical Study of a Complete Sample of Bright ROSAT-Selected AGN Candidates	2.2-m
B-0079	Heines/Wagner	Intra-Day Variability of Quasars Discovered by EGRET	0.9-m Dutch
B-0069	Hjelm/Joersaeter	High-Excitation Circumnuclear Gas in Active Galaxies	1.5-m Danish
D-0115	Holweger/Gummersbach/Kaufer/Rentzsch-Holm/Wolf	High-Resolution Spectroscopy of Late B-Type Main-Sequence Stars	0.5-m
E-0350	Hron/Kerschbaum/Lebzelter	Evolutionary Status of Semi-Regular Variables	1.5-m
E-0350	Hron/Kerschbaum/Lebzelter	Evolutionary Status of Semi-Regular Variables	1.4-m CAT
E-0418	Hubrig/Mathys	Carbon Distribution on the Surface of Magnetic Ap Stars	1.5-m
E-0118	Imbert/Maurice	Vitesses radiales des Céphéides brillantes du LMC	1.5-m Danish
A-0801	Infante/Carlberg/Pritchet	Evolution of Faint Galaxy Pairs and the Redshift Relation	2.2-m
A-0801	Infante/Carlberg/Pritchet	Evolution of Faint Galaxy Pairs and the Redshift Relation	NTT
A-0367	Jaffe/Bremer/Johnstone/Kotilainen	Imaging Shocked Molecular Gas in Cluster-Cooling Flows	2.2-m
E-0336	Jorissen/Mayor/North	The Evolutionary Status of S Stars and Dwarf Barium Stars	1.5-m Danish
C-0003	Käufl/Stanghellini	Morphology of Planetary Nebulae at $\lambda \sim 8\text{--}13\,\mu m$, and Its Implications for Post-AGB Stellar Evolution	3.6-m
D-0402	Koester/Reimers	An Empirical Test for the Mass-Radius Relation of White Dwarfs.	3.6-m
D-0829	Koesterke/Hamann/Leuenhagen/ Wessolowski	Spectroscopy of CSPN of WC-Type in the Magellanic Clouds and the Galaxy	3.6-m
D-0301	Krautter/Baade/Kneer	Low-Mass Star Formation in LMC Dark Clouds	2.2-m
E-0382	Krautter/Metanomski/Pasquini/Schmitt/ Wälde	Nature of Late-Type Stars in the ROSAT All-Sky Survey	0.5-m
E-0382	Krautter/Metanomski/Pasquini/Schmitt/ Wälde	Nature of Late-Type Stars in the ROSAT All-Sky Survey	1.4-m CAT
E-0615	Kunkel/Brandner/Zinnecker	The X-Ray Selected Young Stellar Population in the CMa R Association	1.5-m
E-0615	Kunkel/Brandner/Zinnecker	The X-Ray Selected Young Stellar Population in the CMa R Association	NTT
E-0424	Kürster/Cochran/Dennerl/Döbereiner/ Hatzes	High-Precision Stellar Radial Velocities, Part V	1.4-m CAT
F-0618	Lagerkvist/Dahlgren/Erikson/Lagerros/ Lindgren/Magnusson/Rickman	A Search for Trans-Neptunian Objects	NTT
F-0523	Lagerkvist/Dahlgren/Fitzsimmons/Lahulla/ Williams	Rotational Properties and Shapes of Hilda Asteroids	0.9-m Dutch
E-0957	Lagrange/Beust/Deleuil/Ferlet/Lecavalier/ Mouillet/Tobin/Vidal-Madjar	High-Resolution Spectroscopic Survey of β Pictoris with the CES During Coordinated Ground-Based and HST Observations	1.4-m CAT
E-0093	Leinert/Eckart/Weitzel	Very Low Mass Stars	3.6-m
D-0321	Lennon/Dufton/Kudritzki	An Intermediate-Dispersion Spectroscopic Survey of B-Supergiants in the SMC	NTT
D-0124	Leone/Lanzafame	Helium Stratification in Magnetic Chemically Peculiar Stars	1.4-m CAT
B-0655	Lipari/Tsvetanov/Zheng	Imaging, Spectroscopy and Polarimetry of Galaxies with Strong IR and Fe II Emission	3.6-m
A-0464	Longhetti/Rampazzo/Reduzzi	Nature of Fine Structure in Early-Type Galaxies in Pairs	1.5-m
A-0835	Macchetto/Giavalisco/Sparks/Steidel	Near-Infrared Spectroscopy of Radio-Quiet Galaxies at Red-shift z > 3	NTT
A-0667	Macchetto/Sparks	Light Echoes of Historical Supernovae and the Distances to Galaxies	3.6-m
E-0749	Magain/Zhao	Lanthanum and Europium Abundances in Metal-Poor Stars	1.4-m CAT
E-1001	Magnan/de Laverny/Mennessier	Study of the Repeatability of the UBVRI Light Curves of Mira Variables in Successive Cycles	0.5-m
B-0095	Manfroid/Gosset/Moreau	A Multitechnique Quasar Survey: Extension of the Calibration of the UBVRI Survey	1.5-m Danish
B-0095	Manfroid/Gosset/Moreau	A Multitechnique Quasar Survey: Extension of the Calibration of the UBVRI Survey	0.9-m Dutch
B-0101	Marano/Bonifazi/Gruppioni/Hasinger/ Mignoli/Zamorani/Zitelli	Deep Multi-Colour Imaging for Faint X-Ray and Radio Sources and a Search for Faint Quasar Candidates ($22.0 \leq m_B \leq 24.5$)	NTT
E-0789	Mariotti/Beuzit/Duquennoy/Eckart/Perrier	Diffraction-Limited Imaging of the Brown Dwarf Candidate G29–38B (Part II)	3.6-m
C-0055	Martin/Kohoutek	Extinction-Distances to Planetary Nebulae	0.9-m Dutch
E-0416	Mathys/Hubrig/Landstreet/Lanz/Manfroid	Systematic Search and Study of Ap Stars with Magnetically Resolved Lines	1.4-m CAT
D-0724	Megeath/Bronfman/Cox/Moneti/Roelfsema	A Near-Infrared Study of On-Going Star Formation in the Carina Nebula	2.2-m

ESO No.	Names of PIs (in alphabetical order)	Title of Submitted Programme	Telescope
A-0388	Mellier/Bonnet/Fort	The Dark-Matter Distribution in the Distant Cluster of Galaxies S295 from the Measurement of the Weak Gravitational Shear	NTT
D-0912	Melnick/Brandner/Meylan/Terlevich	The Initial Mass Function of the Ionizing Cluster of 30 Doradus	NTT
E-0812	Mennickent	Mass Ratios, Orbital Periods, System Parameters and Disk Inhomogenities of the SU UMa Stars RZ Leo and HV Vir	2.2-m
E-0392	Mermilliod/Mayor	Constraints on Stellar Formation from Orbital Elements of Cluster Binaries	1.5-m Danish
A-0999	Meylan/Azzopardi/Dubath/Lequeux	Search for Dark Matter in the Fornax Dwarf Spheroidal Galaxy	NTT
B-0998	Meylan/Djorgovski/Smith/Thompson	A Search for Quasar Protoclusters at High Redshifts	NTT
B-0083	Miley/Roettgering/van Ojik	High-Resolution Spectroscopy of z > 2 Radio Galaxies	NTT
E-0990	Minniti/Goudfrooij/Jablonka/Meylan	Search for Globular Clusters in the Inner Parts of NGC 5128	2.2-m
A-0606	Mirabel/Bravo Alfaro/Duc	Dwarf Galaxies of Tidal Origin	NTT
A-0614	Molinari/Chincarini/De Grandi/Böhringer	Photometric Properties of X-Ray Selected Clusters of Galaxies	1.5-m Danish
D-0712	Moorhouse/Brand/Burton/Smith	Mapping the Excitation of Molecular Hydrogen	2.2-m
B-0598	Moorwood/Käufl/van der Werf	Infrared Imaging of Warm Dust in Starburst Galaxies and AGNs	2.2-m
B-0598	Moorwood/Käufl/van der Werf	Infrared Imaging of Warm Dust in Starburst Galaxies and AGNs	3.6-m
B-0793	Moorwood/Oliva/Origlia	The Mass-to-Light Ratio of cD Galaxies	NTT
B-0129	Møller/Warren	The Size and Morphology of Normal Galaxies at $z \simeq 3$	NTT
D-0468	Najarro/Hillier/Kudritzki/Lennon/Lutz	IR Spectroscopy of Ofpe/WN9 Stars in the LMC	NTT
D-0365	Nisini/Lorenzetti/Saraceno/Spinoglio/Zavagno	Infrared Morphology of Mass Outflows in Young Stellar Objects	2.2-m
E-0440	Nissen/Lambert/Smith	The Lithium Isotope Ratio in Galactic Disk Stars	1.4-m CAT
E-0386	North/Betrix/Kuenzli	Lithium in Evolved Metallic A-F Stars	1.4-m CAT
D-0668	Nota/Clampin/Leitherer/Origlia	Near-IR Spectroscopy of Massive, Evolved Stars	NTT
D-0902	Nota/Clampin/Leitherer/Paresce/Pasquali/Robberto	High-Resolution Coronographic Imaging of LBVS and SLASH (Ofpe/WN9) Stars	NTT
D-0870	Nota/Clampin/Origlia/Moneti	IR Narrow- and Broad-Band Imaging of AG Carinae and Other Selected LBVS	2.2-m
E-0661	Nussbaumer/Mürset/Schild/Schmutz	Wind Structure of Red Giants in Symbiotic Systems	1.4-m CAT
B-0766	Oliva/Marconi/Moorwood	Testing Unified Models in the Nearest Seyfert 2 Galaxy	NTT
A-0474	Oliveira/Bolte	Proto-Globular Clusters in Merging Galaxies	2.2-m
A-0900	Ordell/Booth/Horellou	Integrated Star Formation Rates of Arp-Madore Merging Galaxies	1.5-m
D-0521	Orio/Bianchini/Della Valle/Massone/Oegelman	Optical Study and Identification of Supersoft X-Ray Sources	2.2-m
D-0967	Pakull/Koeppen/Motch	Highly Ionized Nebulae Around X-Ray Sources in the Magellanic Clouds	NTT
E-0399	Pallavicini/Pasquini	Lithium in Solar-Like Dwarfs in the Old Cluster M67	3.6-m
E-0892	Pantin/Backman/Fajardo-Acosta/Lagage/Lagrange	Monitoring the 10-μm Flux of the Inner Dust Disk of β Pictoris	3.6-m
C-0935	Paresce/Clampin/Ligori/Robberto	A Search for Circumstellar Disks Around MS Stars	NTT
E-0872	Pasquini/Andersen/Cutispoto/Randich	Hunting Young, Nearby G Stars	1.4-m CAT
E-0880	Pasquini/Molaro/Castelli	Be Abundance in Solar-Type Stars	NTT
A-0538	Patat/Barbon/Benetti/Cappellaro/Turatto	The Intrinsic Colours of Supernovae of Type Ia	0.9-m Dutch
A-0768	Pedersen/Boer/Hurley	Cosmological versus Local Origin for Gamma-Ray Bursts	NTT
A-0029	Pellegrini/Böhringer/Danziger	A Study of a Complete Sample of Galaxy Clusters Detected by ROSAT	3.6-m
A-0025	Pellegrini/Ciotti/Held	Correlation Between X-Ray Emission and Internal Dynamics in S0 Galaxies	1.5-m
A-0025	Pellegrini/Ciotti/Held	Correlation Between X-Ray Emission and Internal Dynamics in S0 Galaxies	0.9-m Dutch
A-0492	Petitjean/Bertrand/Cimatti/Haenelt/di Serego Alighieri	Host Galaxies of AGN	3.6-m
E-0018	Poretti/Bossi/Mantegazza/Riboni/Zerbi	Pulsation Mode Identification of Multiperiodic δ Sct Stars	0.5-m
E-0018	Poretti/Bossi/Mantegazza/Riboni/Zerbi	Pulsation Mode Identification of Multiperiodic δ Sct Stars	1.4-m CAT
E-0371	Pottasch/Garcia-Lario/Manchado/Parthasarathy/Sanz	Spectral Changes in Rapidly Evolving Post-AGB Stars	1.5-m
C-0506	Rauch/Koeppen/Werner	Spectral Analyses of Planetary Nebulae and Their Central Stars	2.2-m
D-0034	Rauw/Gosset/Manfroid/Smette/Vreux	Study of the Eclipses of the SB1 System WR22	0.5-m
D-0035	Rauw/Gosset/Vreux	Study of an Eclipsing Single-Lined (!) Wolf-Rayet Binary	1.5-m
D-0604	Redfern/Cullum/Shearer	A Search for Optical Pulsations From Geminga	NTT
E-0647	Reetz/Axer/Baumüller/Fuhrmann/Gehren	CNO Abundances in Metal-Poor Stars	3.6-m
E-0647	Reetz/Axer/Baumüller/Fuhrmann/Gehren	CNO Abundances in Metal-Poor Stars	1.4-m CAT
D-0828	Reipurth	Jets and Bow Shocks in Herbig-Haro Flows	NTT
A-0058	Röser/Dyer/Kronberg/Perley	Global Mass of Intervenor Galaxies Towards Quasars	3.6-m
F-0806	Rosenqvist/Billebaud/Encrenaz/Gendron/Schmitt/Tiphène	Near Infrared Observations of the Martian North Polar Cap at High Spatial Resolution	3.6-m
C-0693	Rouan/Field/Lacombe/Lai/Rostas	Small Structure of Molecular Clouds: High Angular Resolution Mapping of H_2 Filaments in the Reflection Nebula NGC 2023	3.6-m
A-0024	Saglia/Bender/Gerhard/Jeske	Probing the Gravitational Potential and Anisotropy of Elliptical Galaxies	NTT

ESO No.	Names of PIs (in alphabetical order)	Title of Submitted Programme	Telescope
A-0788	Sams/Brandl/Genzel	Diffraction-Limited K-Band Studies of High-z Galaxy Evolution and Morphology	3.6-m
C-0351	Schild/Miller/Tennyson	H_2 Structure and Temperature of Molecular Clouds	2.2-m
E-0575	Schild/Mürset/Schmid/Schmutz/Vogel	Search for Symbiotic Stars in the LMC	1.5-m Danish
E-0637	Severino/Covino/Gomez/Lopez/Terranegra	Spectroscopic Test of Cool-Star Atmospheres	1.4-m CAT
B-0993	Shaver/Kellermann/Wall	A Search for Radio-Loud Quasars at z > 5	3.6-m
A-0398	Shaw/Axon/Combes	Nuclear Bars and Isophote Twists in Barred Spiral Galaxies	2.2-m
D-0602	Shearer/Cullum/Middleditch/Redfern	A Temporal and Polarimetric Study of SN1987A	NTT
E-0401	Siebenmorgen/Gredel/Zijlstra	The Dust Composition in Herbig-Haro Objects	NTT
C-0452	Sivan/Perrin	Spectrophotometry of Luminescence Processes in Extra-galactic H II Regions	1.5-m
D-0963	Srinivasan Sahu/Blaauw/Murphy	Spectral Classification of YSO Candidates in the IRAS Vela Shell	1.5-m
C-0669	Stark/Boisse/Gredel	Small-Scale Brightness Variations in Interstellar Cirrus Clouds	1.5-m Danish
D-0547	Stefl/Baade/Kaper	Origin and Coupling of Stellar and Circumstellar Balmer Jump Variations in Be Stars	0.5-m
D-0547	Stefl/Baade/Kaper	Origin and Coupling of Stellar and Circumstellar Balmer Jump Variations in Be Stars	1.5-m
D-0547	Stefl/Baade/Kaper	Origin and Coupling of Stellar and Circumstellar Balmer Jump Variations in Be Stars	1.4-m CAT
D-0713	Stefl/Hirata	Atmosphere Instabilities in the Be Star λ Eri – a Multi-Site Campaign	1.4-m CAT
A-0532	Stein/Binggeli/Jerjen	Dynamics of Dwarf Galaxies in the Fornax Cluster	3.6-m
A-0346	Stein/Oliveira	Probing Theories of Formation of cD Galaxies	1.5-m Danish
A-0346	Stein/Oliveira	Probing Theories of Formation of cD Galaxies	1.5-m
A-0507	Tacconi-Garman/Brandl/Eckart/Henning	Adaptive Optics Near-IR Observations of Galaxies in the Zone of Avoidance	3.6-m
B-0497	Tadhunter/Morganti/Simpson/Ward	IR Imaging of a Complete Sample of Radio Galaxies	2.2-m
E-0408	Tagliaferri/Cutispoto/Fleming/Pallavicini/ Pasquini	Spectroscopic and Photometric Studies of Cool Stars Detected Serendipitously by WFC and EUVE	0.5-m
E-0408	Tagliaferri/Cutispoto/Fleming/Pallavicini/ Pasquini	Spectroscopic and Photometric Studies of Cool Stars Detected Serendipitously by WFC and EUVE	1.4-m CAT
E-0411	Testa/Ferraro/Mateo	J,H,K Photometry of Young Magellanic Clusters	2.2-m
D-0112	Testor/Schild	Spectroscopy of Bright Stars in Selected OB Associations in LMC	1.5-m
D-0494	Thé/Bjorkman/Grady/Perez/van den Ancker	Coordinated Optical and UV Spectroscopy of Edge-On Proto-Planetary Disk Systems	1.4-m CAT
D-0363	Thé/Miroshnichenko/van den Ancker	Dust Grains Induced Variable Characteristics of PMS Herbig Ae/Be Stars	1.4-m CAT
A-0459	Théodore/Petitjean	Properties of Galaxies Producing Low z Lyα Absorptions	2.2-m
A-0077	Thimm/Frenk/van Harlem	Infalling Subclusters, Morphology-Density Relation and Gravitational Shearing for CI0500-24 (z = 0.321)	NTT
A-0064	Tiersch/Böhringer/MacGillivray/Oleak/Stoll	Photometrical Investigations of Shakhbazian's Compact Group of Galaxies	1.5-m
A-0040	Tiersch/Böhringer/MacGillivray/Oleak/Stoll	Photometrical Investigations of Shakhbazian's Compact Group of Galaxies	1.5-m Danish
E-0049	Tinney	Parallaxes of VLM Stars	2.2-m
E-0048	Tinney	A Survey for Main-Sequence/Brown Dwarf Transition Objects	1.5-m Danish
D-0450	Tosi/Bragaglia/Ferraro/Fusi Pecci/Marconi	Open Clusters as Tracers of Galactic Evolution	1.5-m Danish
B-0791	Tsvetanov/Ford/Fosbury/Kotilainen/Ward	High-Resolution Infrared Imaging of Seyfert Galaxies with Ionization Cone Morphology	2.2-m
B-0046	Ulrich/Doublier/Molendi	Spectroscopy of Quasars with Extreme α_{ox}	1.5-m
D-0524	van der Hucht/Bouchet/Setia/Gunawan/ Williams	Search and Monitoring of Eruptive Wolf-Rayet Dust Formation	2.2-m
C-0597	van der Hulst/Baluteau/de Graauw/Israel/ Joubert/van der Werf	Excitation of H II Regions in the Magellanic Clouds	3.6-m
A-0338	van der Kruit/de Grijs/Peletier	Near-Infrared Surface Photometry of Edge-On Spiral Galaxies	2.2-m
B-0706	van der Werf/Bremer/Miley/Moorwood/ van Ojik	The Cluster Environment of High-Redshift Radio Galaxies	2.2-m
C-0595	van der Werf/de Graauw/Israel/Laureijs/ van der Hulst	Excitation of Molecular and Ionized Gas in the Magellanic Clouds	NTT
D-0530	van Paradijs/Abbott/Augusteijn/Leibundgut/ Strom	Supernova Light Curves	0.9-m Dutch
D-0723	Waelkens/Waters	Near-IR Spectroscopy of Herbig Ae/Be Stars	NTT
D-0442	Walsh/Chugai/Fridman/Khoruzhij	Unravelling the η Carinae Jet	NTT
C-0444	Walsh/Walton	Imaging and Spectroscopic Survey of the Abell Planetary Nebulae	1.5-m
B-0854	Warren/Bunker/Clements/Hewett	0.3-cm, 2-cm Hα Emission from Galaxies at z > 2	2.2-m
D-0107	Waters/Cox/Käufl/Lacy/Lamers/Roelfsema	10-μm Imaging of the Ejecta of Luminous Blue Variables	3.6-m
D-0809	Waters/de Graauw/Lacy/Lamers/Marl-borough	Mid-IR Spectroscopy of Extended Atmospheres of Hot Stars	3.6-m
D-0054	Weigelt/Appenzeller/Davidson/Reinhei-mer/Schöller/Scholz/Seggewiss/Wagner	Speckle Masking and Speckle Spectroscopy of Stellar Objects and AGNs	2.2-m
D-0574	Werner/Rauch	Search for Hydrogen in Helium-Rich [Pre-] White Dwarfs	3.6-m

ESO No.	Names of PIs (in alphabetical order)	Title of Submitted Programme	Telescope
F-0735	West/Hainaut	Neptunian "Trojans"	NTT
F-0763	West/Hainaut/Marsden/Meech	Activity in Very Distant Comets	NTT
E-0650	Wicenec/Makarov/Wagner	Verification of the Tycho Catalogue	0.9-m Dutch
B-0930	Williger/Elston/Smette	Low-z QSO Absorbers and the UV Background	NTT
D-0006	Wolf/Gummersbach/Kaufer/Mandel/Stahl/ Sterken/Szeifert/Zickgraf	High-Dispersion Spectroscopy of Luminous Blue Variables of the MCs	3.6-m
D-0114	Wolf/Gäng/Gummersbach/Kaufer/Kovacs/ MandelStahl/Sterken/Szeifert	High-Resolution Spectroscopic Monitoring of B-Type Supergiants	0.5-m
C-0341	Yun	T Tauri Stars and HH Objects Associated with Bok Globules	1.5-m Danish
E-0051	Zacs	Barium Star Formation	1.4-m CAT
B-0100	Zamorani/Giacconi/Marano/Mignoli/Zitelli	Spectroscopic Follow-Up of ROSAT Discovered X-Ray Sources in the "Marano Field"	3.6-m
A-0007	Ziegler/Bender	The Age of Elliptical Galaxies in Clusters	NTT
E-0135	Zijlstra/Groenewegen/Loup/Waters	TIMMI Observations of Obscured AGB Stars in the LMC	3.6-m
E-0622	Zijlstra/Loup/Waters/Whitelock	The AGB Mass-Loss Function in the LMC	2.2-m
E-0134	Zijlstra/Minniti	Miras in Nearby Galaxies	NTT
E-1000	Zinnecker	Adaptive Optics Imaging Spectroscopy of T Tau, Z CMa, and NGC 3603	3.6-m
D-0031	Zwitter/Munari	Spectrophotometric Survey of Suspected Cataclysmic Variables	1.5-m

LISA II – Library and Information Services in Astronomy II

ESO, Garching, May 10–12, 1995

LISA I, IAU Colloquium No. 110, was held in Washington D.C. on July 28–August 1, 1988. The aims of LISA II, an IAU Technical Workshop, are twofold: to provide the opportunity for librarians of astronomical observatories and institutes to meet to discuss common problems, and ways of stimulating greater cooperation between libraries and their services; and to raise discussion about, and to throw light on, the interface areas between astronomical libraries and the wide range of on-line and other astronomical computer-based services which are becoming ever more widespread.

Among topics to be covered are:
- **Astronomical information – changing technologies**
- **Impact of electronic publishing on the library**
- **Mastering the information flood**
- **Abstracting and indexing**
- **Future perspectives**

Scientific Organizing Committee: M. Albrecht (ESO), B. Corbin (USNA), M. Cummins (Toronto), B. Hauck (Lausanne), A. Heck (Strasbourg), J.-M. Lloveras (CASLEO), U. Michold (ESO), F. Murtagh (ST-ECF), R. Shobbrook (AAO), G. Shvedova (SAO), W. Warren (GSFC), M. Wolf (Prague).

Local Organizing Committee: M. Albrecht, U. Michold, F. Murtagh, C. Stoffer.

Contact addresses: WWW URL http://http.hq.eso.org/lisa-ii.html

Email: lisaii@eso.org

LISA II, c/o Uta Michold, ESO, Garching. Tel: +49 89 32006-280. Fax: +49 89 32006-480.

The following Workshop Proceedings have recently been published by ESO:

Dwarf Galaxies
(ESO Conference and Workshop Proceedings No. 49)

The price for the 602-p. volume, edited by G. Meylan and P. Prugniel, is DM 90.–.

Handling & Archiving Data from Ground-based Telescopes
(ESO Conference and Workshop Proceedings No. 50)

The Proceedings have been edited by M. Albrecht and F. Pasian (price: DM 35.–). Prepayment is required for both publications.

Payments have to be made to the ESO bank account 2102002 with Commerzbank München or by cheque, addressed to the attention of

ESO Financial Services
Karl-Schwarzschild-Straße 2
D-85748 Garching bei München, Germany.

STAFF MOVEMENTS

Arrivals

Europe
BERGERON, Jacqueline (F), Senior Astronomer
BUSCHMEIER, Wilhelm (D), Head of Administration
CLEMENTS, David (GB), Fellow
GILMOZZI, Roberto (I), Senior Astronomer
ZIJLSTRA, Albert (NL), Astronomer (changed from Fellow to International Staff Member)

Chile
ACHMAD, Lucky (Indon.), Student
MATHYS, Gautier (B), Astronomer (changed from Fellow to International Staff Member)

Departures

Europe
CLASS, Shala (D), Photographer
HAINAUT, Olivier (B), Student
KOTILAINEN, Jari (SF), Fellow

Chile
BRANDNER, Wolfgang (D), Student
MONETI, Andrea (I), Paid Associate

Transfer

Europe
BACHMANN, Gerhard (D), from Head of Administration to Assistant to the Director General

New ESO Publications

Scientific Report No. 14: "Third Catalogue of Stars Measured in the Long-Term Photometry of Variables Project (1990–1992).

Scientific Preprints

1012. M.-H. Ulrich and S. Molendi: Observations and Models of the UV/Soft X-Ray Spectrum of the Quasar PG 1116+215. *Astronomy and Astrophysics*.
1013. R. Siebenmorgen, A.A. Zijlstra and E. Krügel: BD+30°3639: The Infrared Spectrum During Post-AGB Stellar Evolution. *M.N.R.A.S.*
1014. S. Djorgovski and G. Meylan: The Galactic Globular Cluster System. *Astronomical Journal*.
1015. J.D. Smith et al.: Multicolor Detection of High-Redshift Quasars: II. Five Objects with z > 4. *Astronomical Journal*.
1016. M. Spite, L. Pasquini and F. Spite: Lithium in Old Binary Stars. *Astronomy and Astrophysics*.
1017. N. Reid, C. Tinney and J. Mould: VLM M-Dwarfs – Stars or Brown Dwarfs in Disguise. *Astronomical Journal*.
1018. M.R. Rosa and P. Benvenuti: The IMF and the Extinction Law in M101 – HST FOS Spectra of Extragalactic HII Regions. *Astronomy and Astrophysics*.
1019. S. Stefl et al.: Simultaneous Photometric and Spectroscopic Monitoring of Rapid Variations of the Be Star η Cen. *Astronomy and Astrophysics*.
1020. J. Storm et al.: A Baade-Wesselink Analysis of the RR Lyrae Star V9 in 47 Tuc. *Astronomy and Astrophysics*.
1021. E. Cappellaro et al.: The Bright Linear Type II SN 1990 K. *Astronomy and Astrophysics*.
1022. L. Kaper: Stellar Winds in High-Mass X-Ray Binaries. Invited review at IAU Symp. 163, 2–6 May 1994, Elba, Italy. To appear in Proc. IAU Symp. 163, Wolf-Rayet Stars: Binaries, Colliding Winds, Evolution, 1994. Eds. Van der Hucht and Williams, Kluwer Academic Publishers.
1023. C. Lissandrini, S. Cristiani and F. La Franca: Sky Subtraction with Fiber Spectrographs. *Pub. Astr. Soc. Pac.*
1024. R. Gredel: Near-Infrared Spectroscopy and Imaging of Herbig-Haro Objects. *Astronomy and Astrophysics*.
1025. E.K. Grebel and Wm James Roberts: Heterochromatic Extinction. I. Dependence of Interstellar Extinction on Stellar Temperature, Surface Gravity, and Metallicity. *Astronomy and Astrophysics*.
Wm J. Roberts and E.K. Grebel: Heterochromatic Extinction. II. Dependence of Atmospheric Extinction on Stellar Temperature, Surface Gravity, and Metallicity. *Astronomy and Astrophysics*.
1026. A. Caulet, R.N. Hook and R.A.E. Fosbury: Measurements of the Sky Background Using the HST Faint Object Camera. *Astronomy and Astrophysics*.
1027. P. Goodfrooij et al.: Interstellar Matter in Elliptical Galaxies. III. Properties of Dust Extinction. *M.N.R.A.S.*
1028. L.B. Lucy: Fluorescent Excitation of [Ni II] Lines in the Spectra of Gaseous Nebulae. *Astronomy and Astrophysics*.
1029. J.P. Kneib, J. Melnick and Gopal-Krishna: The Cl 2236-04 Lens Cluster. Looking for a Third Gravitational Image? *Astronomy and Astrophysics*.
1030. O. Hainaut et al.: Post-Perihelion Observations of Comet P/Halley. IV. $r = 16.6$ and 18.8 AU. *Astronomy and Astrophysics*.
1031. F. Patat and G. Carraro: A Photometric Study of the Open Cluster Haffner 6. *M.N.R.A.S.*
1032. J.K. Kotilainen and M.A. Prieto: Near-Infrared Imaging of the Seyfert 2 Galaxy NGC 5252. *Astronomy and Astrophysics*.
1033. H. Andernach, R.J. Hanisch and F. Murtagh: Network Resources for Astronomers. *P.A.S.P.*
1034. P.A. Mazzali, I.J. Danziger and M. Turatto: A Study of the Properties of the Peculiar SN Ia 1991 T Through Models of Its Evolving Early-Type Spectrum. *Astronomy and Astrophysics*.
1035. I.R. King, S.A. Stanford and P. Crane: Far-UV Properties of the Nuclear Region of M31. *Astronomical Journal*.
1036. B. Leibundgut and J. Spyromilio: Supernovae and the VLT: More Light to Examine. To appear in *Science with the VLT*, eds. J. Walsh and J. Danziger.

ESO Publications Still Available

A number of books published by ESO are still available. To permit you to complete the series or simply to inform you about any volume that you may have missed, we reproduce here a list of some of the more recent ESO publications.

Proceedings

No.	Title	Price
28	ESA/ESO/ST-ECF Workshop on Astronomy from Large Databases – Scientific Objectives and Methodological Approaches, 1988	DM 50.–
29	NOAO-ESO Conference on High-Resolution Imaging by Interferometry (2 volumes – Part I and Part II), 1988	DM 95.–
30	ESO Conference on Very Large Telescopes and their Instrumentation (2 volumes – Vol. I and Vol. II), 1988	DM 95.–
31	1st ESO/ST-ECF Data Analysis Workshop, 1989	DM 30.–
32	ESO Workshop on Extranuclear Activity in Galaxies, 1989	DM 40.–
33	ESO Workshop on Low Mass Star Formation and Pre-Main Sequence Objects	DM 50.–
34	2nd ESO/ST-ECF Data Analysis Workshop, 1990	DM 20.–
35	ESO/CTIO Workshop on Bulges of Galaxies, 1990	DM 40.–
36	ESO Workshop on Rapid Variability of OB-Stars: Nature and Diagnostic Value, 1991	DM 45.–
37	ESO/EIPC Workshop SN 1987 A and other Supernovae, 1991	DM 80.–
38	3rd ESO/ST-ECF Data Analysis Workshop, 1991	DM 30.–
39	ESO Conference on High-Resolution Imaging by Interferometry II (2 volumes – Part I and Part II), 1993	DM 110.–
40	ESO Workshop on High Resolution Spectroscopy with the VLT, 1992	DM 45.–
41	4th ESO/ST-ECF Data Analysis Workshop, 1992	DM 25.–
42	ESO Conference on Progress in Telescope and Instrumentation Technologies, 1992	DM 90.–
43	Astronomy from Large Databases II, 1992	DM 70.–
44	ESA/ESO/ST-ECF/STScI Workshop on Science with the Hubble Space Telescope, 1993	DM 80.–
45	ESO/EIPC Workshop "Structure, Dynamics and Chemical Evolution of Elliptical Galaxies", 1993	DM 90.–
46	Second ESO/CTIO Workshop on Mass Loss on the AGB and Beyond, 1993	DM 70.–
47	5th ESO/ST-ECF Data Analysis Workshop, 1993	DM 30.–
48	ICO-16 Satellite Conference on "Active and Adaptive Optics", 1994	DM 90.–
49	ESO/OHP Workshop on "Dwarf Galaxies", 1994	DM 90.–
50	ESO/OAT Workshop "Handling and Archiving Data from Ground-based Telescopes", 1994	DM 35.–

Other Publications

ESO's Early History: The European Southern Observatory from Concept to Reality (A. Blaauw), 1991 — DM 25.–

The Strasbourg-ESO Catalogue of Planetary Nebulae, Part I and II (eds. A. Acker, F. Ochsenbein, B. Stenholm, R. Tylenda, J. Marcout, C. Schohn), 1992 — DM 135.–

Contents